THE UNIVERSITY OF MICHIGAN

INDUSTRY PROGRAM OF THE COLLEGE OF ENGINEERING

THE EFFECT OF THE RATE OF ENERGY INPUT UPON THE MINIMUM SPARK IGNITION ENERGY OF LEAN PROPANE-AIR MIXTURES

John C. Steiner

A dissertation submitted in partial fulfillment
of the requirements for the degree of
Doctor of Philosophy in the
University of Michigan
Department of Mechanical Engineering
1964

April, 1964

IP-666

ACKNOWLEDGMENTS

The author expresses his sincere appreciation to Professor William Mirsky, Chairman of the Doctoral Committee, for his constant encouragement, advice and assistance throughout the course of this investigation. The writer also expresses his gratitude to the members of the Committee, Professor J. A. Bolt, Professor S. W. Churchill, Dr. M. E. Milberg and Professor G. J. Van Wylen.

Acknowledgment is due to Professor M. B. Stout of the Electrical Engineering Department of the University for his help on several occasions.

The financial assistance given by General Motors Corporation, Shell Oil Co., Texaco, Incorporated and the Institute of Science and Technology of the University in the form of Fellowships is gratefully acknowledged.

Provision of material and equipment by the Mechanical Engineering Department of the University for this investigation as well as the use of the Computing Center facilities is appreciated. Acknowledgment is also due to the Delco Remy Division of General Motors Corporation for furnishing a special ignition coil.

Thanks is due to my wife, Lucy, for preparation of the manuscript.

TABLE OF CONTENTS

TABLE OF CONTENTS (CONT'D)

LIST OF TABLES

LIST OF ILLUSTRATIONS

LIST OF ILLUSTRATIONS (CONT'D)

LIST OF ILLUSTRATIONS (CONT'D)

NOMENCLATURE

a	Concentration of reactant or fuel
a	Concentration of active particles or chain carriers
a_o	Concentration of active particles at $\omega_1 = 0$, page 56
a_o	Concentration of fuel at source
a_o	Initial concentration of particles inside sphere, page 57
a_o	Value of a as defined on page 54
A	Area
A_r	Constant
B	Constant
C	Capacitance
C_2	Secondary equivalent lumped capacitance in Figure 1.1
c	constant
$\bar{c}_v$	Molar specific heat at constant volume
$\bar{c}_p$	Molar specific heat at constant pressure
c_v	Constant volume specific heat
c_p	Constant pressure specific heat
D	Diffusion coefficient for active particles
D	Constant
D_L	Constant
D_p	Constant
d_q	Quench distance
E_a	Arrhenius activation energy
E_f	Final energy in the kernel

E_H	Total energy in high rate spark component
E_L	Total energy in low rate spark component
E_{MIN}	Minimum ignition energy
E_{MINL}	Minimum ignition energy for a line source
E_{MINP}	Minimum ignition energy for a point source
E_S	Fraction of condenser energy existing as internal energy in the kernel
F	Constant
F/A	Fuel air ratio
G	Mass flow of mixture toward source
g	Geometric factor representing the percentage of photons that reach the cathode.
H	"Heat"
h	Planck's constant
$\bar{h}$	Average convective heat transfer coefficient
I_o	Steady state primary current
i	Current
i_o	Photocurrent
K	Thermal conductivity
K_u	Thermal conductivity of unburned gases
k_b	Second order branching coefficient
k'_b	First order branching coefficient
k_L	First order chain breaking coefficient
L	Inductance
L_1	Primary inductance
M_{AIR}	Molecular weight of air
M_F	Molecular weight of fuel

m	Mass
N_f	Mole fraction of fuel
N_o	Mole fraction of oxygen
n	Total number of moles
n	Order of a reaction
P	Pressure
P_f	Partial pressure of fuel
P_T	Total pressure
P_o	Initial pressure
P_{HA}	Average rate of energy discharge during high rate component
P_{LA}	Average rate of energy discharge during low rate component of the spark
P_p	Peak power
q_I	Rate of heat generation by reaction
q_{II}	Rate of heat loss
R	Resistance
R	Gas constant
R_2	Coil resistance in Figure 1.1
R_2'	Lead resistance in Figure 1.
R_g	Effective gap resistance
r	Radius of spherical flame volume
r_1	Radius of initial self-propagating flame
S_u	Velocity of unburned gases relative to flame front
s	Emperical constant
	Temperature

T_a	An average temperature between T_b and T_u
T_b	Self-ignition temperature
T_f	Adiabatic flame temperature
$T_{S_{LINE}}$	Temperature of the line source
$T_{S_{POINT}}$	Temperature of the point source
T_o	Initial temperature
T_u	Temperature of unburned mixture
T_w	Wall temperature
T_b	Self-ignition temperature
t	Time
U_{RP}	Heat of reaction per unit mass
U_{RP}	Heat of reaction per molecule
U_{RP}	Heat of reaction per mole of fuel
U_{RP}	Heat generation per unit time by each active particle
V	Volume
V	Voltage
V_{BR}	Breakdown voltage
V_{2MAX}	Maximum secondary voltage
V_f	Final volume
V_s	Volume at shock separation
v	Velocity
X	Field strength
X	Reactance
X_r	Radial component of a space charge field

α	Townsend's first ionization coefficient
β	Second Townsend coefficient
γ	Secondary ionization coefficient
γ	Ratio of specific heats, c_p/c_v
Δt_{BR}	Voltage rise time
Δt_{SP}	Total spark discharge duration
δ	Gap length
η	Fraction of photons which produce electrons at the cathode cathode capable of leaving the surface
η	Ratio of actual air to stoichiometric air
θ	Number of photons produced by an electron per centimeter of gap
μ	Average absorption coefficient of the gas molecule for photons
ν	Constant
ν	Light frequency
ρ	Gas density
ρ_o	Density of gas mixture at source
ρ_u	Density of unburned gases
σ_1	Constant
σ_2	Constant
ϕ	Equivalence ratio
ϕ_w	Work function
ω	Reaction rate
ω_1	Rate of initiation of chain carriers due to ignition source
Ω	Constant

I. INTRODUCTION

A. Purpose

Improved thermal efficiency is realized by increasing the compression ratios of spark ignited internal combustion engines. This involves the ignition and burning of lean fuel-air mixtures. The purpose of this investigation was to determine the significance of the rate of energy input by the spark upon ignition of lean propane-air mixtures. The purpose was to conduct a study in which lean, quiescent propane-air mixtures were ignited in a constant volume bomb under fixed initial conditions. The total energy and the rate of energy transfer to the mixture by each spark were controlled.

B. General

Initiation of a self-propagating reaction in the combustible mixture of an internal combustion engine is most frequently performed by an electric discharge called a spark. The quantity of energy and time of discharge can be controlled with relative ease as opposed to heated surfaces and flames.

Two basic types of electrical discharges have been used to initiate combustion: capacitance and inductance sparks. The characteristic difference between these discharges is the rate at which the energy is released in the electrode gap.

Pure capacitance sparks are produced by the discharge of capacitors which are charged to the breakdown voltage of the electrode gap. Pure capacitance implies that the circuit resistance and inductance

are negligible. The time duration of such a spark is in many cases less than one microsecond for low energies and more than 100 microseconds if the energy is high. The latter long duration is due to non-negligible circuit resistances. The current can reach peak values as high as 300 amps with this type of spark. Therefore, the resultant rate of energy input is high during this type discharge.

Inductance sparks are generated by high impedance coils when the circuit is interrupted by opening contacts. The current is low, (i.e., less than 200 milliamps) but the time duration is as long as 2 or 3 milliseconds. Hence, the rate of energy input is low compared to capacitance sparks.

The conventional ignition system produces a spark which consists of two components. The first part of the spark is stored in the inter-electrode capacitance of the coil in addition to any other secondary lead capacitance. Figure 1.1 illustrates a conventional ignition system circuit for a one cylinder engine.

C_2 represents the total equivalent lumped capacitance of the secondary circuit and the energy stored in the capacitance at breakdown is equal to $1/2\ C_2 V_{BR}^2$, where V_{BR} is the voltage at the instant spark breakdown occurs, as shown in Figure 1.2. The time for the voltage to rise to the breakdown value for the given electrode spacing and gas is represented as Δt_{BR}, or voltage risetime. During the buildup of voltage to the breakdown value, the current in the secondary circuit follows the middle curve which shows current versus time in Figure 1.2 The current during Δt_{BR} is required to charge the secondary capacitance, C_2 and does not represent current flow in the electrode gap.

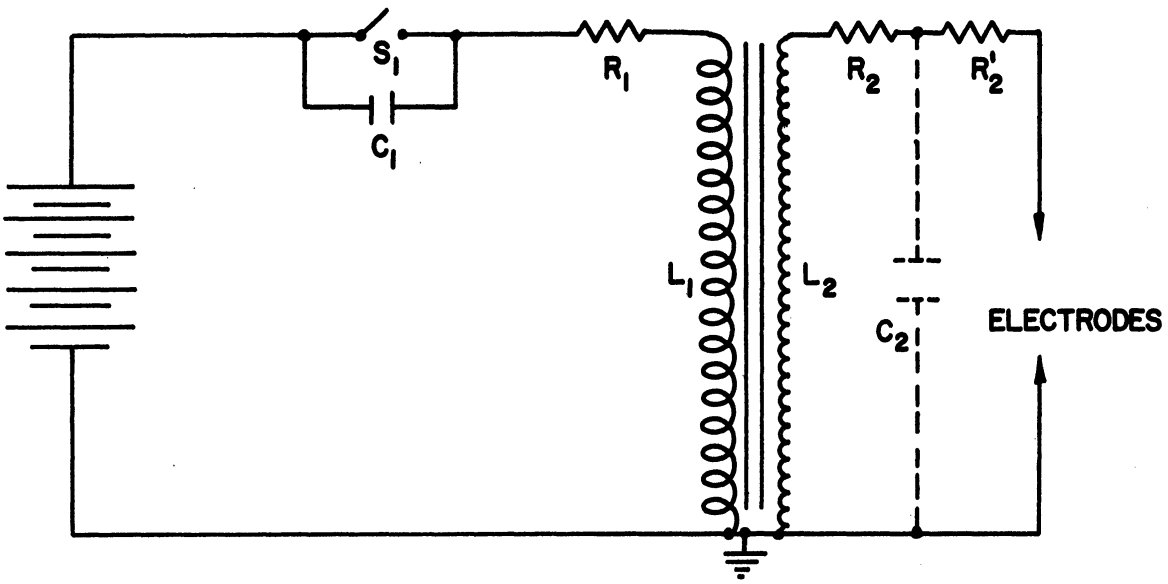

Figure 1.1. Conventional Ignition Circuit.

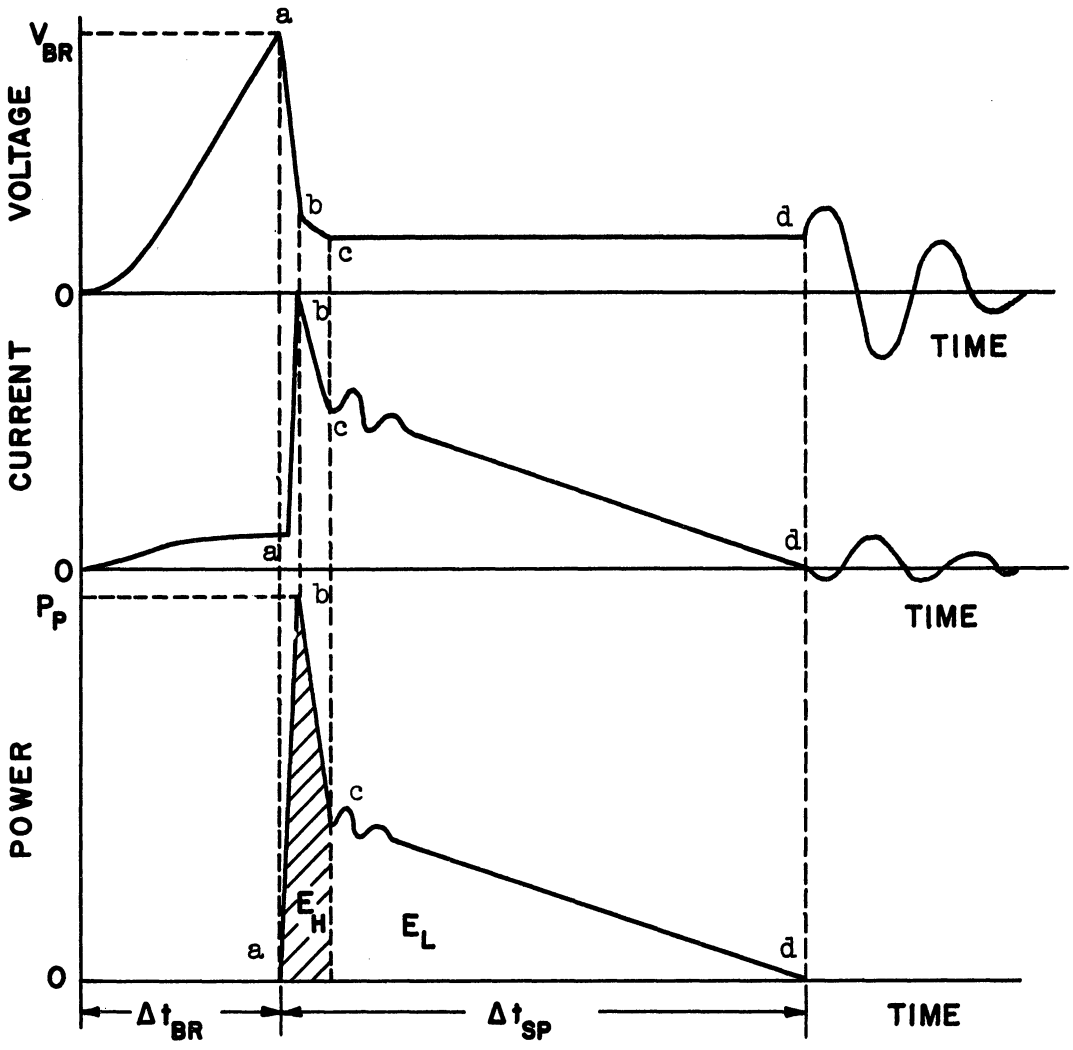

Figure 1.2. Voltage, Current and Power as a Function of Time in a Conventional Ignition Spark.

After breakdown, the current in the electrode gap rises to a maximum in 2 to 8 microseconds while the voltage drops off from a to b as shown in Figure 1.2. The current then falls to point c as the voltage levels off between b and c . This initial current pulse is due to the discharge of the secondary capacitance and is limited by the secondary resistance R_2' and the effective gap resistance. Actually, the capacitive component is not a pure capacitive discharge. It is a spark component which discharges energy at a high rate. The instantaneous rate of energy input, (i.e., power) is merely the product of voltage and current as illustrated in Figure 1.2.

The area under the power curve between a and c is equal to energy in the high rate of capacitive discharge of the spark and is designated, E_H .

Before the high rate energy is completely dissipated, the energy stored in the ignition coil inductance begins to contribute energy but at a low rate. The peak current during the high rate discharge can be as high as 200 to 300 amps, but the maximum current during the low rate component is usually less than 200 milliamps. The area under the power curve of Figure 1.2, between c and d is equal to the energy in the low rate component and is designated, E_L . This low rate component is commonly referred to as the inductive component since the energy dissipated during this time was stored in the inductance of the coil. However, the energy E_L must be discharged through the coil resistance R_2 and the lead resistance R_2' in addition to the electrode gap resistance. Thus, it is not a pure inductance spark. The combustible gas

located between the electrodes sees only the energy transmitted to it and the rate at which it is received. From this viewpoint, "high rate component" and "low rate component" will be used to refer to the respective components of the spark discharge.

Immediately following the high rate component, the current trace shows a unidirectional oscillation. This oscillation is due to coupling between the secondary and primary circuit after the switch S_1 opens.

The total spark duration is designated as Δt_{SP} in Figure 1.2. Δt_{BR} refers to the total time between opening of switch S_1 and spark breakdown. The sine wave oscillation of the voltage and current which occurs after the spark is extinguished, is due to the secondary "tank" circuit decay.

Control of the rate of energy input to the fuel-air mixture was carried out by adjustment of the secondary resistance and capacitance. The total spark energy was adjusted by control of the total time duration Δt_{SP} of the electrical discharge, for a given peak rate of energy input.

II. SURVEY OF PREVIOUS WORK

A few of the early investigators noted that the electrodes seemed to affect the minimum energy required for ignition. Later it was shown that for a fixed set of initial conditions (i.e., fuel, fuel-air ratio, initial pressure and temperature, electrode shape and material), the energy required for ignition decreases to a minimum as the electrode spacing is increased. The electrode gap at which the minimum is reached is defined as the "quench distance". Many early investigations were performed with electrode spacings smaller than the quench distance. Those works which were performed at electrode spacings smaller than the quench distance will be designated as such in the remainder of this section wherever it is significant to the conclusions drawn.

One of the first methods used to determine the energy in a spark was the calorimeter method. Silsbee, Loeb and Fonseca[1,2] presented results of direct measurement of the total energy supplied to the spark gap by different types of ignition systems operating at various frequencies in an early attempt to obtain design information for new ignition systems. While this work provided information about the energy in the spark, it did not describe the structure of the individual sparks.

Wheeler[3] examined the spark structure using a smear camera. He found that the spark consisted of an initial bright spark followed by others of less intensity or by a striated luminous zone which indicated

an oscillating unidirectional discharge of current. He established that the first bright spark was what is today referred to as the capacitive component and the second spark is commonly referred to as the inductive component. His investigations also showed that the primary current required for ignition decreased to a minimum as the fuel-air ratio increased from a lean mixture to stoichiometric. Further increases in fuel-air ratio required a corresponding increase in primary current for ignition. Wheeler[4] continued his work and found that the above mentioned relation for primary current versus fuel-air ratio was the characteristic shape for most hydrocarbons. That is, the primary current required for ignition is high for lean mixtures, decreases to minimum and increases again as the fuel-air ratio is increased. Further, he noted some cooling effect of the electrodes on the initial combustion process.

Taylor-Jones[5] et al., presented mathematical solutions of the heat conduction equation starting from either point of spherical sources and applied them to the spark ignition problem. They showed that if the source of ignition is solely regarded as a source of heat, the effectiveness of a given quantity of energy depends upon the way the energy is transferred to a given volume of mixture. They concluded that an instantaneous point source of ignition was the best. Therefore, the capacitive component of the spark would prove to be the most effective, since the rate of energy input is highest in this component.

Further work by Taylor-Jones[6] et al. showed that a capacitive spark when discharged between two spherical electrodes passed between the

electrodes at the shortest distance. On the otherhand, an inductive spark moved out away from the narrowest gap distance. They surmised that the capacitive spark was in a position relative to the electrodes such that it could transfer heat most readily to the electrodes and less heat to the gas than would the inductive spark. However, they performed calorimeter tests with small spherical carbon electrodes and found that the capacitive sparks transferred more heat to the gas than the inductive sparks transferred with the same primary current. Consequently, they felt that the thermal theory was still valid.

Coward and Meiter[7] determined the volumes of methane-air mixtures that were burned by sparks which were not sufficient to cause a self propagating reaction to occur in the mixture. These volumes were roughly proportional to the square of the primary current of the induction coil. In other words, the columns were approximately proportional to the spark energy. They concluded that the spark acted "mainly perhaps entirely as a source for thermal energy in igniting a gas mixture".

Finch and Thompson[8] and also Bradford and Finch[9] on the otherhand, concluded from their works that "ignition is determined by the setting up of a sufficient concentration of suitably activated molecules". They determined minimum igniting pressures for sparks of different energies and of different current oscillatory frequencies. Their results showed that the total energy and the rate of energy dissipation were unimportant, but the oscillatory frequency of the current was an important factor.

In an attempt to shed some light on the reaction mechanism of hydrogen and oxygen, Thompson[10] and then Linnett, Rayor and Frost[11]

conducted experiments on spark ignition of mixtures of hydrogen and oxygen. The combustible gases were ignited inside 2 to 5 centimeter glass tubes by sparks formed from induction coils. Over a series of runs the spark energy and gap were held constant and the least igniting pressures were determinedfor various mixture ratios. Both investigators found that the partial pressure of the $2H_2 + O_2$ mixture in the gas could be reduced when moderate amounts of inert gas were added at the least igniting pressure. They interpreted this as meaning that the diffusion of chain carriers from the spark volume was inhibited. Linnett[11] et al., found that larger additions of inert gases cause an increase in the partial pressure of $2H_2 + O_2$ at the least igniting pressure. Lewis and von Elbe[12] explain this latter effect as due to thermal factors. The flame temperature is decreased and the thermal diffusivity of the mixture changes. Linnett and Nutbourne[13] found that the partial pressure of the $H_2 + 3N_2O$ mixture in the least-igniting pressure mixture was always increased by the addition of inert gases. They concluded that the absence of a branched chain in the $H_2 + 3N_2O$ reaction was the reason that their results differed from those obtained with the $2H_2 + O_2$ mixtures. Lewis and von Elbe[12] indicate that the results of the preceding experiments are only qualitative and cannot be compared with experiments on minimum ignition energies, because the electrode gap was arbitrarily chosen to be constant. In minimum ignition energy determination, the electrode spacing must be carefully determined to be larger than the flame quenching distance for each fuel-air ratio and initial condition.

Morgan[14,15] in his works indicated that the "incendivity" of a capacity spark is greater than that of an inductance spark when each spark dissipates the same energy. He operated a conventional type ignition system and added a variable capacitor to the secondary, in parallel with the electrodes.

The primary current was fixed, and when the secondary capacitor was set at zero, the spark (capacitive plus inductive) did not cause ignition. However, the spark caused ignition if the secondary capacitance was increased while using the same primary current. Therefore, Morgan concluded that the capacitive component was the most effective in igniting a mixture. It must be pointed out that the experiment was carried out with non-pointed electrodes and was presumably confined to gaps which were smaller than the quench distance, and therefore the results do not establish an absolute trend.

Contradictory work was carried out by Bradford, Finch and Prior[16]. In this case, the ignition occurred in a 250 cc glass explosion vessel. The secondary voltage and current in the spark were recorded using a cathode ray-oscillograph. A mixture of $CO-O_2-H_2$ was ignited at a pressure of 100 mm of mercury with a primary current of 3 amps and the spark breakdown voltage was 4000 volts. The total duration for the spark was 2.81 milliseconds. Then, for the same conditions only the total time duration of the spark was reduced to 2.6 milliseconds, the mixture would not ignite until the pressure was increased to 109 mm of mercury. The following table illustrates further the results obtained.

TABLE I

BRANDFORD, FINCH AND PRIOR[16] DATA

Time Duration Milliseconds	Energy Millijoules	Pressure at Ignition mmHg. abs.
0.79	9.2	130
0.39	5.2	154
0.20	2.4	195
0.02	0.15	235

Bradford et al., concluded from these results that the inductive component, if not most important, at least was necessary for ignition under the conditions of their experiment.

The conclusions presented by Bradford, et al. would seem valid since it was stipulated that the breakdown voltage and thus the capacity component was maintained constant throughout all of the runs. However, Lewis and von Elbe[12] indicate that they obtained minimum ignition energies for a $CH_4 + 2O_2$ mixture with a pure capacitive spark of 0.04 mjoules at a pressure of 252 mm of mercury. But, Bradford, et al., failed to ignite the same mixture at 263 mm Hg. with a 5.0 mjoule spark which consisted of only the capacitive component. Gap lengths were not reported by Bradford, Finch and Prior. Consequently, the explanation of the extremely large energy value cannot be directly attributed to the quench effect, but indicates that the results are not meaningful.

Finch and Sutton[17] verified the theory of the ignition coil through the use of a cathode-ray oscillograph. They confirmed experimentally that the closing of the primary circuit, (i.e., turning the primary current on), during the life of the inductive component stops the secondary discharge. These results enabled them to design a system whereby the duration of the spark could be controlled by control of the time that the primary circuit was open, (i.e., primary current off). Basically, the control of the spark duration controls only the inductive component. The regulation of the capacity component was attained by limiting the secondary current. This limitation was accomplished through the use of a diode which was run under conditions such that the peak current was lower than the normal high capacity component current.

Finch and Mole[18, 19] investigated the influence of the inductive component of the spark on ignition in an engine. The initial pressures and temperatures encountered in the engine were substantially higher than those used in the works of Bradford, Finch and Prior[16] Their results indicated that the output, efficiency and speed of the engine remained unchanged when the inductive component time duration was reduced from 2 to 0.5 milliseconds. Therefore, they concluded that in the engine the capacity component is sufficient for ignition.

Lewis, von Elbe, Blanc, and Guest[20,21,22] were the first investigators to perform really meaningful experiments to obtain minimum ignition energies as a function of fuel-air ratio. All of their work was performed at an initial pressure of one atmosphere or lower at atmospheric temperature. Their electrical circuit is illustrated in Figure 2.1. The variable air capacitors were charged very

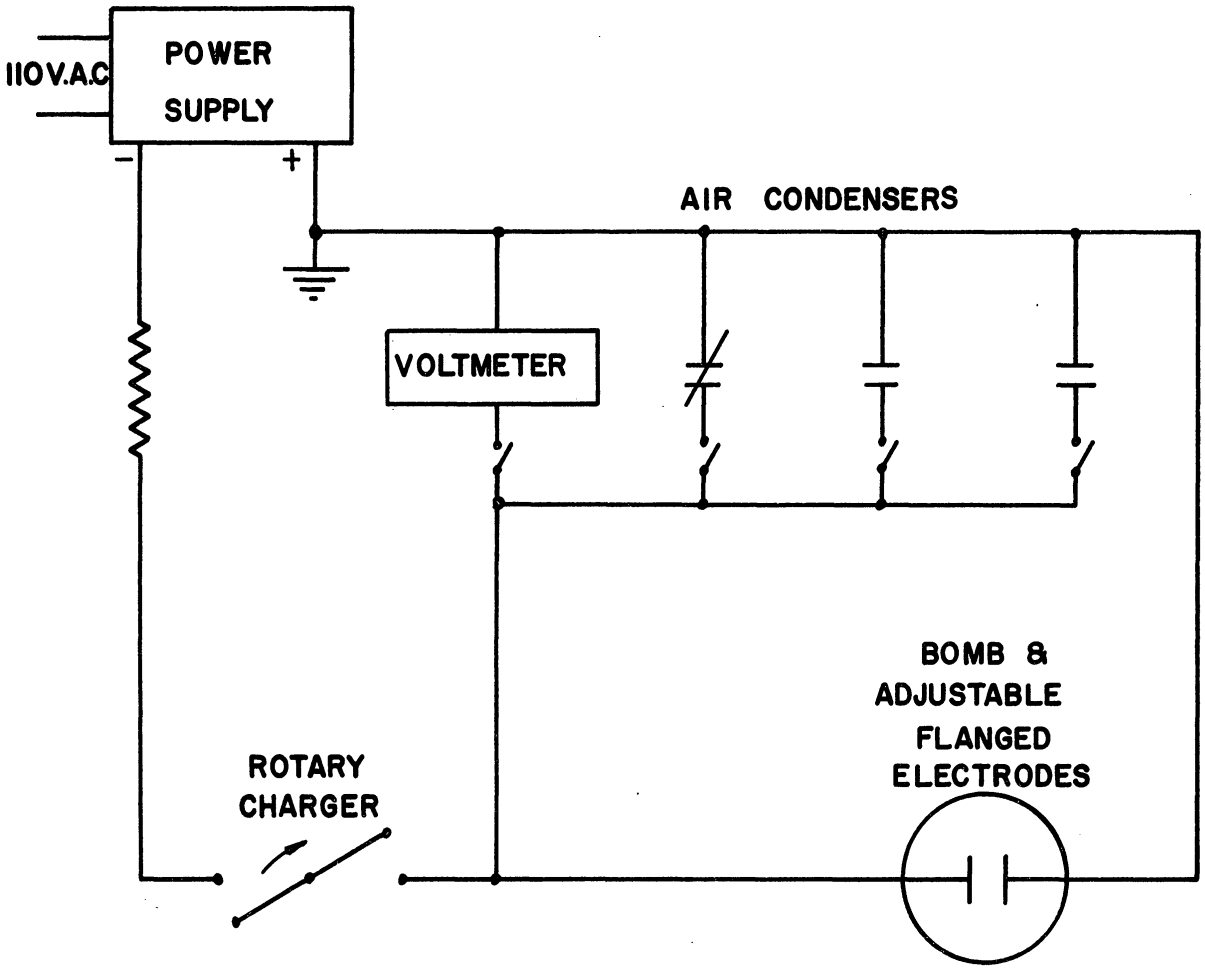

Figure 2.1. Ignition System Used by Lewis and von Elbe.

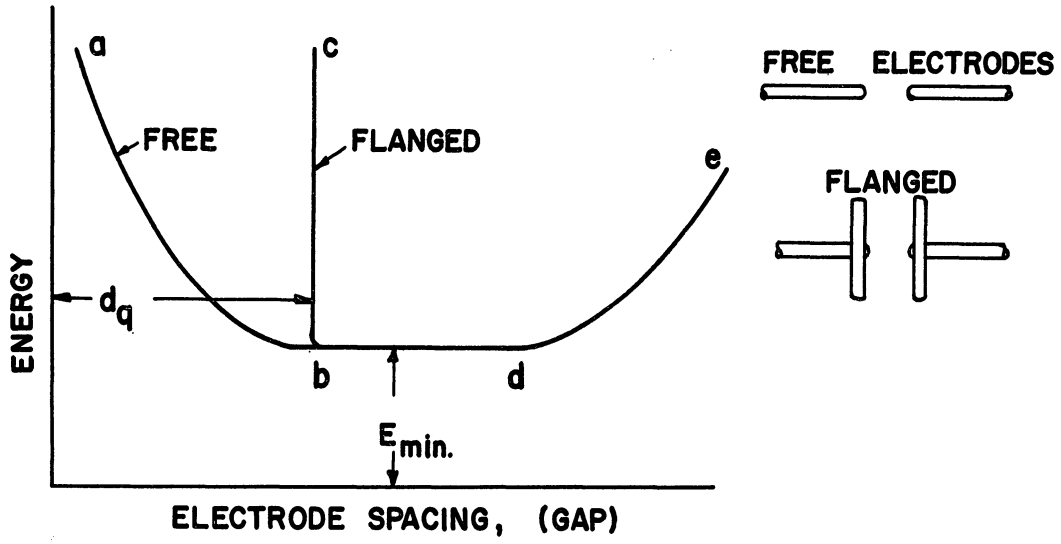

Figure 2.2. Minimum Ignition Energies for Various Electrode Configurations.

slowly by the rotary charger until the breakdown voltage of the spark gap was reached. The voltage at which the spark occurred was observed and the voltage on the capacitors after the spark was recorded. The net energy change in the capacitors was assumed to be the energy dissipated by the spark. It was felt that resistance losses were negligible since the circuit resistance was less than 0.1 ohm, and as compared to an effective gap resistance assumed to be much larger. A test of this point was made by the addition of up to 30 ohms of resistance to the circuit before any effect was noted in the energy required.

Further tests were run to determine the effect of inductance on the ignition process. The resistance in the previous test was replaced by a helix of heavy wire. This helix did not show any effect of moderate changes of inductance on the minimum ignition energy.

It appears that the conclusions that may be drawn from the result are either that the added inductance did not change the spark characteristic or the inductively changed capacitive spark is as effective in the process of ignition as the pure capacitive spark.

One of the most important contributions made by Lewis and von Elbe *et al.*[14,20,21,23] is the determination of quench distances for spark ignition studies. The quench distance is illustrated in Figure 2.2.

They found that where free electrodes, as shown in Figure 2.2, are used, the minimum ignition energy goes through a minimum as the electrode spacing is increased. The quench effect shown by the curve ab for free electrodes was attributed to chain breaking of the initial reactions

at the electrodes as well as heat transfer to the electrodes. Proof of this is shown by the curve cb for flanged electrodes. In this case, glass flanges were added to the free electrodes. The effect was to increase the required ignition energy to infinity for electrode spacings less than d_q, which is defined as the "quench distance". Thus, it is clear that measurement of minimum ignition energies at electrode spacings, δ, less than d_q with anything other than flanged electrodes would leadto erroneous results. Therefore, minimum ignition energy in the true sense refers only to the value E_{MIN} illustrated in Figure 2.2.

The flat section bd of Figure 2.2 suggests that most of the energy is transferred to the gas over a small fraction of the gap length. Rise of the curve, d to e is attributable to distribution of the spark energy over a volume which exceeds a critical volume.

Lewis and von Elbe[12,20,21,23] also found that the minimum ignition energy decreases as the initial pressure is increased from 0.2 atmospheres up to 1.00 atmosphere. In addition, the minimum ignition energy follows a U shaped curve as a function of the percent fuel in air as shown in Figure 2.3. This is a characteristic shape for all hydrocarbons. In addition, the quench distance follows an analogous U shape as a function of the percent fuel in air as illustrated in Figure 2.4.

Morris[24] discusses some general relationships applicable to the results obtained by Lewis and von Elbe.[20,25] He found that the quench distances are related to the pressure according to a general equation

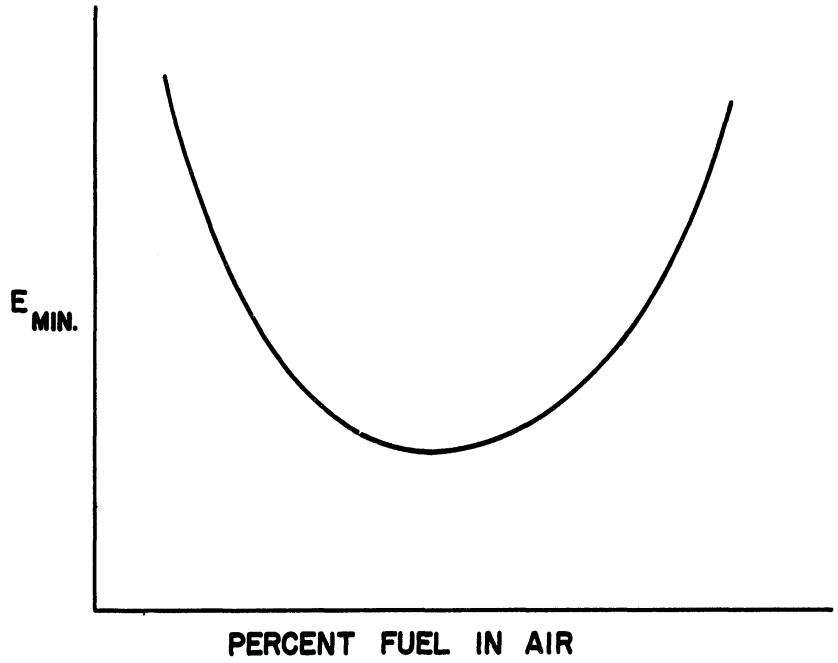

Figure 2.3. Minimum Ignition Energy E_{MIN} as a Function of the Percent Fuel in Air.

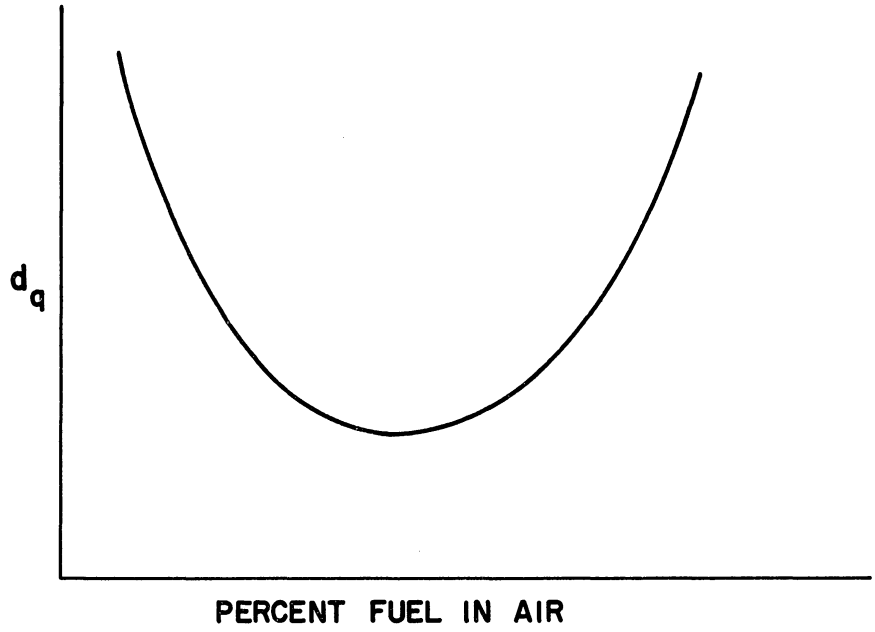

Figure 2.4. Quench Distance d_q as a Function of the Percent Fuel in Air.

where is

$$d_q = c + \frac{s}{p} \tag{2.1}$$

always positive, varying from 0.005 to 0.18 centimeters. Composition changes affect the value of s in an irregular manner. In addition, the minimum ignition energies follow a general relationship

$$E_{MIN} = \frac{e}{p^2} \tag{2.2}$$

where e is a constant for the mixture.

Belles and Swett[26] point out that the quench distances obtained in ignition energy experiments are the same as those obtained in flame quench experiments. In both cases, the quench effect is due to heat transfer from the flame or diffusion of active particles from the flame to the solid surfaces and the surrounding gas. The flame quench experiments involve flashback of flames burning at the port of rectangular burners. The spacing between the long walls of the rectangular burner are varied for a series of flashbacks until the spacing is determined for which the flame will not propagate back into the burner when the fuel-air flow is suddenly stopped. Investigations carried out by Friedman et al.[27] and Harris et al.[28] both show that the quench distance follows the same "U shape" function as indicated by Figure 2.4. In addition, the quenching distance decreases with increases in temperature and pressure.

A comprehensive discussion of the pure capacitive spark is included in the report by Belles and Swett.[26] They indicate that the time duration of the spark can be less than 0.01 microseconds for

low energies and as long as 100 microseconds for energies greater than 1 joule. The time duration of the spark is dependent upon the inherent properties of the circuit. Long duration capacitive sparks are obtained by the addition of series resistance to the circuit and when enough resistance is added, the discharge is very similar to that of a pure inductance spark.

An extensive experiment on capacitive spark discharges was carried out by Rose and Priede.[29] Since no suitable instrument was available at the time, the authors built a high speed oscillograph that had a resolution of one nanosecond.* They recorded the voltage across the spark and the current through the spark as a function of time. Voltage was measured by means of a capacitance potential divider and the current was measured by determination of the voltage across a resistor on the ground side of the circuit. For essentially pure capacitive sparks,** the discharge was oscillatory. By plotting the successive positive and negative peaks on semi-log paper versus time, they calculated the resistance of the spark gap from the slope of the curve. They found that the gap resistance increased markedly as the system capacitance was decreased. Also, reduction of the capacitance reduced the maximum value of the current. It was quite common to record peak currents as high as 300 amps. In their work, they found that the gap resistance followed the following emperical equation.

---

* 1 nanosecond = 10^{-3} microseconds

**System used was very similar to that of Lewis and von Elbe.

$$R_g = 0.4\, e^{3.4 \times 10^{-2} Z} \tag{2.3}$$

where

$$Z = \left(\frac{L}{C}\right)^{1/2} + R \tag{2.4}$$

When a large series resistance of 11K ohms was introduced, the current was critically damped and unidirectional or aperiodic with a peak value of 0.4 amps.

Rose and Priede[30] extended their investigations to determine the effect that electrode configuration had upon the ignition energy and breakdown voltage. They found that the breakdown voltage of a given gap increased when the radius of curvature of the electrode tips were increased. However, addition of a large radius insulting material around a small radius electrode did not change the breakdown voltage. In addition, they found the electrode material affected the energy required for ignition of a given mixture. The minimum energy decreased in the order platinum, aluminum, silver and cadmium. Also, the minimum ignition energy decreases with an increase in the value of the resistance in series with the capacitance spark. Reduction of the minimum ignition energy occurs with reduction of electrode size and reduction of the energy required for a critical area of the electrode material to reach its boiling point. Any decrease in discharge time resulted in a decrease ofthe minimum ignition energy.

Clyde Swett[31,32,33,34,35] studied the ignition of flowing gases by long duration capacitive sparks, (i.e., up to 24,400 micro-seconds duration). In these experiments the long duration capacitive

discharge was obtained by addition of resistance to the circuit. His results showed that decreasing the spark duration from approximately 25000 microseconds to 125 microseconds decreased the amount of energy required for ignition. In addition, he reported that the energy required for ignition with a spark of short duration (i.e., 1 microsecond) was considerably larger than that required by most of the long duration sparks, (i.e., 600 microseconds). The energy required for ignition decreased and then increased again as the gap was increased and for small diameter electrodes the minimum was not sharply defined. Small diameter electrodes required less energy than large diameter electrodes and the required energy for ignition increased with increased turbulence of the gas stream.

In a capacitive spark the energy is transmitted to the gas almost instantaneously. Then the heat is transferred from the gas to the electrodes. Lewis and von Elbe *et al.*[36] conducted some experiments to determine the heat generation by capacitive sparks and the heat transferred to the electrodes. They mounted electrodes in a small vessel containing a monoatomic gas and recorded the pressure change at constant volume or the volume change at constant pressure during the ignition process. From these records the spark generated "heat", H, that is present in the gas at any instant was determined as follows:

$$H = \int_{o}^{n} \bar{c}_v \, (T - T_o) \, dn \qquad (2.5)$$

For constant pressure, $\bar{c}_p$ is used. Then from the ideal gas law:

$$V\Delta P = R \int_{o}^{n} (T - T_o)\, dn \quad \text{for constant volume} \tag{2.6}$$

and

$$P\Delta V = R \int_{o}^{n} (T - T_o)\, dn \quad \text{for constant pressure} \tag{2.7}$$

where

n = total number of moles

T = temperature in volume element

T_o = initial temperature

$\bar{c}_v$ = molar apec heat at constant volume

Then if $\bar{c}_v$ and $\bar{c}_p$ are constant, the spark generated "heat" is represented by the following for monoatomic gases.

$$H = 1.5\, V\Delta P \quad \text{for constant volume} \tag{2.8}$$

$$H = 2.5\, P\Delta V \quad \text{for constant pressure} \tag{2.9}$$

By plotting the ratio of "heat" to energy supplied by the capacitor as percent, versus the square root of the product of thermal diffusivity and time, the curves were extrapolated back to zero time, in xenon, argon and helium 95 percent of the spark energy is present in the form of, "heat".

Olsen et al.[37,38] studied the capacitive spark using a schlieren technique and used ideal gas assumptions in their solution. They developed an equation to describe the fractional loss of energy by the kernel due to expansion after separation of the initial shock in pure argon. The expression is as follows:

$$\frac{E_s - E_f}{E_s} = \frac{(V_f/V_s)^{\gamma-1} - 1}{(V_f/V_s)^{\gamma-1}} \tag{2.10}$$

where

V_f = final volume

V_s = volume at shock separation

E_s = fraction of cond. energy existing as internal energy in the kernel

E_f = final energy in the kernel

Thus the energy in the kernel decreases due to the work that must be done on the surrounding gas during expansion and the remaining energy in the kernel is the energy available for ignition.

Further, their results showed that the energy in the capacitance sparks followed the rules:

For argon: $$1/2\ C\ V_{BR}^2 \propto V_f^{1.23} \tag{2.11}$$

for oxygen: $$1/2\ C\ V_{BR}^2 \propto V_f^{1.57} \tag{2.12}$$

where

V_{BR} = voltage at breakdown

C = capacitance

Olsen and associates[39] also investigated the initial flame kernel growth of hydrogen-air and propane-air mixtures using the same equipment as in the preceding discussion. Their observations enabled them to determine the steady state flame velocity for hydrogen and

propane mixtures. In addition, they found, that for sparks which had less than the minimum amount of energy, the flame velocity approached zero in less than 200 microseconds while sparks having more than the minimum energy caused the flame velocity to approach the steady state value in approximately 900 microseconds.

Interesting results were obtained by Arnold and Sherburne[40] in their investigation of the initial flame kernel growth following ignition by a spark. The observations were made with a schlieren system by photographing the kernel at small time increments following the spark. They found that after a certain fixed time for a given fuel-air ratio that if the kernel had not reached a "critical" radius, the flame would extinguish as it progressed further downstream. Also, the critical radius decreases to a minimum andthen rises again (i.e., U shaped curve) as the equivalence ratio is increased. The minima of these curves agree very well with those published by Lewis and von Elbe[20,21] for minimum ignition energy as a function of equivalence ratio.

Schlieren photographs were used by Kumagai et al.[41] to observe the effect that ultrasonic waves have upon spark ignition and flame propagation. A flame front assumes a ragged form when exposed to ultrasonic waves. It is felt that this is due to acceleration of the flame. The major effect was considered to be promotion of heat transfer and diffusion of active particles from the burned to the unburned mixture. The waves had no observable effect on the spark ignition. This suggested that the agitating action of the spark was similar to that resulting from ultrasonic waves.

The effect of the molecular structure of hydrocarbons on spark ignition was examined by Calcote, Gregory, Barnett and Gilmer.[42] They used a constant volume bomb for their studies and ignited the mixture with pure capacitance sparks. The results indicated that knowledge of the structural configuration of the fuel could enable one to predict the effect of a change in fuel on minimum ignition energy.

Metzler[43] measured the minimum spark ignition energies of 12 pure hydrocarbon fuels at reduced pressure and extrapolated the data back to one atmosphere. He ignited the fuels with long duration capacitance sparks. All paraffins and cycloparaffins including the branched members had essentially the same minimum spark-ignition energies. The equivalence ratio at which the minimum spark ignition energy occurred was established by the length of the carbon chain and was relatively insensitive to pressure. He found that the minimum energy was approximately proportional to the inverse of the pressure to the 1.82 power for most fuels and the flame velocity was inversely proportional to the minimum energy to the 0.8 power. And finally, the minimum ignition energy was related to the quenching distance by the following expression.

$$E_{MIN} = 6.36\, d_q^{1.79} \tag{2.13}$$

King and Calcote[44] reported the effect of initial temperature on the minimum spark ignition energy using capacitive sparks. They found that the log of the energy was proportional to the inverse of temperature above -30°C as the initial temperature was increased. Also, the minimum ignition energy shifted to leaner mixtures.

The effects of radiation at the point of ignition of constant volume combustion were studied by Harnsberger and Van Wylen.[45] Results indicated that the breakdown voltages of the spark gap were reduced by approximately one-half by the presence of a 1.6 curie radiation source at pressures below 60 inches of mercury absolute. Also, the ignition energy requirement can be reduced 30 to 50 percent by the presence of radiation at the ignition point if the electrode spacing is set at greater than the quench distance.

Further investigation of the influence of radiation upon constant volume combustion was carried out by Souka.[46] The results indicated that the so-called ignition delay period was unaffected by irradiating the spark gap with alpha radiation. However, a decrease in delay period occurred in the case of ethane. No discernable change was noted in the rate of pressure rise when the spark gap was irradiated. Ethane required less energy for ignition when the electrodes were irradiated but ethylene required more energy for ignition for wide gaps and no change was noted for narrow gaps when the electrodes were irradiated. Furthermore, the energy necessary for ignition of acetylene was increased by irradiation for narrow gaps and decreased for wider gaps.

J. S. Clarke[47] indicates that probably the most important property of the spark in an engine is the electrode gap. The electrode gap which is required for stable combustion at idle is larger than that required for combustion at half-load or higher. This is due to the quenching effect that the electrodes cause at the lower pressure

idle condition. He also points out that the way in which the spark energy is released in the gap has little effect on the ignition process in an engine. This manner of energy release refers to single or multiple sparks.

According to Morgan[15] the capacitive or high rate of energy component of the conventional ignition spark is the only part of the spark necessary for ignition. From a design standpoint, it would prove most fruitful to have a large secondary capacitance in the ignition coil. Miller[48] discusses in detail one limitation on the maximum secondary capacitance. For a given primary current, the peak secondary voltage is limited by secondary capacitance according to the following equation, if the energy losses in the secondary circuit can be neglected.

$$V_{2MAX} = I_o \sqrt{L_1/L_2} \tag{2.14}$$

where

L_1 = primary inductance

I_o = primary current before switch is opened.

This equation assumes that the primary current can be instantaneously stopped when the switch is opened. Thus, if C_2 is large enough, the maximum secondary voltage can be limited to a value smaller than the gap breakdown voltage V_{BR} and no spark will form.

A second design problem involves the erosion of the spark gap. The high rate of energy component of the spark is of a short duration, but the current can be very high. Obert[49] indicates that this high

current 20 to 200 amps is responsible for a large portion of the spark plug electrode erosion. The erosion can be reduced by reduction of the secondary capacitance and/or addition of a large resistance in series with the electrode gap.

The Ethyl Corporation conducted a series of studies[50,51,52,53] during the Second World War to evaluate the dependability and durability of aircraft ignition systems with emphasis on electrode wear.

In one study,[50] various high tension spark generators were evaluated with regard to electrode wear. The magneto systems which provided high energy release caused considerably more erosion than the conventional battery coil systems having equivalent secondary capacitances. Therefore, the conclusion was drawn that the high energy sparks caused more erosion. An auxiliary gap added to a system caused slightly more electrode wear.

Addition of 1000 ohms of series resistance to the secondary circuit reduced the electrode wear by 35 to 40 percent.[51] The report[51] indicates that the high intensity discharge of the secondary capacitance is the major cause of spark plug erosion. Further tests[52] indicated that an increase in the secondary capacitance from 50 picofarads (i.e., 10^{-12} farads) to 95 picofarads increased the electrode wear by 100 percent.

Another study[53] indicated that the electrode material affected the spark breakdown voltage in the engine. As the electrical resistivity of the center electrode materials increased, the breakdown voltages decreased. The breakdown voltages decreased as the thermal conductivity of the center electrodes decreased.

Allsop and Guenault[54] discuss the effect that inductance, voltage, frequency of the voltage, rate of separation of electrodes and

electrode material have upon ignition of combustible gas mixtures in relation to safety devices. They indicate some of the devides that may be used for prevention of explosions and describe their applicability.

Cipriani and Middleton[55] discuss the thermal, ionization and chain theories of spark ignition and their application to automotive ignition systems. They describe how an understanding of the theories lead to larger spark plug gaps so that leaner mixtures could be burned in the spark ignited engines.

III. THE MECHANISM OF SPARK BREAKDOWN

A. General

The electrical spark is defined by Loeb and Meek[56] as follows: "The spark is an unstable, irreversible and transient phenomenon sometimes marking the transition from one more or less stable condition of current between electrodes in a gas to another more stable one under imposed conditions." In this chapter a brief description is made of the fundamentals of the initial more or less stable conditions leading up to spark breakdown. In particular, a description of the pre-breakdown currents is essential for a thorough understanding of the spark breakdown mechanism.

B. Photoelectric Emission

Emission of an electron from the cathode in a spark system is most commonly due to the impingment of a light photon of sufficient energy upon the cathode surface. An electron can leave the surface of the cathode if:

$$h\nu \geq \phi_w \tag{3.1}$$

Electrons close to the surface which have their maximum energy directed normal to the surface leave the cathode at a substantial velocity when the quantum of light energy, $h\nu$ is larger than the work function, ϕ_w. These emitted electrons have a velocity given by Einstein's Photoelectric Law[57]

$$1/2\ mv^2 = h\nu - \phi_w \tag{3.2}$$

Actually, most of the electrons possess less energy than represented by Equation (3.2) because most of the electrons which escape have less than the maximum velocity perpendicular to the surface and also lose energy due to internal encounters other than the gross work function ϕ_w, so that:[58]

$$1/2\ mv^2 \leqq h\nu - \phi_w \tag{3.3}$$

The intensity of the incident light which is related to the number of photons does not affect the energy distribution of the escaping electrons, but the number of electrons ejected from the cathode per unit time is directly proportional to the light intensity.[59]

C. Townsend Theory

Consider two electrodes connected to a variable D.C. voltage supply with an electrometer in series to measure the low pre-breakdown currents as shown in Figure 3.1. Current is initiated when an electron leaves the cathode and progresses to the anode under the influence of the applied voltage.

Each electron emitted by the cathode undergoes an acceleration due to the externally applied voltage. During acceleration, the electron soon collides with a gas molecule. In most cases, this collision is elastic if the collision occurs in the region near the cathode surface where the kinetic energy of the electron is still low. Since the mean free path of an electron between collisions in air at one atmosphere is 5×10^{-5} centimeters,[60] an electron will make 3×10^{5} collisions/cm of

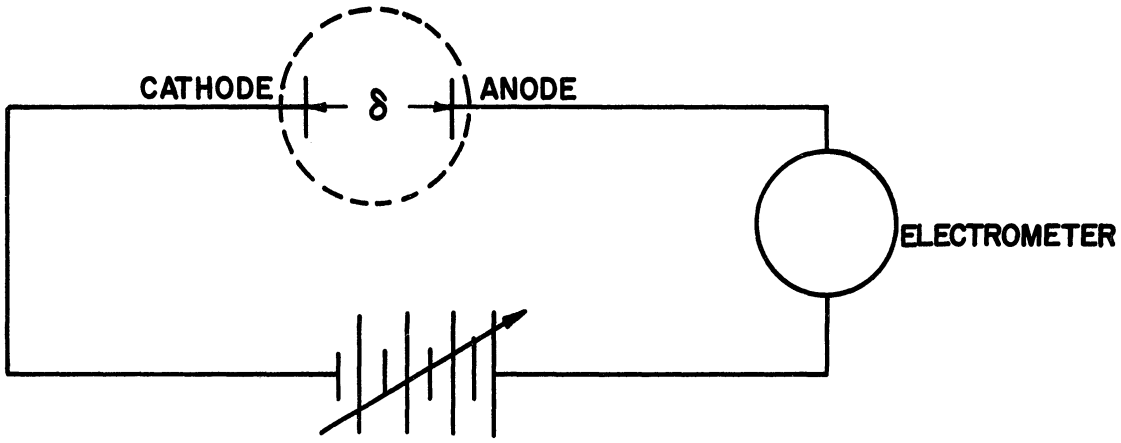

Figure 3.1. Circuit for Measurement of Pre-Breakdown Currents.

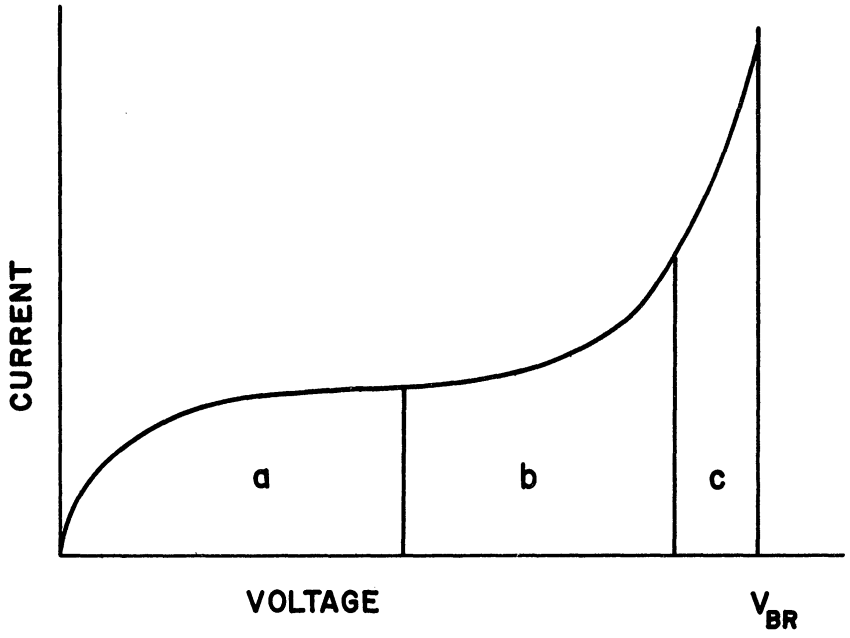

Figure 3.2. Pre-Breakdown Current-Voltage Characteristics.

electrode gap, and the net drift velocity just after ejection from the cathode is about one tenth of the random velocity.[60] As a result, most of the emitted electrons suffer collisions which return them to the cathode if the applied voltage is low. This is called "back diffusion." Higher voltages result in electron diffusion to the anode. Electrons which reach the anode are measured as current by the external electrometer shown in Figure 3.1. The current is shown as a function of the applied voltage in Figure 3.2.[61,62] At very low voltages, most of the emitted electrons back diffuse with a resultant low current as shown at the left of region a , of Figure 3.2. An increase in the field strength causes more and more electrons to diffuse to the anode until the saturation current is reached which is equal to the photocurrent, i_o . The magnitude of the saturation current is dependent upon the light intensity of impinging light.

Further increase of the external voltage causes a rise in current above the photocurrent, i_o . Therefore, electrons are being generated in the gas by some other mechanism. The phenomenon is due to inelastic collisions between the electrons and gas molecules, with resultant ionization of some molecules of the gas. This increased current, region b of Figure 3.2 is expressed by the following equation which was originated by Townsend,[59,60,61,63]

$$i = i_o e^{\alpha\delta} \quad * \tag{3.4}$$

---

* Derivation of this equation may be found in Appendix A.

α is the first Townsend coefficient and is defined as the number of electrons produced by ionizing collision in the path of a single electron traveling a distance of one centimeter.[59,60,61,63] Equation (3.4) indicates that $e^{\alpha\delta} - 1$ new electrons reach the anode for each electron emitted by the cathode. This phenomenon is known as an "electron avalanche" and as "gas amplification" in electron tube parlance. Since the photo-current is increased tremendously by the increased field strength, the ionization is sometimes called, field-intensified ionization.

Townsend showed experimentally that the first ionization coefficient α, is proportional to the gas density ρ and the field strength X [59] in the following manner.

$$\alpha = \rho f \left(\frac{X}{\rho}\right) \tag{3.5}$$

In addition, his experiments indicated that if the external voltage is raised beyond that of region b, the current increased still more than that represented by Equation (3.4). He concluded that a secondary mechanism was the cause. Townsend felt that the secondary electrons were liberated by positive ion bombardment of the cathode and by collision between positive ions and gas molecules. For secondary emission of electrons due to ionization of gas molecules by positive ions, Townsend developed the following equation.[63]

$$i = i_o \frac{(\alpha-\beta)\, e^{(\alpha-\beta)\delta}}{\alpha - \beta\, e^{(\alpha-\beta)\delta}} \quad * \tag{3.6}$$

β is the second Townsend coefficient and it is related to the gas density and field strength according to the equation[62]

---

* Derivation of this equation is left for Appendix A.

$$\beta = \rho g \left(\frac{X}{\rho}\right) \tag{3.7}$$

Under most conditions, the probability is very small that a positive ion will obtain enough energy to ionize a gas molecule.[64]

An equation similar in form to Equation (3.6) can be derived from secondary emission at the cathode due to positive ion bombardment.[63]

$$i = i_o \frac{e^{\alpha\delta}}{1 - \gamma\,(e^{\alpha\delta} - 1)} \quad * \tag{3.8}$$

if α is substituted for $(\alpha-\beta)$ and γ for $\beta/(\alpha-\beta)$ in Equation (3.6), the Equations (3.6) and (3.8) would be identical

More recently, physicists have stated that a third possible process of secondary emission of electrons from the cathode is due to photon impact from excited gas atoms and is expressed as follows:[64,65]

$$i = i_o \frac{(\alpha-\mu)\, e^{\alpha\delta}}{(\alpha-\mu) - \Theta\eta g\, e^{(\alpha-\mu)\delta}} \quad * \tag{3.9}$$

where Θ is the number of photons produced by an electron per centimeter of gap, η is the fraction of the photons which produce electrons at the cathode capable of leaving the surface, g is the geometric factor which represents the percentage of photons that reach the cathode, μ is the average absorption coefficient of the gas molecules for photons. Equation (3.9) resembles Equations (3.6) and (3.8) and since the net effect of the processes are indistinguishable, it is common to express the secondary ionization effects by the coefficient, γ . Probably both positive ions and photons cause emission at the cathode. Therefore,

---

* Derivation of this equation is left for Appendix A.

Equation (3.8) is useful for determination of breakdown voltages under steady state conditions.

Wheatcroft[59] defines electrical breakdown as the point of transition of the gas from insulator to conductor. This causes an abrupt increase in the current. In Figure 3.5 $di/dV = \infty$ at the end of region c where breakdown occurs. In reality the current is finite and limited to a maximum value by the external circuit parameters. From Equation (3.8) the Townsend criterion for spark breakdown at the end of region c is:

$$\gamma(e^{\alpha\delta} - 1) = 1 \qquad (3.10)$$

so that i approaches infinity.

γ , is the number of secondary electrons generated per primary electron causing an avalanche in the gap. Since $(e^{\alpha\delta} - 1)$, represents the number of electrons formed in the gap by each electron ejected from the cathode, the Townsend criterion of breakdown guarantees that the discharge is self-sustaining.

Equation (3.8) indicates that breakdown is dependent upon α , γ , the type of gas and upon the cathode material (i.e., indirectly through γ), while α and γ are both proportional to the ratio of field strength to gas density.

D. Streamer Theory

In 1940 Meek[66] and Raether[67] independently proposed the streamer theory of spark breakdown. This theory was developed to account for inadequacies in the Townsend mechanism at atmospheric pressure and

above. One major problem encountered with the Townsend theory was that time for formation of an avalanche at higher pressures is shorter than the corresponding time it would take for a positive ion to progress across the gap and cause secondary ionization at the cathode. Experimental observations of long sparks indicated a need for a new theory of spark breakdown.

Consider an external voltage V applied across the electrodes of Figure 3.1, such that the field strength X is high enough to cause an avalanche which extends to a distance x, across the gap. Electrons travel on the order of 2×10^7 cm/sec as compared to 2×10^5 cm/sec for positive ions.[61] Therefore, the positive ions are essentially stationary with regard to the electrons, and the electrons leave a positive space charge behind as illustrated in Figure 3.3 This space charge distorts the field to which the electrons at the head of the avalanche are subjected. The distortion of the field is the greatest at the head of the avalanche where the ion density is the highest. The conical space charge due to this avalanche induces a radial component X_r to the overall field which enhances the external field X. The electrons at the head of the avalanche move into the anode when the avalanche has crossed the gap. Then the positive space charge is extremely high at the anode and decreased toward the cathode as shown in Figure 3.4a. Photons are produced in the region surrounding the avalanche by the recombination of ions and electrons and by decay of electronically excited molecules. It is assumed that these photons ionize the gas. The resultant electrons initiate secondary avalanches which are directed toward the anode base of

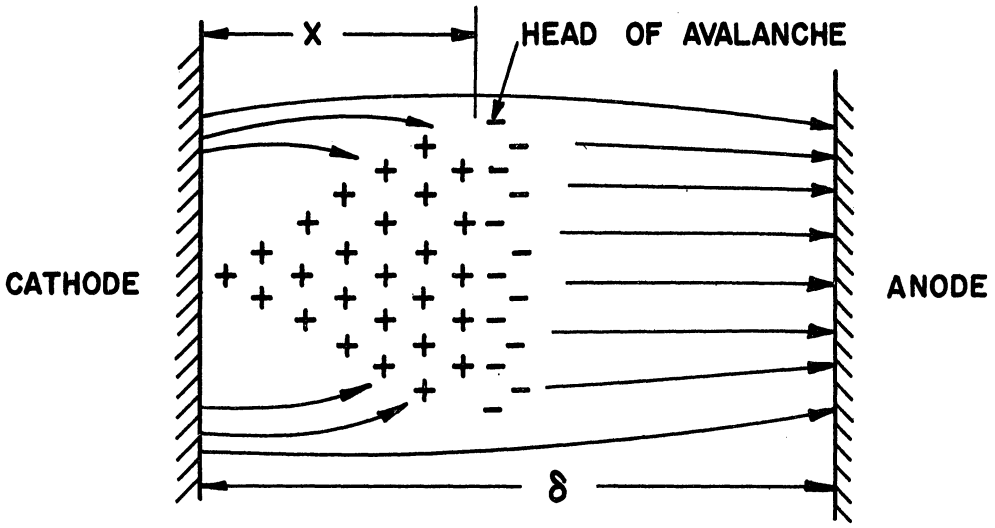

Figure 3.3. Electron Avalanche.

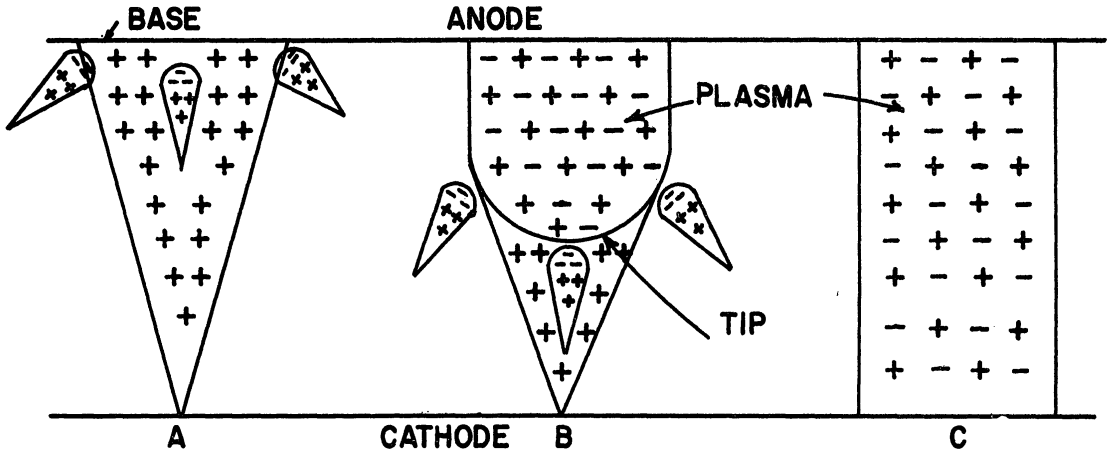

Figure 3.4. Formation of a Streamer.

the main avalanche is the space-charge field X_r , is of the same order as the external field X . The greatest number of seconsary avalanches feed electrons and positive ions into the head of the main avalanche. A conducting plasma is thus formed as shown in Figure 3.4b, and this plasma effectively reduces the gap length. The positive ions behind the auxiliary avalanches intensify the field at the tip of the plasma. Therefore the plasma, which is called a streamer, moves toward the cathode at an accelerating rate until it reaches the cathode. Whereupon, the gap is bridged by a conducting plasma which is the initial spark channel through which the external circuit energy is discharged.

The streamer breakdown criterion as stated by Devins and Sharbaugh[60] is: "When enough positive ion space charge is generated at the original avalanche head so as to cause a space charge field of the same order as the applied field, then the streamer breakdown will occur."

In other words, breakdown occurs when X_r is equal to X .

If the applied external voltage is larger than the minimum breakdown voltage, the main avalanche may form a space charge field as large as the external field before the avalanche traverses the gap. Under these conditions mig-gap streamers have been observed to form.

Devins and Sharbaugh[60] indicate that the Townsend mechanism of breakdown sets the low breakdown limit up to one atmosphere and at electrode spacings of one centimeter or less. However, the streamer theory is applicable for high pressures and larger gaps. Also, the streamer theory seems applicable for overvoltaged gaps at one atmosphere.

E. Paschen's Law and Similitude

In 1889 Paschen introduced an expression for electrical breakdown which has since been used very extensively. Paschen's Law states that in a uniform field the breakdown voltage of a gas depends only upon the product of the gas pressure and the electrode spacing. If temperature variations are considered, the breakdown voltage is dependent upon the product of gas density and spacing.

The Townsend theory of spark breakdown established an explanation for the experimental observations of Paschen. The Townsend coefficient, γ can be expressed by the following equation:[61]

$$\gamma = f\left(\frac{X}{\rho}\right) \tag{3.11}$$

Substitution of Equations (3.11) and (3.5) into Equation (3.10) the criterion for Townsend breakdown gives:

$$f\left(\frac{X}{\rho}\right)\left[e^{\rho f\left(\frac{X}{\rho}\right)\delta} - 1\right] = 1 \tag{3.12}$$

Since the breakdown voltage V_{BR} is equal to $X\delta$, Equation (3.12) is expressed as follows:

$$f\left(\frac{V_{BR}}{\rho\delta}\right)\left[e^{\rho\delta f\left(\frac{V_{BR}}{\rho\delta}\right)} - 1\right] = 1 \tag{3.13}$$

The variables of the equation are only V_{BR} and $\rho\delta$, and explicit solution for V_{BR} would be:

$$V_{BR} = \psi(\rho\delta) \tag{3.14}$$

which is a mathematical expression of Paschen's Law.

Paschen Law is a particular case of the Similarity Principle. The Principle of Similarity states that if the voltage applied to two different sets of electrodes is the same, the current flow between the electrodes each set will be the same when the gas density is multiplied by a factor K and all linear dimensions are divided by K. Take two plane-parallel plates in a uniform field and increase the gas denisty by K and divide the linear dimensions by K.

$$\rho_2 = K\rho_1 \qquad \text{and} \qquad \delta_2 = \frac{\delta_1}{K} \tag{3.15}$$

$$X_2 = K X_1 \tag{3.16}$$

Substituting Equations (3.15) and (3.16) into Equation (3.5) for the first Townsens coefficient and Equation (3.11) for the γ coefficient yields:

$$\frac{\alpha_2}{\rho_2} = f\left(\frac{X_2}{\rho_2}\right) = f\left(\frac{KX_1}{K\rho_1}\right) = \frac{\alpha_1}{\rho_1}$$

and

$$\alpha_2 = \frac{\rho_2}{\rho_1}\alpha_1 \tag{3.17}$$

or

$$\alpha_2 = K\alpha_1 \tag{3.18}$$

Also,

$$\gamma_2 = f\left(\frac{X_2}{\rho_2}\right) = f\left(\frac{X_1}{\rho_1}\right) = \gamma_1 \tag{3.19}$$

Finally, substitution of Equations (3.18) and (3.19) reduces Equation (3.8) to the following:

$$i_2 = i_o \frac{e^{\alpha_1 K \delta_2}}{1 - \gamma_1 \left(e^{\alpha_1 K \delta_2} - 1 \right)} \tag{3.20}$$

Recall that δ_2 is equal to $\frac{\delta_1}{K}$

$$i_2 = i_o \frac{e^{\alpha_1 \delta_1}}{1 - \gamma \left(e^{\alpha_1 \delta_1} - 1 \right)} \tag{3.21}$$

Therefore, the current i_2 will be the same for both systems and consequently the breakdown voltage will be the same. Equations (3.15) reduce to:

$$\rho_2 \delta_2 = \rho_1 \delta_1 \tag{3.22}$$

which is an expression of Paschen's Law.

F. Time Lags

The preceding discussion of conditions before breakdown dealt exclusively with a steady state mechanism. In practice, the time duration of the voltage application plays an important part in determination of the pre-breakdown current and breakdown voltage. A spark does not occur immediately upon application of a sufficiently large voltage to the electrodes. Therefore, there is a time lag before breakdown. This time delay may be divided into two periods: (1) statistical time lag is the time required for one or more electrons emitted by the cathode to acquire a favorable position in the gap for avalanche formation, (2) formative time lag is the time required to develop an avalanche which leads to Townsend breakdown or streamer formation. If the duration of the voltage

pulse is less than the time lag (i.e., statistical plus formative) breakdown may not occur even though the peak voltage is equal to the steady state breakdown voltage. This can be illustrated by Figure 3.5

The voltage drops below V_{BR} before the time lag has elapsed. Consider another voltage pulse that continues to rise at the same rate beyond V_{BR}, Figure 3.6. In this case breakdown will occur after the time lag and at the higher voltage V'_{BR}. Consequently, a fast rising voltage will result in a higher breakdown voltage for the same conditions. A recent paper by Eason[68] indicates that a faster voltage rise in an automotive ignition system improves the ability to fire fouled plugs. A disadvantage of such a system is the necessary increase in breakdown voltage due to the time lag. Fortunately, the time lags encountered in the conventional automotive ignition systems are short enough so that no major difficulty has been noted concerning increased breakdown voltages with decreased risetimes.

Examination of secondary voltage traces of an automotive spark indicates a wide variation in breakdown voltage from spark to spark. This variation appears to be statistical. It is just this variation which lead to the term statistical time lag. The statistical time lag may be controlled by control of the rate of electron emission by the cathode in the following ways.

1. Reduction in the work function of the cathode material, i.e., choice of cathode material, see Section A.
2. Irradiation of the cathode with ultraviolet light of high intensity, see Section A.
3. Irradiation of the gas by radioactive materials.

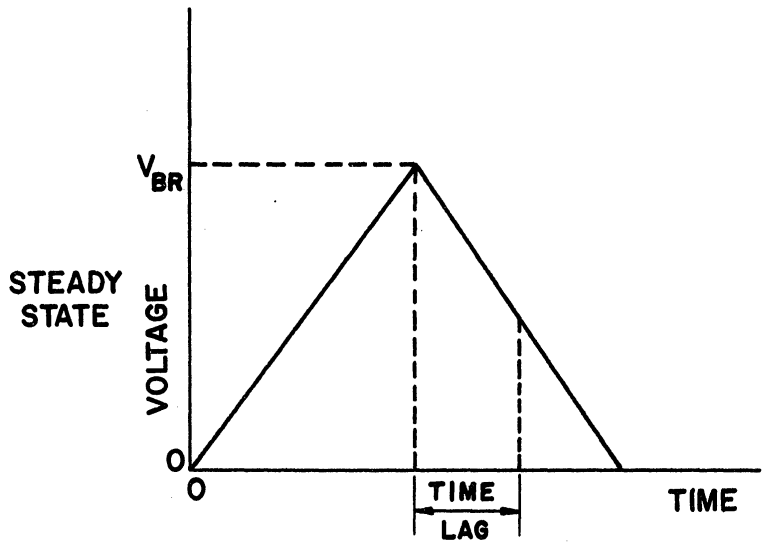

Figure 3.5. Effect of Time Lag Upon Breakdown.

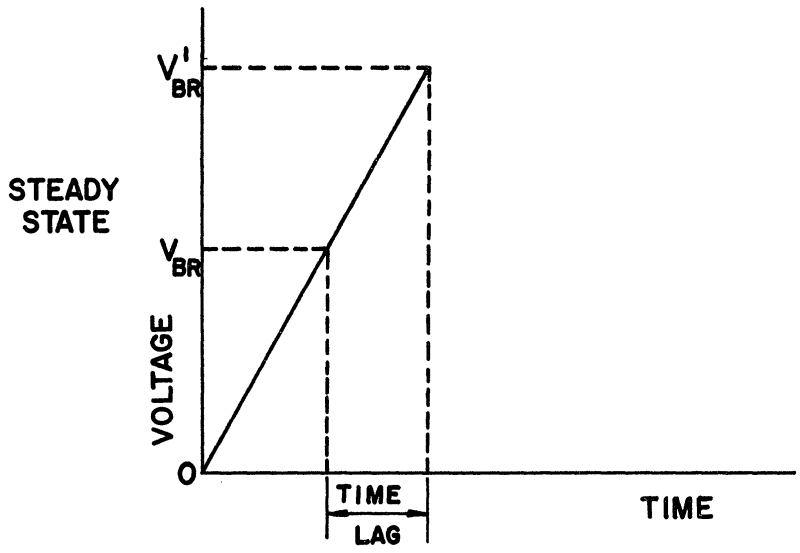

Figure 3.6. Increased Breakdown Voltage Due to Time Lag.

If the cathode is irradiated by ultraviolet light of sufficient energy and intensity, the statistical time lag can be reduced so that the major portion of the time lag is due to the formative lag. This technique is used to separate and measure the time lags. Time lags have been measured that range from less than one microsecond up to 560 microseconds.

Irradiation of the gap by a radioactive source emitting for instance alpha particles has been used to reduce the time lag. Alpha particles cause ionization of the gas molecules as opposed to emission of electrons by the cathode.

The use of both light and particle radiation are impractical in the automotive ignition system. However, their use is a helpful tool in laboratory studies of spark phenomena.

IV. SURVEY OF IGNITION THEORIES

A. General

An analysis of the spark ignition process which includes all of the phenomena involved has not been reported in the literature. The ignition process is a combined problem of ionization, diffusion of active particles, chemical reaction, surface quenching and heat transfer. Thus, an analysis must be a simplification of the problem in order to reduce the basic differential equations to a solvable form.

B. Thermal Theory

In 1920 Wheeler[3] first advocated the thermal theory which he stated as follows, "Ignition depends on the heating of a sufficient volume of the gas to a sufficient temperature." Later Taylor-Jones[5] et al. obtained solutions of the transient heat conduction equation in spherical coordinates. Their results indicated that if the source of energy is strictly thermal, the effectiveness of a given quantity of energy for ignition depends on the manner in which the energy is transferred to the mixture. If a quantity of energy is transferred instantaneously to a given volume of gas, the maximum temperature which the volume attains is higher than if the same quantity of energy is transferred over a finite time allowing heat loss to occur to the surroundings. It follows that the maximum temperature to which a large volume of gas can be raised by an instantaneous energy source is lower than if the same energy were transferred instantaneously to a smaller volume. Thus, it is concluded that an instantaneous point source of energy is the most effective for ignition.

C. Semenov's Self-Ignition Theory

Semenov[69,70] developed an expression for the condition which is required for self ignition to take place in a fuel-air mixture. According to the following procedure he equates the rate of heat generation due to chemical reaction with the rate of heat loss. It is known that a combustible mixture reacts at a slow rate as the temperature increases until a certain ignition temperature is obtained. Then the reaction becomes self-sustaining. The energy liberated by the chemical reaction is expressed as follows*

$$q_I = A_r \cdot V \cdot U_{RP} \cdot a^n e^{-\frac{E_a}{RT}} \qquad (4.1)$$

where

A_r = constant

V = volume of the reacting vessel, cm^3

U_{RP} = heat of reaction per molecule, cal./molecule

a = concentration of reactant, $\frac{\text{number of molecules}}{cm^3}$

n = order of the reaction

E_q = arrhenius activation energy, cal./mole.

R = gas constant, 1.986 cal./mole °K

T = absolute temperature of mixture, °K

Heat is transferred from the gas mixture to the vessel walls (i.e., heat loss) according to the equation:

$$q_{II} = hA(T - T_w) \qquad (4.2)$$

---

* Discussion of the reaction rate, order of the reaction and activation energy may be found in References 71 and 72.

where

$\bar{h}$ = average convective heat transfer coefficient

A = vessel wall area

T_w = wall temperature

To illustrate the necessary conditions under which self-ignition ofa combustible mixture will occur according to Semenov, it is advantageous to consider the shape of the functions q_I and q_{II} with respect to the mixture temperature and their relationships to each other. Consider three different cases of heat liberation q_I as shown in Figure 4.1. Cases 1, 2, and 3 represent small, medium and large initial values of the concentration of the reactant a. The heat loss is represented by the straight line q_{II} in Figure 4.1. This is the case for one fixed wall temperature T_w. In case 1, q_{II} is lower than q_I for mixture temperatures lower than T_a. Therefore, the temperature of the gas will rise to the temperature T_a where q_I and q_{II} intersect at point a and are equal. Beyond point a the heat loss to the walls q_{II} is greater than q_I and the reaction will cause a return of the mixture temperature to T_a. At point c, q_I and q_{II} again intersect. An unstable condition exists at this point. Below T_c, q_{II} is greater than q_I and the temperature will decrease to T_a. Above T_c, q_I is greater than q_{II} and a self-propagating reaction will occur. An external source of energy must be supplied if point c is to be reached. q_I is always larger than q_{II} for case 3 representing the highest concentration. Self-ignition will occur in this case. For the intermediate concentration, case 2, curves q_I and q_{II} intersect and are tangent at point b which corresponds to temperature T_b

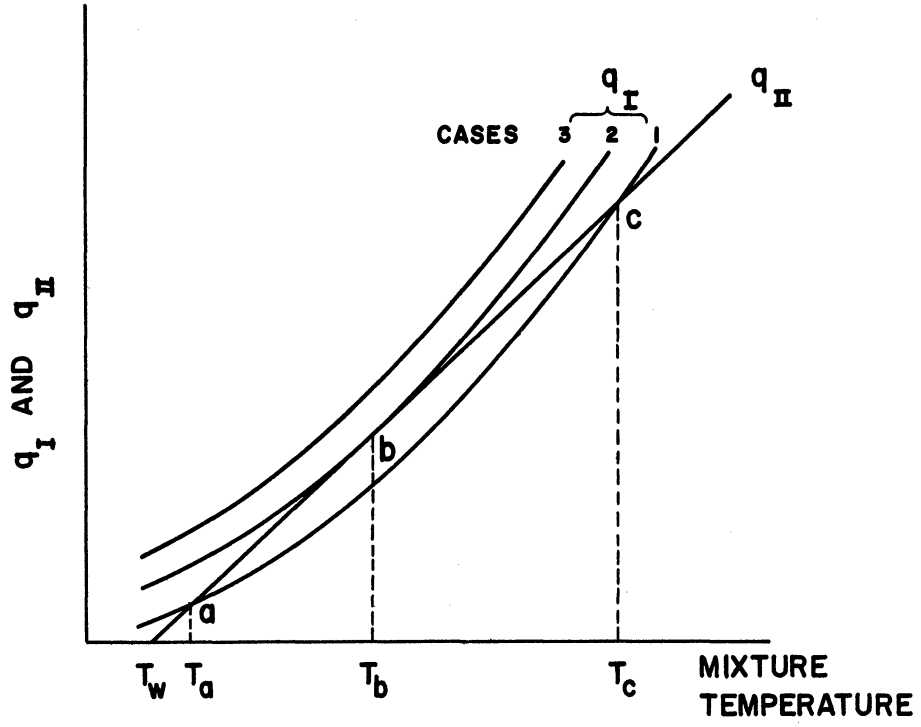

Figure 4.1. Effect of Initial Gas Concentration on Self-Ignition.

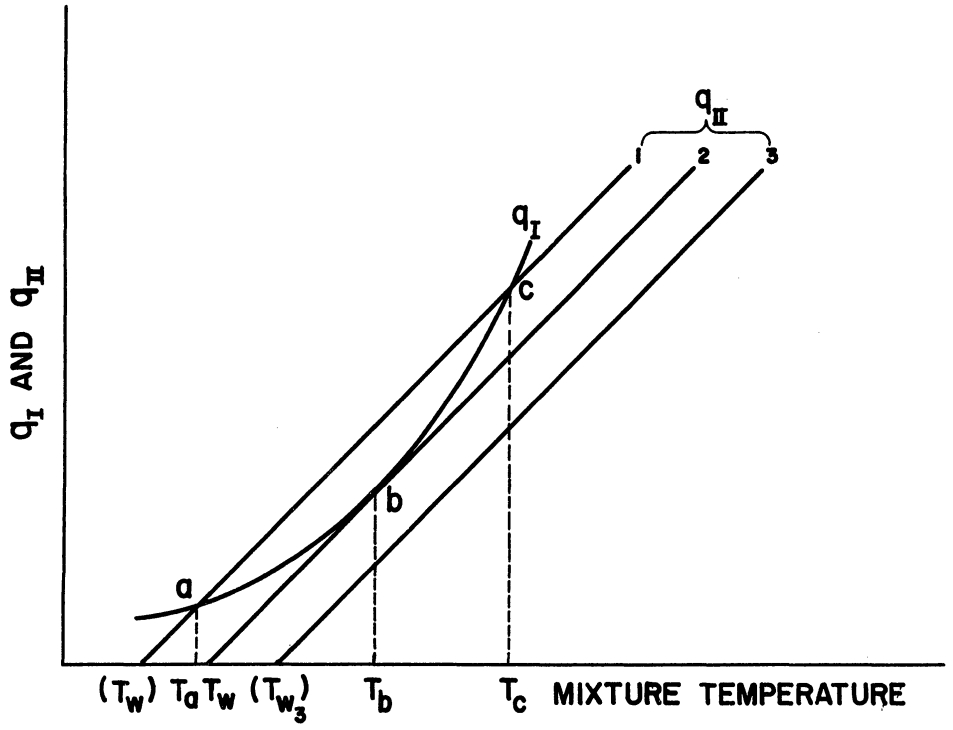

Figure 4.2. Effect of Wall Temperature on Self-Ignition.

This condition defined the critical concentration a for which self-ignition will occur with the given wall temperature T_w.

Figure 4.2 illustrates the effect that wall temperature has upon self-ignition for a single gas concentration. By the same reasoning as above, self-ignition will not occur for $(T_w)_1$ less than T_w whereas for $(T_w)_3$ greater than T_w, self-ignition will always occur. The condition at point b that q_I is tangent to q_{II} defines the ignition temperature T_b for the given reactant concentration.

At points b of Figures 4.1 and 4.2 the following conditions hold:

$$q_I = q_{II} \qquad \text{at} \qquad T = T_b \tag{4.3}$$

and

$$\left(\frac{dq_I}{dT}\right)_{T=T_b} = \left(\frac{dq_{II}}{dT}\right)_{T=T_b} \tag{4.4}$$

Substitution into Equations 4.3 and 4.4 and then solving simultaneously for T_b gives

$$T_b = \frac{1 \pm \sqrt{1 - \frac{4RT_w}{E_a}}}{2\frac{R}{E_a}} \tag{4.5}$$

The smaller root

$$T_b = \frac{1 - \sqrt{1 - \frac{4RT_w}{E_a}}}{2\frac{R}{E_a}} \tag{4.6}$$

is the solution for the ignition temperature.* Equation (4.6) can be expanded in a Maclaurin series and if all terms of higher order than $\frac{RT_w^2}{E_a}$ are neglected the following equation results

$$T_b - T_w = \frac{RT_w^2}{E_a} \tag{4.7}$$

For $(T_b - T_w)$ less than $\frac{RT_w^2}{E_a}$, self-ignition is impossible whereas for $(T_b - T_w)$ greater than $\frac{RT_w^2}{E_a}$ self-ignition would take place.

D. Fenn's Analysis

Fenn's[73] approach is similar to that of Semenov.[69] That is, he equates the heat generation to the heat loss. He assumes that the temperature of the small spherical volume of gas that surrounds the spark rises to a value such that the heat generation equals or exceeds the heat lost. This condition is analogous to point c of Figure 4.1. The minimum

---

* The larger root corresponds to the intersection of q_I and q_{II} at a point beyond the inflection point of q_I as shown below.

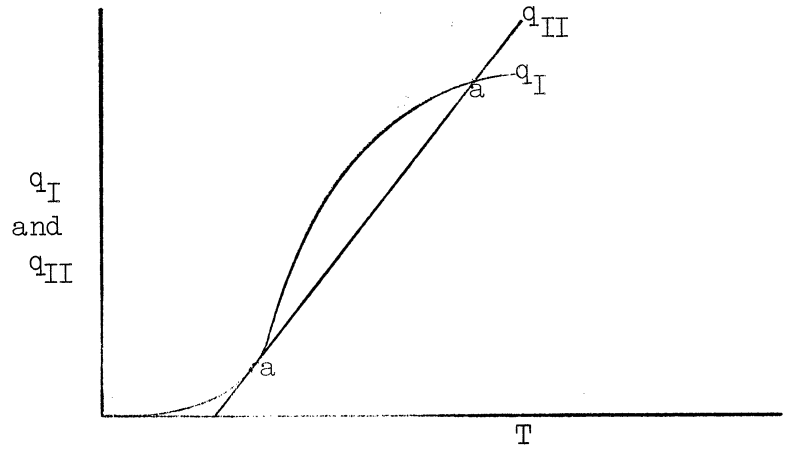

The larger root is therefore not considered because it yields an extremely high temperature.

energy necessary to raise the temperature of the volume of gas to the ignition temperature is related to the smallest self-propagating flame possible at the given initial conditions. By equating the heat loss to the heat generation in this small spherical volume, an expression for the radius of this smallest self-propagating flame can be found.

Heat generation = Heat loss

$$\frac{4}{3}\pi r^3 \left(A_r \bar{U}_{RP} N_f N_o \rho^2 e^{-\frac{E_a}{RT_f}} \right) = 4\pi r^2 K \left(\frac{T_f - T_u}{c \cdot r} \right) \qquad (4.8)$$

where

$\bar{U}_{RP}$ = heat of reaction, cal./mole of fuel

N_f = mole fraction of fuel

N_o = mole fraction of oxygen

A_r = constant

E_a = Arrhenius activation energy, cal./mole

R = gas constant, 1.986 cal./mole °K

T_f = adiabatic flame temperature, °K

T_u = temperature of unburned mixture

K = thermal conductivity, cal./cm °K second

ρ = gas density, gm/cm^3

c = constant

r = radius of the spherical flame volume

According to Fenn, the radius of the small flame volume or reaction zone should be inversely proportional to the square root of the reaction rate. This result is obtained by solving for r in Equation (4.8) showing that the use of r in the denominator of (4.8) is justified.

$$r = \sqrt{\frac{3K\,(T_f - T_u)}{cA_r\bar{U}_{RP}N_fN_o\rho^2 - e^{E_a/(RT_f)}}} \tag{4.9}$$

By assuming that $(T_f - T_u)$ is proportional to $N_f\bar{U}_{RP}$ Equation (4.9) reduces to the following where B is a constant into which all other constants from (4.9) are combined.

$$r = \sqrt{B(N_o\rho^2)^{-1}\, e^{E_a/RT_f}} \tag{4.10}$$

Once the initial composition and temperature are chosen T_f and therefore r become fixed.

The minimum ignition energy is calculated according to the following equation

$$E_{MIN} = D\,\frac{4}{3}\,\pi\, r^3 c_p \rho (T_f - T_u) \tag{4.11}$$

where

c_p = mean constant pressure specific heat

D = proportionality constant

Substitution of Equation (4.10) into Equation (4.11) gives an expression for the minimum ignition energy where σ_1 combines all of the constants.

$$E_{MIN} = \sigma_1 N_o^{-3/2} \rho^{-2} (T_f - T_u)\, e^{\frac{3E_a}{2RT_f}} \tag{4.12}$$

Swett[74,75] modified Fenn's analysis for use with line sources of ignition. In this case, the initial small value of gas surrounding the spark is assumed to be a cylinder of radius r and length d_q between the electrodes. The resulting equation is as follows for the same assumptions as made by Fenn

$$E_{MIN} = \sigma_2 N_o^{-1} d_q (T_f - T_u) e^{\frac{3E_a}{2RT_f}} \qquad (4.13)$$

where

σ_2 = constant

E. Excess Energy Theory[25]

Lewis and von Elbe define a quantity called "excess energy" which is equal to the minimum ignition energy. This excess energy is the same energy that is necessary to raise the temperature of the initial spherical volume surrounding the spark to a temperature such that a self-propagating reaction will occur. That is, the chemical heat generation in the small volume will equal or exceed the heat lost from the volume. Briefly, the solution involves an evaluation of the energy gain of a mass element of mixture by conduction from the hot gases preceding it as it progresses toward the flame. This same "excess energy" is lost by conduction to the cooler gases following the element as it moves out of the flame. The initial small flame receives this "excess energy" from the spark and it is equal to the minimum ignition energy. The reader is referred to the original work for a complete discussion. Their result is stated below,

$$E_{MIN} = 4\pi r_1^2 \frac{K_u}{S_u} \left(\frac{T_u}{T_a}\right)^{1/2} (T_f - T_u) \left(\frac{a_\infty}{a}\right)^2 \times \frac{1 + 1.3\, a\, r_1}{1 + a_\infty r_1 \left[1 - \left(\frac{3}{a r_1}\right)^{1/3}\right]} \qquad (4.14)$$

where

r_1 = initial self-propagating flame radius

$a = \frac{c_p \rho_u S_u}{K_u}$

a_∞ = value of a at r_1

c_p = constant pressure specific heat, cal/cm^3

ρ_u = density of the unburned gases, gm/cm^3

S_u = velocity of the unburned gases relative to the flame front

K_u = thermal conductivity of the unburned gases, $cal/cm°K\ sec.$

T_a = an average temperature between T_b and T_u

T_b = ignition temperature

T_u = temperature of the unburned gases

T_f = temperature of the burned gases.

F. Work of Yang

Yang[76] develops equations which predict the minimum ignition energy as a function of the time duration of the energy source. Three source configurations are considered. They are plane, line and point sources. He considers that a simple fuel plus oxidant reaction occurs at the surface of each source and then writes the time dependent energy and diffusion equations for a small volume element of the surrounding gas. He assumes that fresh mixture flows toward the source and thus places a mass sink at the source to exhaust the burned gases. Yangs equations for point and line sources are the more appropriate for spark ignition work and they are stated below.

$$E_{\substack{MIN \\ LINE}} = 16\, \rho_o c_v \left[\frac{U_{RP}\, G(1-a_o)}{16 A_r (a\rho_o)^n}\right]^{1/\Omega} \left(\frac{Kt_o}{\pi}\right)^{1 - 1/\Omega} \qquad (4.15)$$

$$E_{\substack{MIN \\ POINT}} = 64\rho_o c_v \left[\frac{U_{RP}G(1 - a_o)\ \Omega^{3/2}}{64\ A_r(a\rho_o)^n}\right]^{1/\Omega} \left(\frac{Kt_o}{\pi}\right)^{3/2(1-1/\Omega)} \quad (4.16)$$

where

δ = length of the line source

G = mass flow of the mixture toward the source of flame speed S times the density of the gas ρ, $\frac{gm}{cm^2 sec}$

a = concentration of the fuel

a_o = concentration of the fuel at the source

U_{RP}= heat of reaction, cal/gm

A_r = constant

ρ_o = density of the mixture at the source, $\frac{gm}{cm^3}$

K = thermal conductivity, $\frac{cal}{cm\ ^\circ K\ sec}$

n = order of the chemical reaction

t_o = time duration of the energy addition

Ω = constant

c_v = constant volume specific heat $\frac{cal}{gm}$

The corresponding source temperatures for the line and point sources are given as follows by Yang.

$$T_{\substack{S \\ LINE}} = \left[\frac{U_{RP}G(1-a_o)}{16\ A_r(a\rho_o)^n}\right]^{1/\Omega} \left(\frac{\Omega\pi}{Kt_o}\right)^{1/\Omega} \quad (4.17)$$

$$T_{\substack{S \\ POINT}} = \left[\frac{U_{RP}G(1-a_o)}{64\ A_r(a\rho_o)^n}\right]^{1/\Omega} \left(\frac{\Omega\pi}{Kt_o}\right)^{3/2\Omega} \quad (4.18)$$

G. Work of Mole[77]

Finch,[8,9] et al. stated the activation theory as, "The necessary prerequisite for ignition of an explosive gaseous mixture is the setting up of a sufficient concentration of suitably activated molecules". Mole assumes that the source of ignition introduces a number of active particles into the small volume of gas surrounding the source. Ignition results if this number of particles increases without limit. They multiply by chain branching and are lost by chain breaking reaction whereas effects due to temperature change are neglected. Mole considered a second order chain branching reaction to take place. The resulting equation for the rate of change of concentration of the active particles is

$$\frac{da}{dt} = \omega_1 + k_b a^2 - k_L a \tag{4.19}$$

where

a = concentration of active particles or chain carriers

ω_1 = rate of intiation of chain carriers due to ignition source

k_b = second order branching coefficient

k_L = first order breaking coefficient

Ignition occurs if the reaction continues when $\omega_1 = 0$. The solution of Equation (4.19) in this case is

$$a = \frac{k_L}{k_b}\left\{1 + \left[\frac{1}{(k_b/k_1)a_o} - 1\right] e^{k_L t}\right\} \tag{4.20}$$

For a_o less than $\frac{k_L}{k_b}$ the quantity inside the brackets is greater than one and the reaction becomes explosive. If a_o is greater than $\frac{k_L}{k_b}$, the reaction stops. Therefore a_o has a critical value defined by $\frac{k_L}{k_b}$.

H. Landau's[78] Work

A compromise between the Thermal Theory and the Chain Theory set down by Mole[77] is the theory of Landau. Landau assumes that the chemical processes surrounding the source are of a chain branching type and that an initial concentration of active particles is introduced into the small volume surrounding the ignition source. His criterion for ignition is that, "the temperature of the center of the sphere", surrounding the source, "shall never fall". He states and solves time dependent differential equations for the condentration of the particles and the temperature surrounding the source. By applying his criterion for ignition he obtains a relationship between the physical constants for which ignition can take place. His results are best illustrated by Figure 4.3. The quantities A and M are defined as follows:

$$A = \frac{4(T_f - T_u)K}{\dot{U}_{RP}\, a_o r_1^2} \tag{4.21}$$

$$M = k_b' \left(\frac{r_1}{2\sqrt{D}}\right)^2 \tag{4.22}$$

where

T_f = initial temperature inside the small sphere surround the ignition source, °K

T_u = temperature of the unburned mixture surrounding the sphere, °K

K = thermal conductivity, $\frac{\text{cal}}{\text{cm °K sec}}$

$\dot{U}_{RP}$ = the quantity of heat generated per unit time by each active particle, $\frac{\text{cal}}{\text{particle sec}}$

a_o = initial concentration of particles inside the sphere

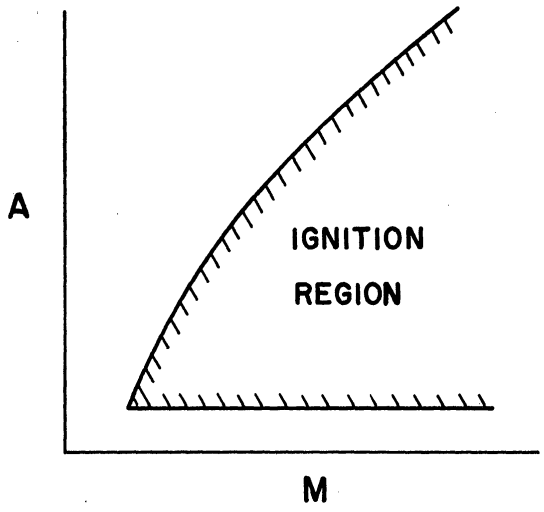

Figure 4.3. Criterion for Ignition.

r_1 = radius of the sphere

k'_b = first order branching coefficient

D = diffusion coefficient for active particles

According to Figure 4.3 Landau indicates that if A is of such a value dependent upon M that it lies inside the shaded area for Figure 4.3, ignition will occur.

I. Application to Present Investigation

The present investigation is primarily concerned with the rate at which the spark energy is discharged into the combustible mixture and the influence this rate has upon the minimum ignition energy. Semenov's[69] approach does not provide an analytical expression to evaluate the ignition energy. However, the conclusions drawn by Taylor-Jones[5] et al. do indicate that an instantaneous point source of ignition is the most effective means of igniting a combustible mixture. In other words, a pure capacitive discharge would be the most effective.

The analysis by Yang[76] is applicable to the present investigation. Equations (4.15) and (4.17) are repeated here for convenience. For Line Source:

$$E_{MINL} = 16\delta\rho_o c_v \left[\frac{U_{RP}\, G\, (1 - a_o)}{16\, A_r\, (a\rho_o)^n}\right]^{\frac{1}{\Omega}} \left(\frac{Kt_o}{\pi}\right)^{1 - \frac{1}{\Omega}} \tag{4.15}$$

$$T_{SL} = \left[\frac{U_{RP}\, G\, (1 - a_o)}{16\, A_r\, (a\rho_o)^n}\right]^{\frac{1}{\Omega}} \left(\frac{\Omega\pi}{Kt_o}\right)^{\frac{1}{\Omega}} \tag{4.17}$$

It would be advantageous to have an espression for E_{MINL} in terms of the source temperature since for a given t_o, E_{MIN} is a function of T_S.

Solving explicitly for t_o in Equation (4.17) and then substituting into Equation (4.15) gives an expression for E_{MINL} as a function of T_{SL}.

$$E_{MINL} = 16\delta\rho_o c_v \frac{U_{RP}\, G\, (1 - a_o)}{16\, A_r\, (a\rho_o)^n} \Omega^{1 - \frac{1}{\Omega}} T_{SL}^{1-\Omega} \tag{4.23}$$

By similar means Equations (4.16) and (4.18) for a point source can be reduced to the following.

$$E_{MINP} = 64\rho_o c_v \frac{U_{RP}\, G\, (1 - a_o)}{64\, A_r\, (a\rho_o)^n} \Omega\, T_{SP}^{1-\Omega} \tag{4.24}$$

For a given set of initial condition, (i.e, fuel, fuel-air ratio, pressure, temperature, electrode configuration and spark length δ or electrode spacing), all of the terms to the left of $T^{1-\Omega}$ in Equations (4.23) and (4.24) can be combined into constants, D_L and D_P. Therefore,

$$E_{MINL} = D_L \frac{1}{T_{SL}^{\Omega-1}} \tag{4.25}$$

$$E_{MINP} = D_P \frac{1}{T_{SP}^{\Omega-1}} \tag{4.26}$$

Yang[76] states that Ω is a constant used as a temperature exponent to approximate the reaction rate in the following manner

$$\omega = A_r' (a\rho_o)^n e^{-\frac{E_a}{RT}} \approx A_r (a\rho_o)^n T^{\Omega} \tag{4.27}$$

He indicates that Equation (4.27) is a good approximation over specific temperature ranges and that Ω is much larger than one. Reference will be made to these results in Chapter VII.

V. EXPERIMENTAL APPARATUS

A. Description of Equipment

Spark ignition of the combustible mixture occurred inside a stainless steel cylindrical constant volume bomb which is shown in Figures 5.2 and 5.3. The spark control panel and peripheral equipment are illustrated in Figure 5.1. The equipment consists of the following nine basic components.

1. Constant volume bomb
2. Bomb heater and cooler
3. Manifold system
4. Temperature measurement equipment
5. Bomb pressure transducer
6. Spark control circuit
7. Voltage and current measurement circuit
8. Photomultiplier circuit
9. Ultraviolet light source.

1. Constant Volume Bomb

The combustion chamber is fitted with two quartz windows, 5 inches in diameter and 1 inch thick for viewing the ignition and combustion processes. The inside diameter of the cylinder is 4 inches, and it is 1-1/4 inches in depth with an outside diameter of 6-1/2 inches. The cylinder and two heads are constructed of 316 stainless steel, and the bomb is mounted on an aluminum pedestal. Two stainless steel ball valves which are designed for high pressure and high vacuum operation were

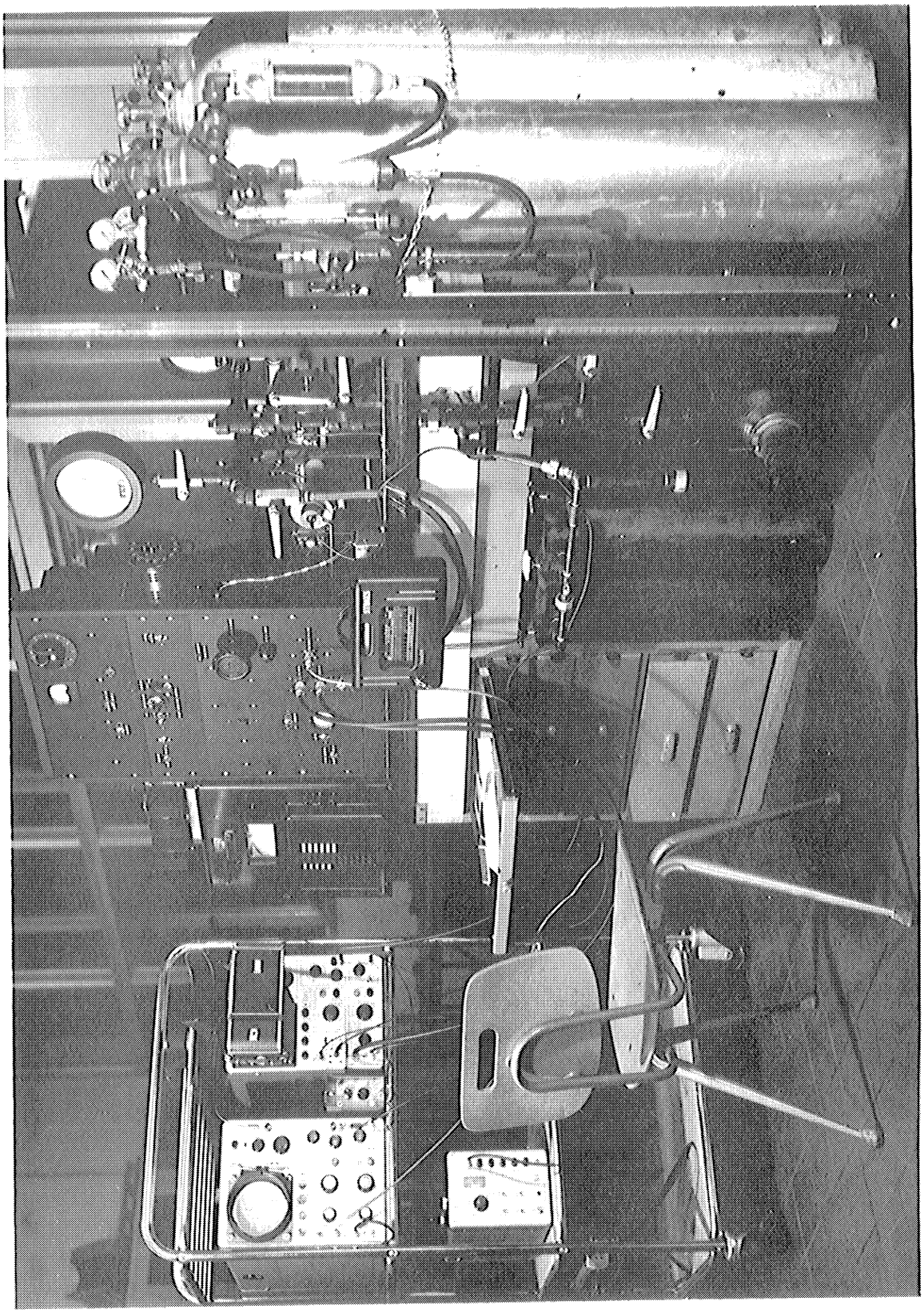

Figure 5.1. Control Panel and Associated Equipment.

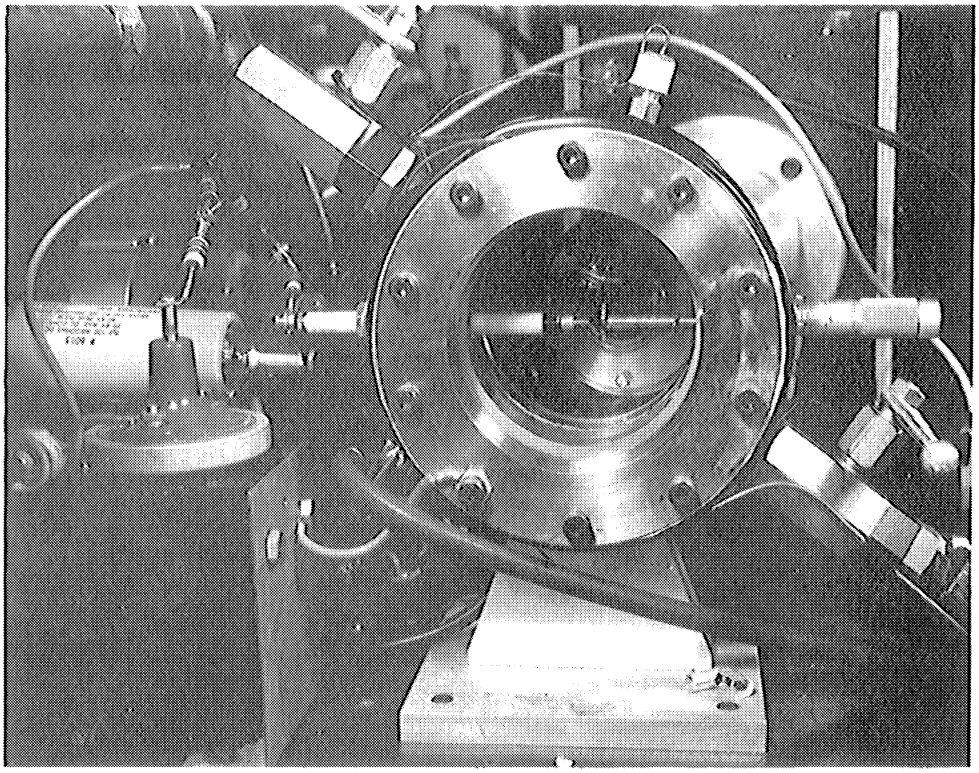

Figure 5.2. Constant Volume Bomb.

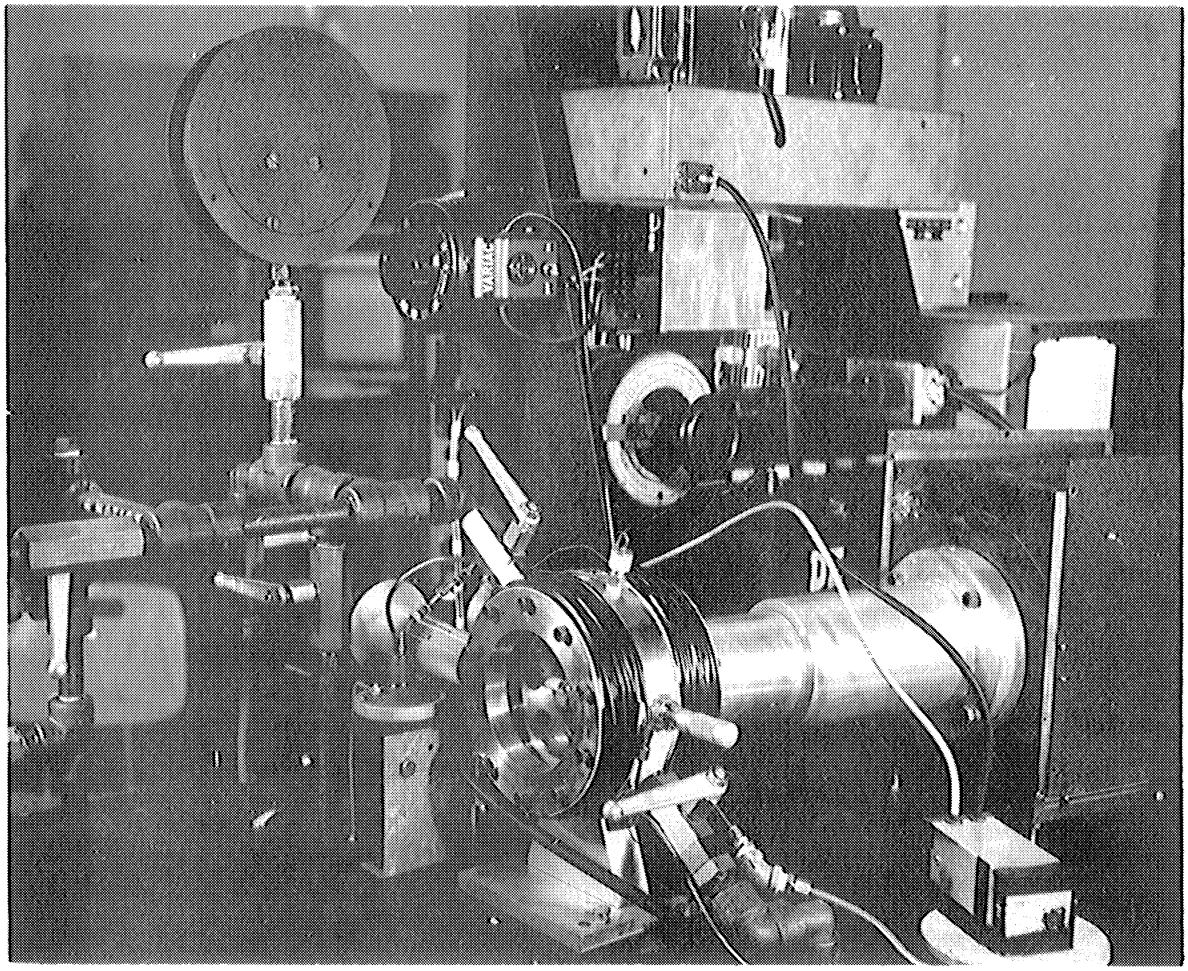

Figure 5.3. Bomb and Rear View of Control Panel.

used for charging and exhausting the bomb. Ten 5/16 - 20 NC high strength bolts fasten each head to the cylinder. A 1/8 inch thick, soft rubber gasket functions in much the same manner as an O-ring to seal the quartz windows against the cylinder. That is, the gasket is compressed to seal, but does not carry the full compressive load exerted by the ten headbolts.

Both electrode assemblies which are shown in Figure 5.2 are installed horizontally in the bomb. The assemblies may be easily removed to clean the electrodes and each electrode is replaceable. The three basic type electrodes used in this study are shown in Figure 5.4. The assemblies are sealed with teflon O-rings. The cathode which is located on the left side of the bomb shown in Figure 5.2, is electrically insulated by the long teflon sleeve. This cathode is the high voltage electrode. The adjustable electrode assembly on the right side of the bomb is the anode. It is equipped with a micrometer handle so that the electrode spacing can be accurately set.

A pressure transducer is attached to the bomb cylinder through a 14 mm threaded hole located in Figure 5.2 just below the cathode.

Temperatures of the combustible gases are measured by a thermocouple which is inserted from the top of the bomb as shown in Figures 5.2 and 5.3. The wires are sealed by a Conax high pressure connector.

2. Bomb Heater and Cooler

Initial temperature of the mixture before ignition is controlled manually by heating or cooling the outside bomb surface as required. Two hundred ohms of electrical heating element wire are wrapped around each head.

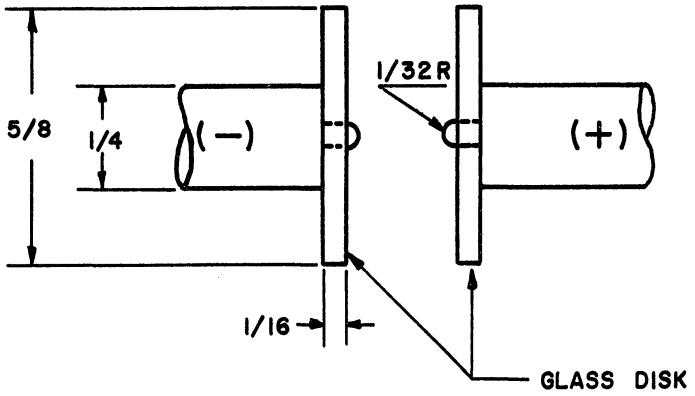

Type "A"; Cathode-Aluminum; Anode - 302 S. S.

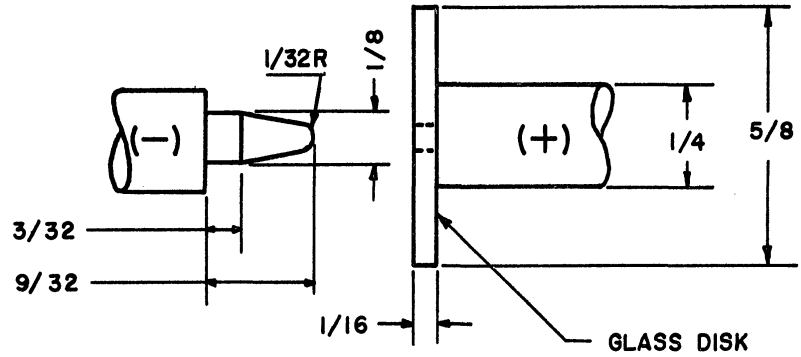

Type "B"; Cathode-Aluminum; Anode - 302 S. S.

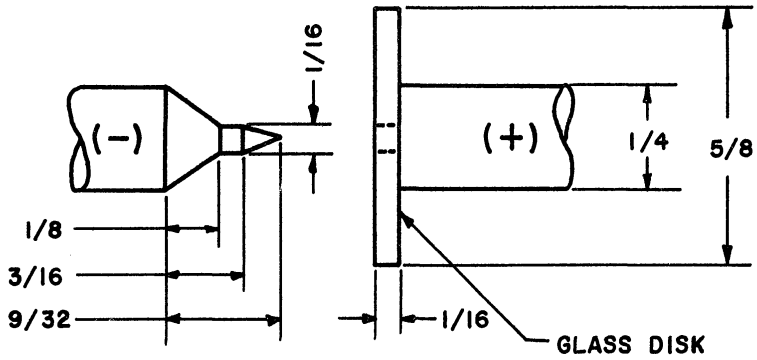

Type "C"; Cathode-Aluminum; Anode - 302 S. S.

Figure 5.4. Electrode Configurations.

High temperature electrical tape is used for insulation between the heating element wires. The heaters are connected in series with a variac to control the current, and thus the rate at which the bomb and gas are heated. Four turns of 1/8 inch copper tubing are wrapped around each head over the top of the heating element wire. This tubing carries tap water as a coolant.

3. Manifold System

The fuel-air mixtures were premixed in three small mixing tanks shown below the bench in Figure 5.1 and shown in the schematic diagram of Figure 5.5. Each tank is equipped with two valves, one valve is used to throttle the mixture is used in conjunction with the first when scavenging the tank before evacuation. This procedure is described in Chapter VI. Ball valves are used at all points where throttling is not required. Piping is schedule 80, 1/2 inch black iron pipe. This large diameter was chosen to reduce the evacuation time to a minimum. One Cenco vacuum pump is used. The system can be evacuated to less than 100 microns of mercury absolute with this pump. Small absolute pressure measurements are made with a McCleod gage having a scale of 0 to 5000 microns. Pressures from 0 to 67 inches of mercury absolute are measured with a mercury manometer which can be read to the nearest one-hundredth of an inch. Higher pressures are measured with either of two bourdon pressure gages. Figure 5.1 shows the location of the gages and the schematic in Figure 5.5 illustrates their location in the manifold system.

Both nitrogen and dry-air are passed through Drierite desiccant to assure a negligible content of moisture. The desiccant is contained in two 8 inch lengths of pipe of 1-1/2 and 2 inch diameters respectively.

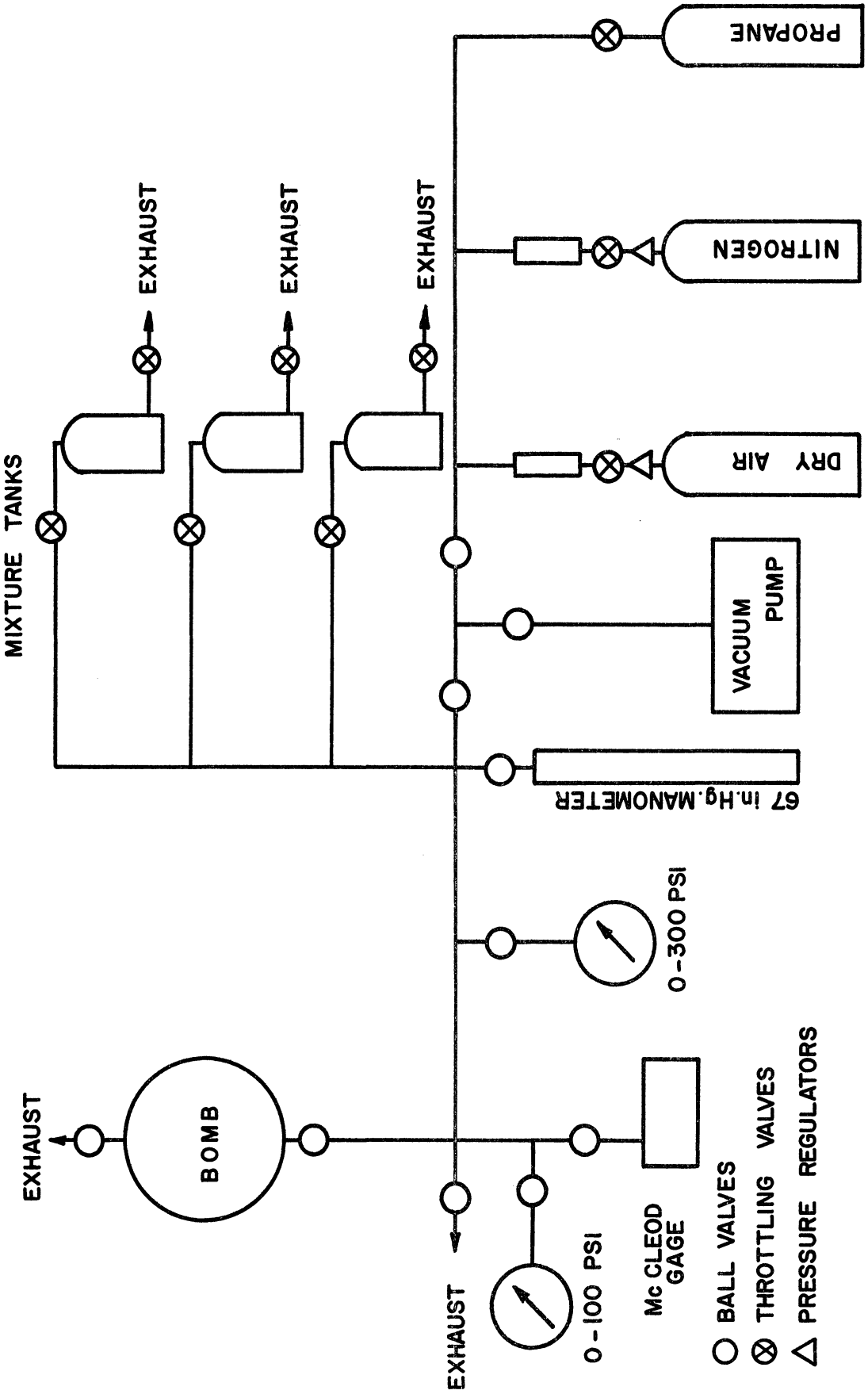

Figure 5.5. Manifold System.

The lengths of pipe are fitted with screens and reducing pipe couplings at each end. They are shown on the right hand side of Figure 5.1 in front of the gas cylinders. The nitrogen and dry-air size 1-A cylinders are equipped with pressure regulators shown in Figures 5.1 and 5.5.

4. Temperature Measurement Equipment

Iron-constantan thermocouples are used for all temperature measurements in conjunction with a Minneapolis Honeywell Brown model 156X63P24 continuous reading potentiometer. Temperatures of the combustible gas mixture inside the bomb are measured by a thermocouple constructed of 24 gauge wire. The length of wire exposed to the gas was looped once to increase the length of exposure and thus reduce the error due to conduction along the wire. This thermocouple is double radiation shielded according to the method described in Reference 79. The shield is shown protruding into the bomb from the top in Figure 5.2. Four thermocouple junctions were taped to the outside bomb surface on the top surface of each head and top and bottom of the cylinder. Top and bottom refer to the top and bottom of the bomb as it is shown installed in Figure 5.2.

Well-type thermocouples were used to determine the gas temperature inside the mixture tanks.

5. Bomb Pressure Transducer

Time dependent pressure indications were used to determine whether or not ignition occurs inside the bomb. A Kistler model 601 piezoelectric transducer is used in conjunction with a Kistler model 568 electrostatic charge amplifier. The amplified signal is displayed on a model 502 Tektronix

oscilloscope. In Figure 5.1, the charge amplifier is located between the two oscilloscopes. A water cooled adaptor was used to mount the pickup on the cylinder of the bomb.

6. Spark Control Circuit

It is desired to control the time duration of the spark discharge. The method chosen in this investigation is the method first used by Finch and Sutton.[17] They showed that the spark can be extinguished at a predetermined time during the discharge by turning the primary current on. Referring again to Figure 1.1, a spark is initiated when the primary current is turned off by opening switch S_1. By closing S_1 again during the discharge, the primary current is turned back on again. This causes the flux in the coil to change and reverse the voltage and extinguish the spark. Finch and Sutton used two switches connected in parallel where one is open while the other is closed. They were actuated by a cam as in a conventional distributor. Thus, the spark could be extinguished at set intervals of time after the spark was initiated.

The use of a switch or relay to turn on the primary current poses the difficult problem of switch bounce. Therefore, it was decided to use transistor switching in this investigation. Figure 5.6 shows the circuit used to control the spark duration. The system can also be used to produce a conventional spark of uncontrolled time duration. With switches S_6 and S_8 in positions 2, switch S_7 is used just as switch S_1 of Figure 1.1. The transistor network should be ignored for this description. Switch S_4 must be closed for either the conventional or for transistor operation. Closing switch S_{10} energizes relay

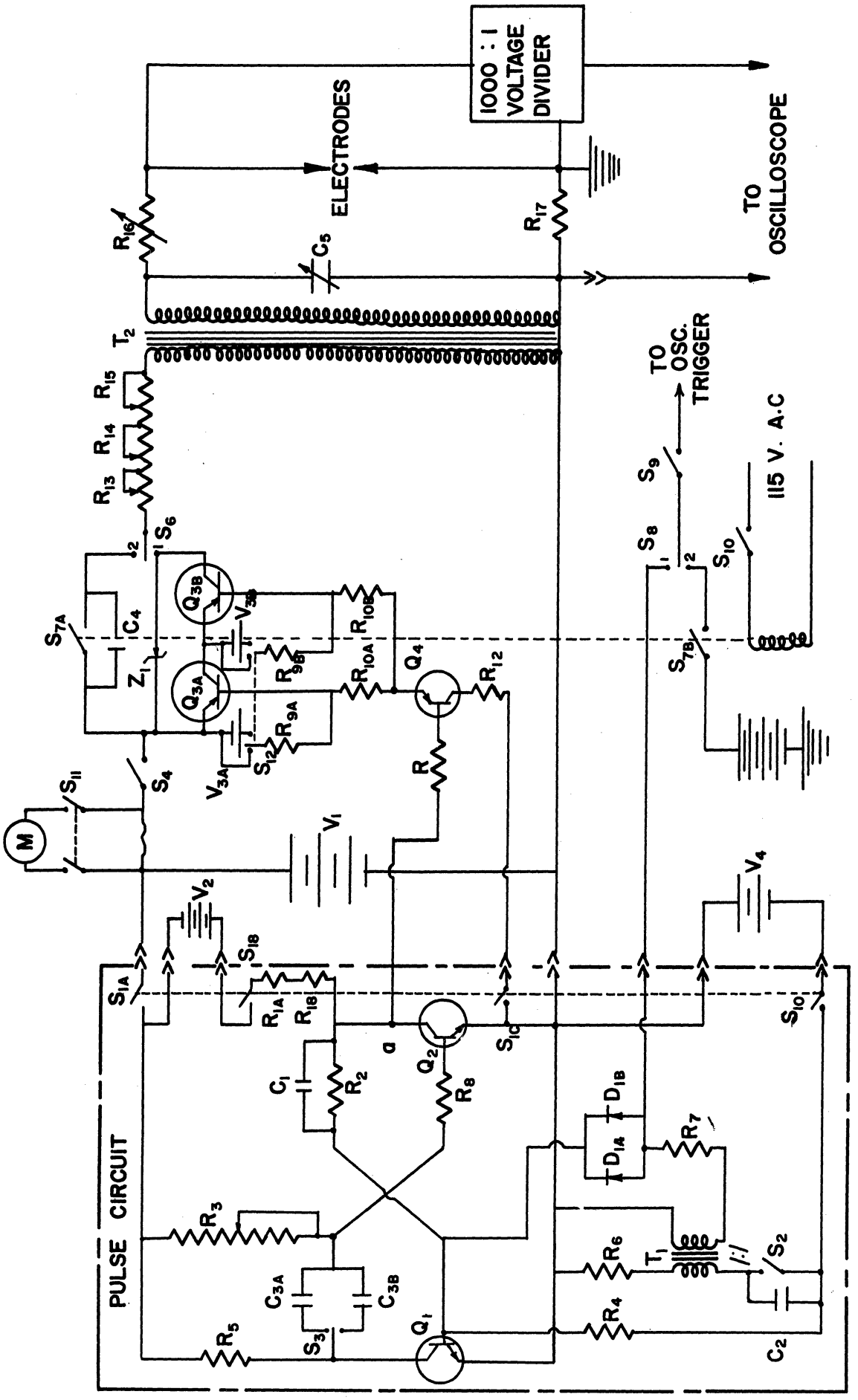

Figure 5.6. Spark Control Circuit.

switch S_7 and contacts S_{7A} and S_{7B} open. S_{7A} turns the primary current off and S_{7B} reduces the voltage at the oscilloscope trigger to zero and triggers the oscilloscope sweep mechanism to record the spark voltage and current. S_{7B} is adjusted so that is opens about 40 microseconds before S_{7A}. Voltage and current measurements are covered in the next section.

All of the minimum ignition energy data was obtained using the transistor switching circuitry. Switches S_6 and S_8 must be in position 1 for transistor operation. Transistors Q_{3A} and Q_{3B} functionally replace S_{7A}. These transistors turn the primary current on and off. The combined base currents of Q_{3A} and Q_{3B} are controlled by transistor Q_4. A monostable multivibrator circuit is used to control transistor Q_4. The reader is referred to References 80, 81, 82, and 83 for a thorough description of multivibrator circuits. Transformer T_1 and switch S_1 were added to the multivibrator circuit to provide a positive pulse to upset the stable operating point of the circuit as shown in Figure 5.6. The multivibrator and added transformer circuit is referred to as the pulse circuit in the figure.

Switch S_1 is normally in a closed position. Transistor Q_1 is negatively biased and thus turned off. Q_2 is based positive and operates in saturation. Point a is at the same voltage as the emitter of Q_2. Opening S_2 causes a flux change in T_1 which transmits a positive voltage pulse through diodes D_{1A} and D_{1B} to the base of Q_1 Q_1 begins to conduct and its decreasing collector voltage is transmitted through either capacitor C_{3A} or C_{3B} to the base of Q_2. Thus, the

collector current of Q_2 begins to decrease with resultant increase in the base voltage of Q_1. This process quickly drives transistor Q_1 into saturation and Q_2 to cutoff. The base of Q_2 is then at a negative voltage. Capacitor C_{3A} or C_{3B} then discharges through R_3. The time duration of the output voltage at point a is determined by the time constant of the C_3R_3 network. The waveshape at point a is shown in Figure 5.7.

Normally the waveshape at point a in a multivibrator circuit would be square as indicated in Figure 5.7 by the dashed lines. However, the resistor R_8 was added as shown in Figure 5.6 to obtain the waveshape indicated by the solid lines in Figure 5.7. This was necessary to decrease the rate at which Q_4 is switched on. This positive voltage at point a and the base of Q_4 maintains the transistor Q_4 off until the voltage at point a begins to decrease along the line 1-2 of Figure 5.7. This gradual decrease in voltage gradually turns transistor Q_4 on. Q_4, in turn, controls Q_{3A} and Q_{3B} which are turned back on at a slower rate than they were turned off by Q_4 during the initial rise in voltage at point a. The transistors Q_{3A} and Q_{3B} must turn the primary current on at a slower rate than they turn the current off to prevent a rapid change in flux in the ignition coil T2. A rapid change in flux causes the cathode to become positive and anode negative at such a rapid rate that a second spark is discharged in the gap. Zener protection of the transistors Q_{3A} and Q_{3B} follows one of the methods suggested by Larges[84] et al.

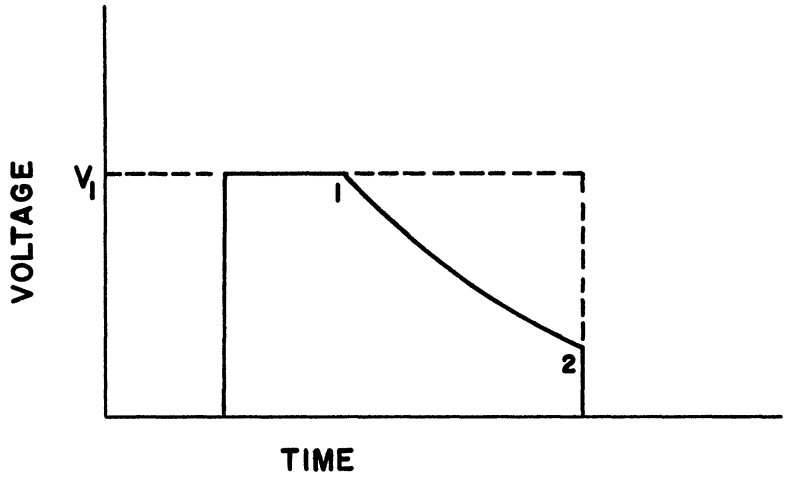

Figure 5.7. Waveshape at Point a in Figure 5.6.

Batteries V_{3A} and V_{3B} when connected in series with resistors R_{9A} and R_{9B} respectively through switch S_{12} . are used to drive the bases of Q_{3A} and Q_{3B} slightly positive when transistor Q_4 goes off. This positive voltage speeds up the cutoff of transistors Q_{3A} and Q_{3B} which results in a faster rate of voltage rise in the secondary circuit. At larger electrode spacings the breakdown voltage becomes very high. This breakdown voltage can be reduced slightly by switching the batteries out of the base circuits using switch S_{12} . The breakdown voltage is reduced because of the effect that the statistical time lag has upon breakdown as was discussed in Chapter III.

The ignition coils used in this investigation were a Mallory model F-12T coil and a special low capacitance coil made for this investigation by Delco-Remy Division of General Motors Corporation. The Mallory coil has a secondary capacitance of 52 picofarads. The Delco coil has a secondary capacitance of only 29 picofarads. Determination of the capacitance of these coils was carried out by a procedure outlined by Stout.(86) This method and the data for the measurements of the Delco and Mallory coils are found in Appendix B. The circuit and coils are equipped with plugs so that the coils can be interchanged as desired.

Total time duration $\Delta t_{BR} + \Delta t_{SP}$ of Figure 1.2 can be adjusted from 100 to 1500 microseconds with the circuit shown in conjunction with either the Mallory or Delco coil. The values of all the electrical components in Figure 5.6 are listed in Table IX, Appendix D.

Figure 5.12 shows the voltage and current traces for a series of sparks each having a different time duration.

7. Voltage and Current Measurement

The high voltages necessary to cause spark breakdown are too large to be measured directly by the oscilloscope. Consequently, a voltage divider is necessary to reduce this voltage to a value compatible with the type oscilloscope being used. Appendix C deals with the necessary design criterion for a voltage divider. A Tektronix P6015 high voltage probe was used in this investigation and is shown in Figure 5.2 connected to the cathode. It has an attenuation ratio of 1000 to 1 and can be used with peak voltages up to 40,000 volts.

Current measurement is accomplished by recording the voltage drop across the known resistor R_{17} in Figure 5.6.

The voltage and current signals are simultaneously fed to a dual beam model 502 Tektronix oscilloscope. The two traces are recorded using a Hewlett Packard Oscilloscope camera which is equipped with a Polaroid back. It is necessary to use ASA 3000 speed film to obtain good photographs of voltage and current as a function of time in the spark.

The oscilloscope is triggered by the same signal that initiates the operation of the multivibrator circuit.

8. Photomultiplier Circuit

The bomb was fitted with a 931-A photomultiplier tube to obtain a signal which was proportional to the light intensity of the spark. This was useful in the initial stage of the equipment development to correlate spark light output duration with the voltage and current traces. Also, the photomultiplier was used to examine the spark structure. Figure 5.8

shows the photomultiplier in position on the right side of the bomb. A typical trace which is proportional to the light intensity of the spark versus time is shown in Figure 5.10. The photomultiplier circuit diagram is shown in Figure 5.9. The circuit used by Saad[85] was modified as required for the present investigation.

9. Ultraviolet Light Source

Ultraviolet light is impinged upon the cathode to overcome the work function and reduce the statistical time lag for breakdown as described in Chapter III. A General Electric, 100 watt, H4AB lamp is used as the source for the ultraviolet light. The outer safety shell of the lamp is glass and it was removed to increase the intensity of the shorter wavelength light. The light is focused upon the cathode with a quartz lens. Figures 5.2 and 5.3 show the light system. The effect of the ultraviolet light in decreasing variations of the breakdown voltage is shown in Figure 5.11.

B. Calibration of Instruments

1. Oscilloscope Sweep Rate

The horizontal deflection system calibration is most important to the energy calculations since the energy is obtained by graphically integrating power as a function of time. An Erie model 400 counter-timer was checked against the National Bureau of Standards time signal broadcast over station WWV. The counter was setup to count its own crystal oscillator output for 5, 40, and 45 minute time intervals. Table X in Appendix D shows the calibration points taken. The maximum error was 0.04 percent.

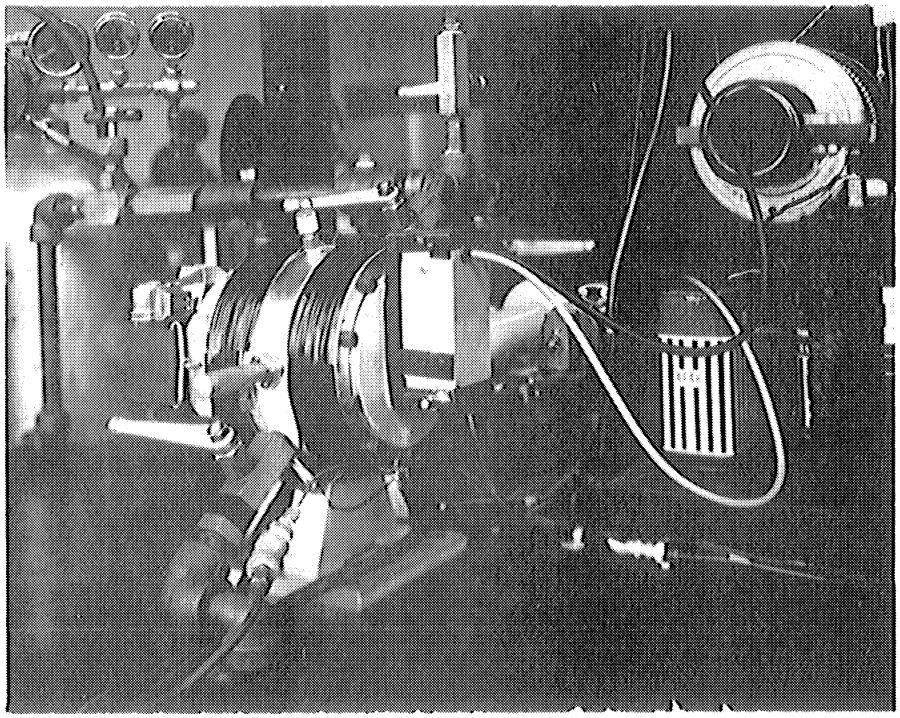

Figure 5.8. Bomb With Photomultiplier Detector Installed and 35 mm Camera Attached.

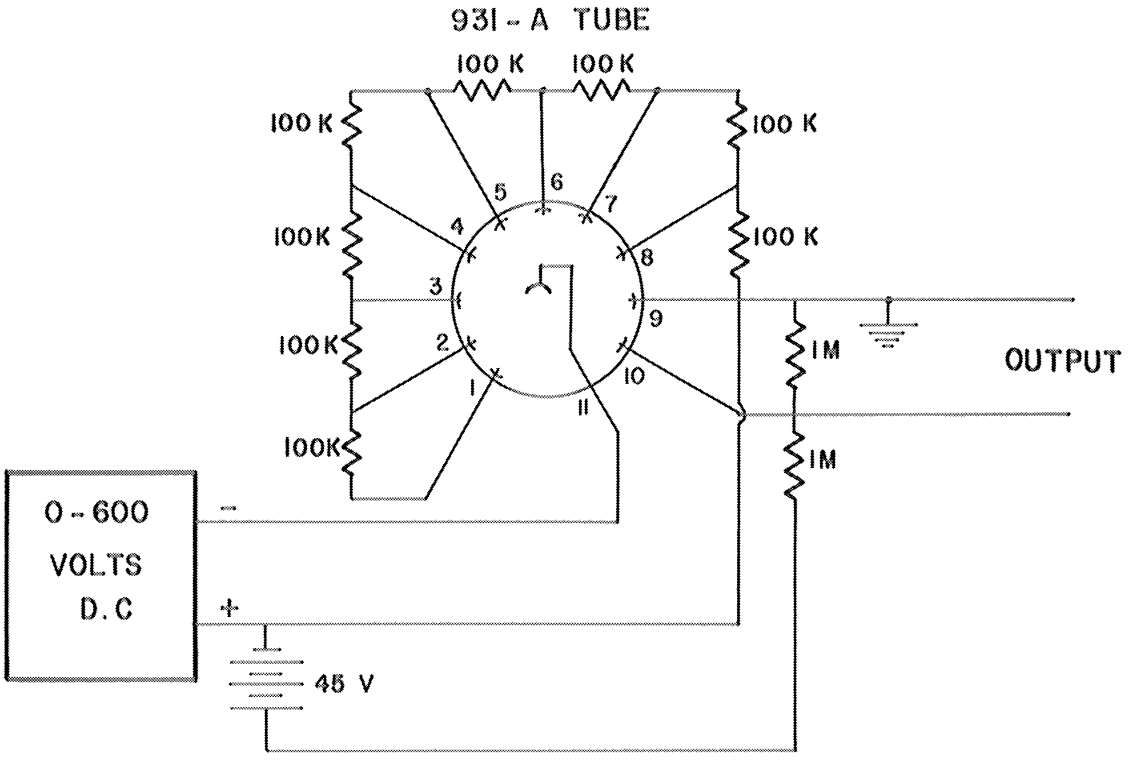

Figure 5.9. Photomultiplier Circuit.

Next, the output from a model 181 Tektronix time marker was compared with the output of the Erie counter and found to be within the accuracy that the oscilloscope can be read. The time marker is a standard instrument sold by Tektronix to be used for oscilloscope calibration. Finally, the sweep rate of the oscilloscope was calibrated using the time marker. Table XI of Appendix D shows the data and the corrected sweep rates which were used for the energy calculations.

2. Voltage and Current

The vertical amplifier deflections were checked be measurement of the voltage of two mercury bias cells. The vertical deflections were within the three percent accuracy stated by the manufacturers of the oscilloscope. Next, the square wave calibrator vertical amplitude was checked with the vertical amplifiers and found to be within the three percent accuracy. The high voltage Tektronix P6015 Probe or voltage divider was frequency compensated and the attenuation was adjusted to 1000 : 1 according to the procedure outlined in the probe manual. A discussion of the conditions that must be satisfied for frequency compensation and design of a voltage divider is included in Appendix C.

No calibration was necessary for current measurement. Voltage drop was recorded as a function of time across a one percent, 150 ohm carbon resistor which was connected in series with the secondary circuit as illustrated in Figure 5.6.

3. Pressure Gages

The 0-100 and 0-300 psi bourdon gages were calibrated using a dead-weight tester. The calibration data and corrections are found in Table XII of Appendix D. The corrections were applied to all of the gage readings made.

4. Pressure Transducer

No pressure calibrations were necessary since the pressure time trace was only used to determine whether or not ignition occurred inside the bomb.

5. Thermocouple Calibration

An iron-constantan thermocouple was calibrated in conjunction with the Brown potentiometer. The ice-point and boiling-point of water were used. The calibration correction curve is shown in Figure D-1 in Appendix D.

6. Frequency Response of Photomultiplier

The response of the photomultiplier tube was determined by exposing the tube to light through four tiny pinholes. A rotating disc having six holes was rotated at high speed between the light source and the photomultiplier tube. The output signal was displayed on an oscilloscope and photographed. Calculations were made to determine the frequency response from Figure 5.13. The calculations show that the initial rising portion of the wave rises at an equivalent frequency of 4000 cycles per second. The falling portion has an equivalent frequency of approximately 2000 cycles per second. This frequency response would be higher if a more intense light source were used with only one small pinhole.

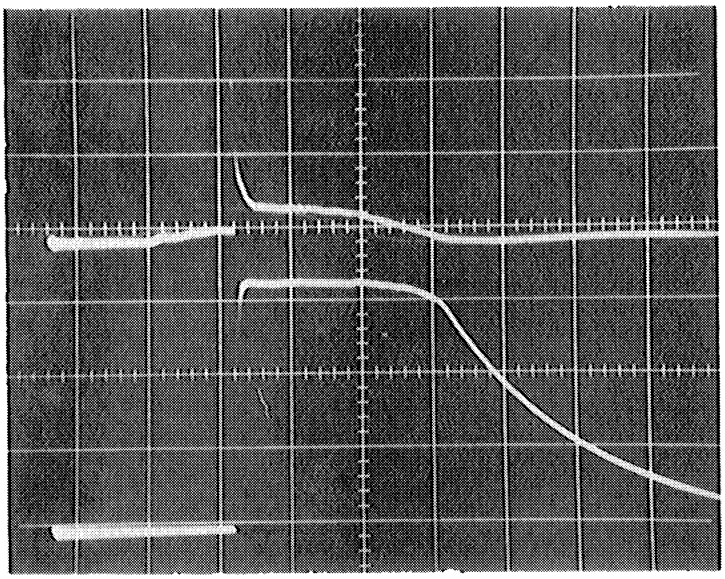

Figure 5.10. Typical Current and Corresponding Light Trace; Upper-current, Lower-light.

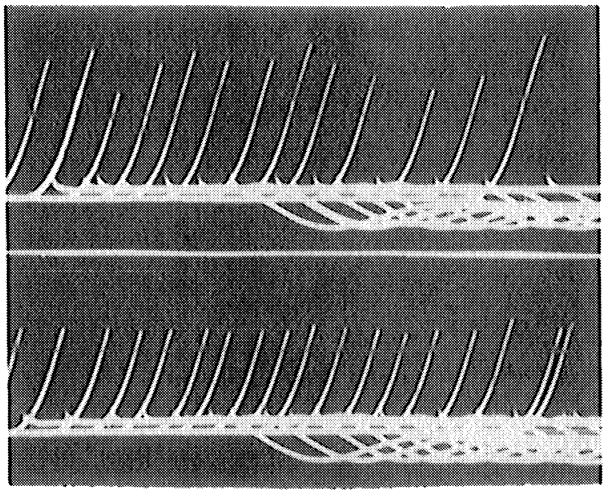

Figure 5.11. Effect of Ultra-violet light Upon Breakdown Voltage; Upper-UV not Used, Lower-UV used.

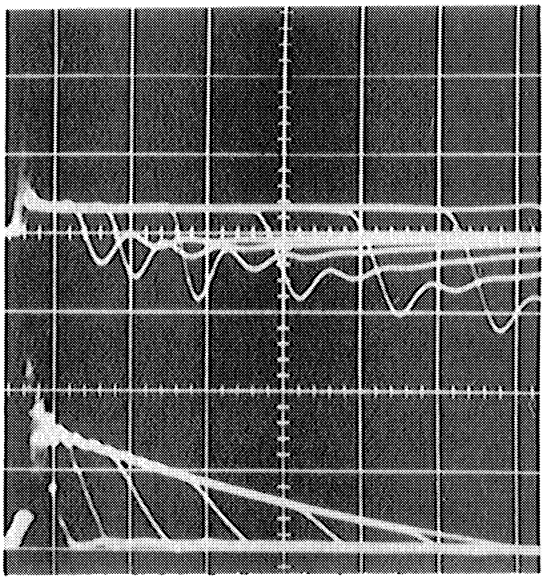

Figure 5.12. Illustration of Spark Time Duration Control; Upper-Voltage, Lower-current.

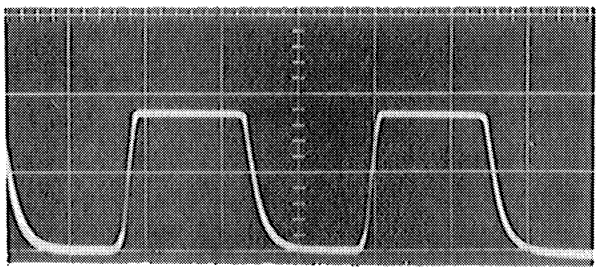

Figure 5.13. Photomultiplier Calibration Trace; Sweep Rate = 500 μsec/cm.

VI. EXPERIMENTAL PROCEDURE

A. Fuel-Air Mixing

The fuel used in this study was chemically pure, 99.0% propane which was purchased from Matheson Company. Air was also purchased from the Matheson Company in cylinders at 2000 psi. The dry-air has a dew point temperature of -75°F.

Each mixture tank was scavenged with dried nitrogen before evacuation to less than 300 microns. Propane was then introduced until the proper pressure for the desired equivalence ratio was reached. The tank valve was closed and the remainder of the system evacuated. Finally, the mixture tanks were charged with dry-air to the required total pressure for the desired equivalence ratio. Care was taken not to open the mixture tank valve before the charging air pressure was well above the fuel pressure in the tank. Thus, there was little chance for fuel to diffuse out of the tank. The partial pressures were calculated according to the following equations.

Propane-air reaction

$$C_3H_8 + \eta 5O_2 + \eta(5)(3.76)N_2 \rightarrow \eta 3CO_2 + \eta 4H_2O + \eta 5(3.76)N_2 \qquad (6.1)$$

where

$$\eta = \frac{\text{Actual air-fuel ratio}}{\text{Stoichiometric air-fuel ratio}}$$

The partial pressure ratio of the fuel is expressed as follows:

$$\frac{P_f}{P_T} = \frac{1}{\eta(23.8) + 1} \qquad (6.2)$$

where

P_f = partial pressure of fuel

P_T = total pressure of fuel plus air

A check calculation showed that the assumption of an ideal gas involves negligible error.

The equivalence ratio is defined as the ratio of the actual fuel-air ratio to the stoichiometric fuel-air ratio.

$$(F/A)_{Volume} = \frac{1}{5\eta 4.76} = \frac{1}{23.8\eta} \tag{6.3}$$

$$(F/A)_{Mass} = \frac{M_f}{23.8\eta M_{air}} = \frac{1}{15.66\eta} \tag{6.4}$$

where

F/A = fuel-air ratio

M_f = molecular weight of fuel

M_{air} = molecular weight of air

Therefore, the equivalence ratio is expressed as follows:

$$\phi = 1/\eta \tag{6.5}$$

A tabulation of the pertinent mixing data is included in Table XIII, Appendix E. This table also includes the required fuel pressures for a total mixing pressure of fuel plus air of 200 psia. Table XIV in Appendix E shows the original data for the mixtures used in this investigation.

B. Measurements of Ignition Energy

The equipment is designed so that the total ignition energy is easily controlled by means of the time duration of the discharge as discussed in Chapter V. The peak power was maintained nearly constant for a given set of runs while the time duration of the sparks was varied. With very short duration sparks and a given peak power, ignition does not occur, provided the peak power setting is not too high. The energy was increased for each consecutive run, by increasing the time duration, until consistent ignition was obtained. The same procedure was followed for three different peak power values at each equivalence ratio.

The peak power is dependent upon the breakdown voltage and the peak current as described in Chapter I and shown in Figure 1.2. An ultraviolet light was used to maintain an approximately constant breakdown voltage. Variation was approximately $\pm$ 10%, but it was considerably better than when no ultraviolet light was used.

The peak current was set by adjustments of the secondary series resistance and parallel capacitance as shown in Figure 5.6. To the left of the large ignition coil in Figure 5.2 one of the ceramic capacitors used for this purpose can be seen. The series resistors are shown in the same Figure 5.2 connected between the high tension terminal of the coil and the cathode on the bomb.

Each set of runs was performed with the same electrode spacing and electrodes. Type "B" electrodes were used in those runs where the electrode spacing was larger than the quench distance, whereas type "A" were used for gaps less than the quench distance.

For each run, the bomb and associated piping were evacuated to less than 300 microns before being charged with a fuel-air mixture. Correct temperature of the mixture inside the bomb was obtained by manual control of the bomb heater or cooler. When the desired temperature was reached, the bomb pressure was again checked and readjusted if required. Then the charging valve was closed, the cathode exposed to the ultraviolet light, camera shutter opened and the spark fired. The criterion for ignition was whether or not the observed pressure time trace showed a pressure rise. This trace was visually observed and not photographed. In addition, a temperature increase was indicated on the potentiometer if combustion occurred. Regardless of whether or not ignition occurred, the exhaust and inlet valves were opened and the bomb was scavenged with dried nitrogen and the charging process was repeated for the next run.

C. Electrode Spacing

Zero spacing was obtained by an electrical continuity check. An ohmmeter was connected across the two electrodes and the electrode spacing was reduced to the point where the ohmmeter reading indicated that the electrode tips touched. The corresponding micrometer reading was recorded. All electrode spacings were then set relative to this reading. Each time the electrode assemblies were replaced after cleaning, etc., a new zero reading was made.

D. Quench Distance

Type "A" electrodes shown in Figure 5.4 were modified slightly for use in the determination of the quench distances. The modification

consisted of removing the 1/32 inch radius from the tips of the electrodes so as to make them flush with the glass flanges like the anode of the type "B" electrodes shown in Figure 5.4. The change was necessary because the results obtained with the type "A" electrodes proves to be erroneous. A discussion of the results obtained with the type "A" electrodes modified and unmodified is found in Chapter VII.

Evaluation of the quench distance for a given fuel-air ratio, etc., involved a series of runs at different electrode spacings. Each run was made with a fresh mixture and the electrode spacing was increased for each run until ignition occurred. Then the electrode spacing was reduced in small increments until the quench distance was defined. The mixtures were exhausted from the bomb after each spark was fired. All of the spark were of the same duration and peak power.

VII. RESULTS AND DISCUSSION

A. Results

The electrode spacings used for determining minimum ignition energies in this investigation are shown in Figure 7.1. Quench distances obtained by three other investigations are also shown on the same figure.

Minimum ignition energies for propane-air mixtures were obtained for equivalence ratios of 0.69, 0.73 and 0.83. Two electrode spacings were used when determining the ignition energies for an equivalence ratio of 0.83, one smaller and the other larger than the reported quench distance shown in Figure 7.1. The total energy is plotted as a function of the peak power P_p in Figures 7.2 through 7.5 for each of the preceding equivalence ratios. The circles are points at which ignition occurred and the squares represent non-ignition points. These same total energies are plotted as a function of P_{LA}/P_{HA} in Figures 7.6 through 7.9. P_{LA} is the average power or average rate of energy discharge during the low rate component of the spark. The average power is obtained by dividing the total energy dissipated during the low rate component E_L by the time duration of that part of the discharge. P_{HA} is the average power or average rate of energy discharge during the high rate component. It is determined in a manner similar to that used for P_{LA}

For convenience, a plot of the minimum ignition energies which were reported by Lewis and von Elbe[21] for pure capacitive sparks are shown in Figure 7.10 as a function of equivalence ratio. The dashed portion

of the curve is an extrapolation of their data to the smallest equivalence ratio used in this study.

All of the data reduction calculations were performed on an IBM 7090 digital computer. Details of these calculations are described in Appendix F and the results are shown in Tables III through VI. The original data readings are shown in Tables XV through XVIII. The last three digits of the run number listed in these tables correspond to the mixture number. Data such as equivalence ratio, etc., relating to each mixture number are found in Table XIV.

B. Discussion

The quench distances reported by References 21, 27, and 28 and shown in Figure 7.1 are seen to approach the same value at the richer mixtures. In the present investigation a quench distance of 0.091 inches was measured at an equivalence ratio of 0.83 using type "A" electrodes. Since this value was smaller by 0.023 inches than that reported by Reference 28, modifications were made on the electrodes to see if better agreement could be obtained. Use of the modified type "A" electrodes gave a 0.120 inch quench distance which was only 0.006 inches larger than the reported value of Reference 28. Therefore, the modified type "A" electrodes were used for the remainder of the quench distances measurements.

Disagreement in the values for d_q exists in the literature for lean mixtures as shown in Figure 7.1. Similar results were obtained in the present investigation, in that the quench distances showed larger scatter at the smaller equivalence ratios. To be assured that tests would

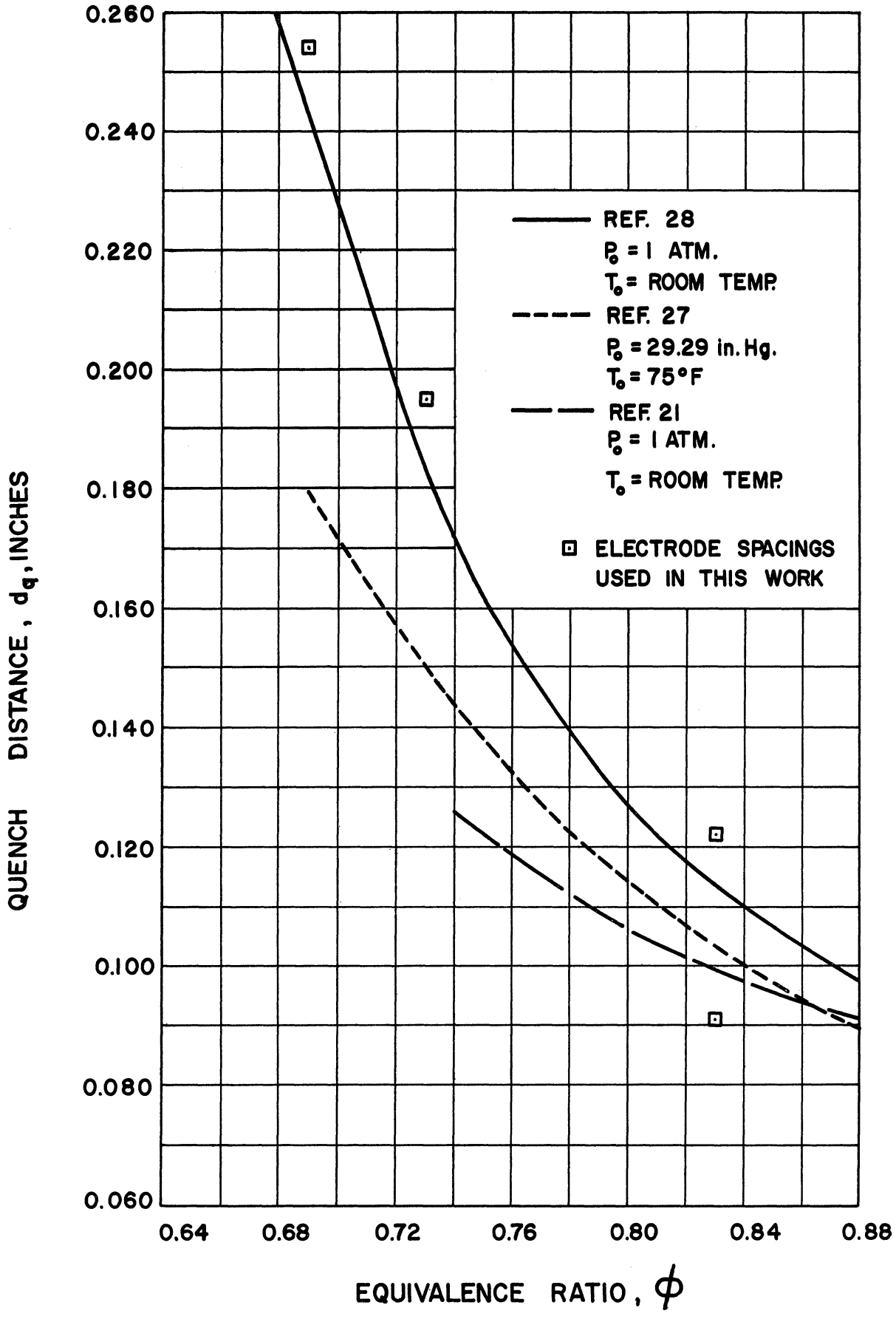

Figure 7.1. Dependence of Quench Distance Upon Equivalence Ratio for Propane-Air Mixtures.

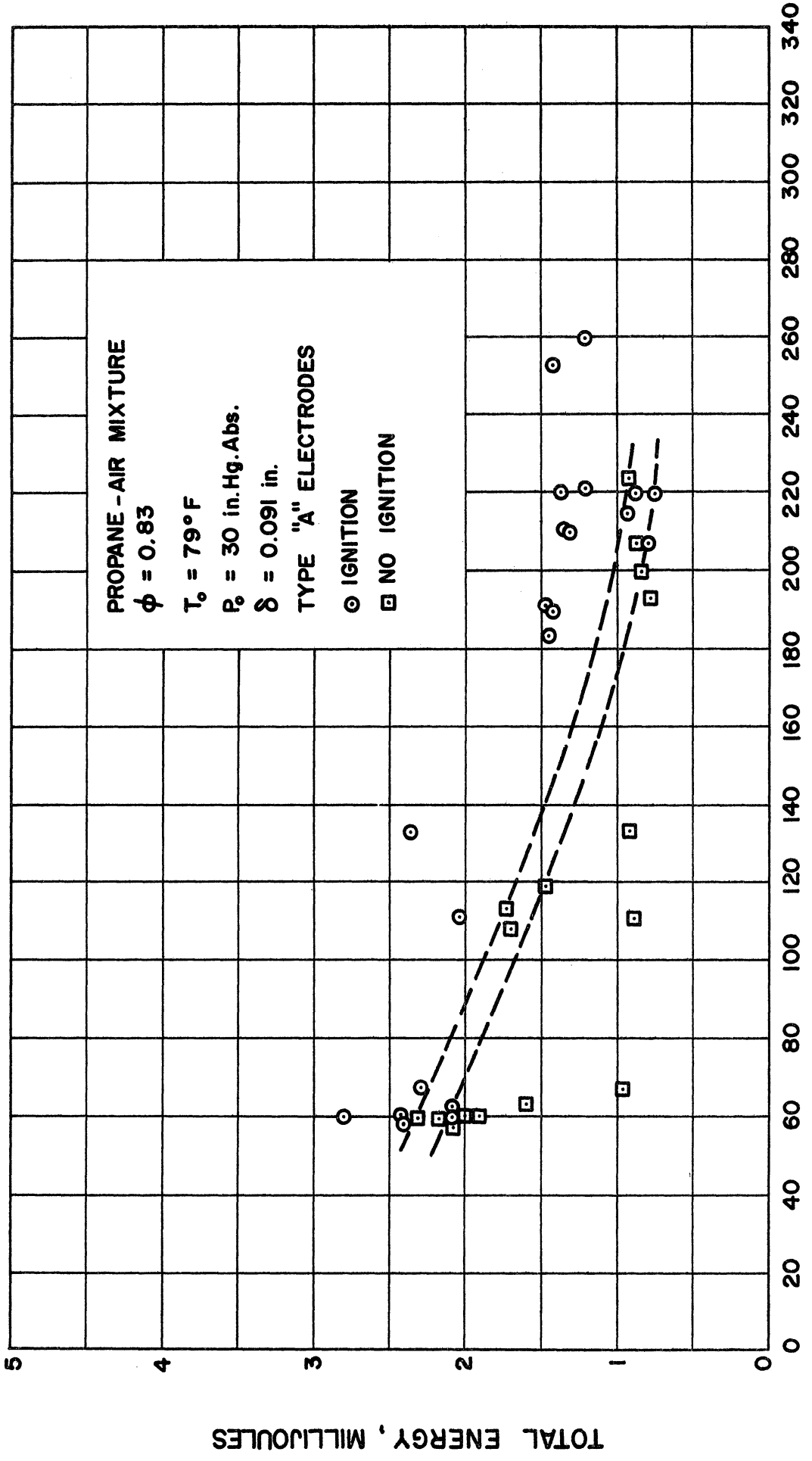

Figure 7.2. Effect of Peak Power Upon Minimum Ignition Energy for δ Less than Quench Distance.

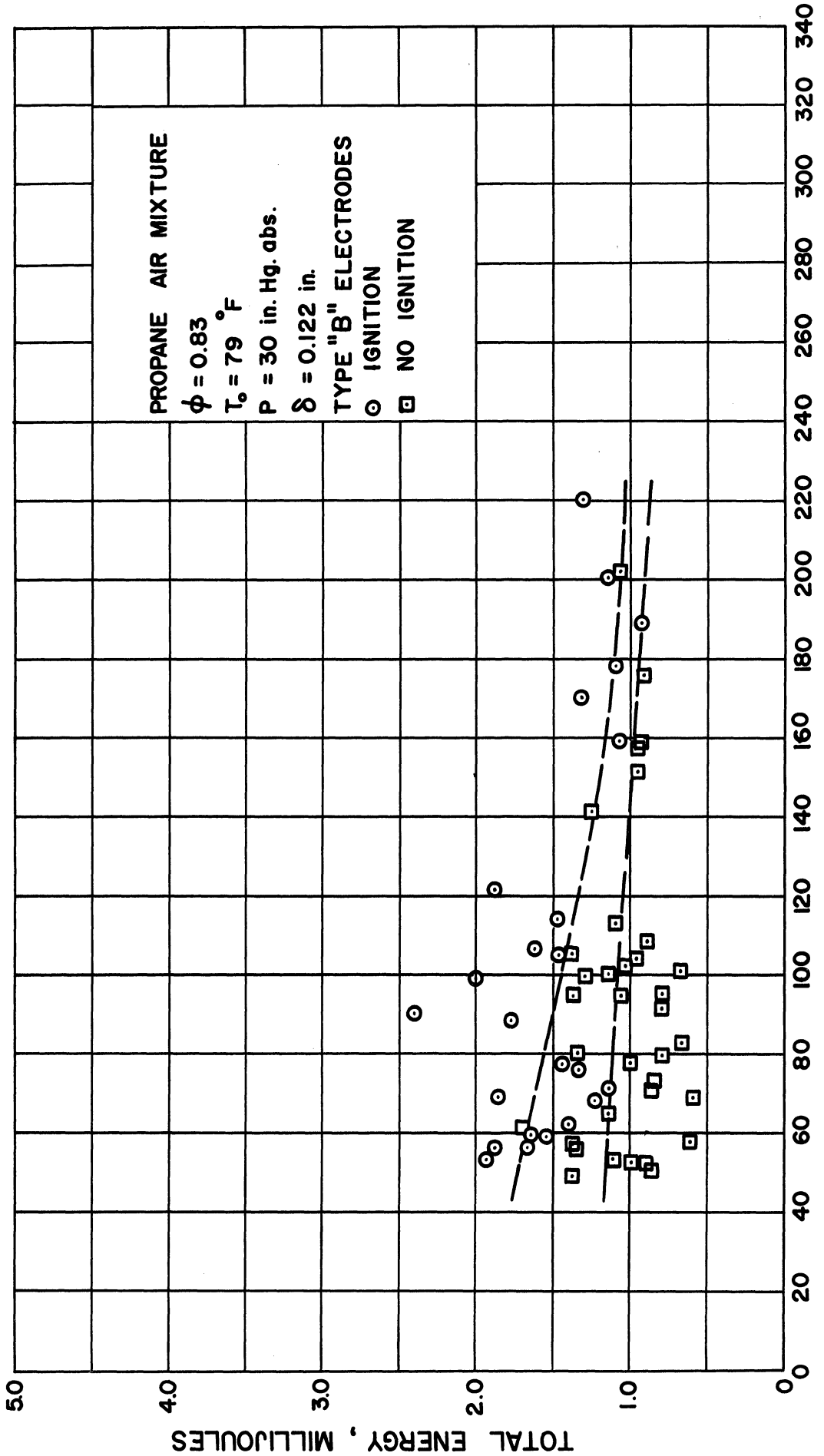

Figure 7.3. Effect of Peak Power Upon Minimum Ignition Energy.

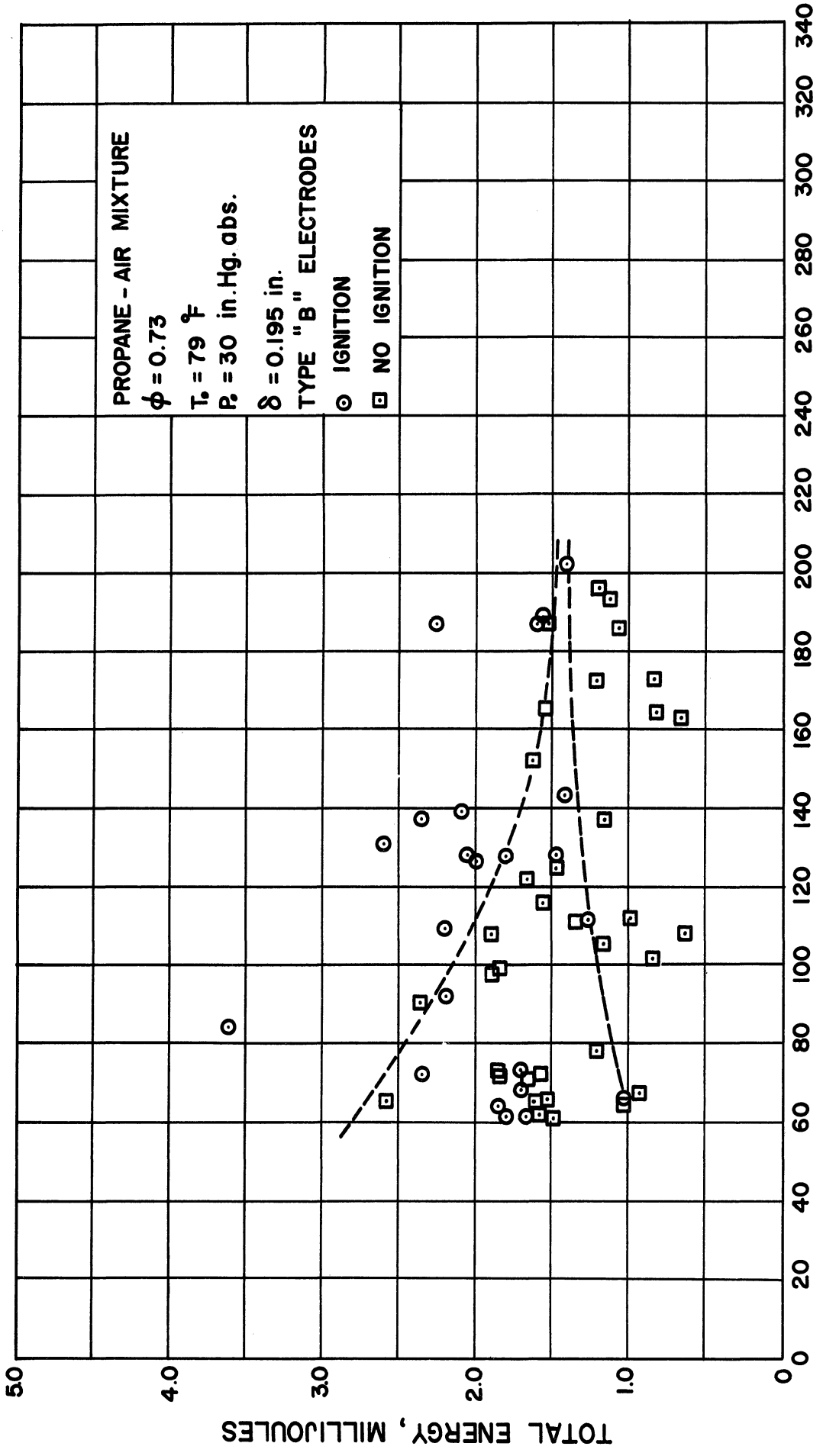

Figure 7.4. Effect of Peak Power Upon Minimum Ignition Energy.

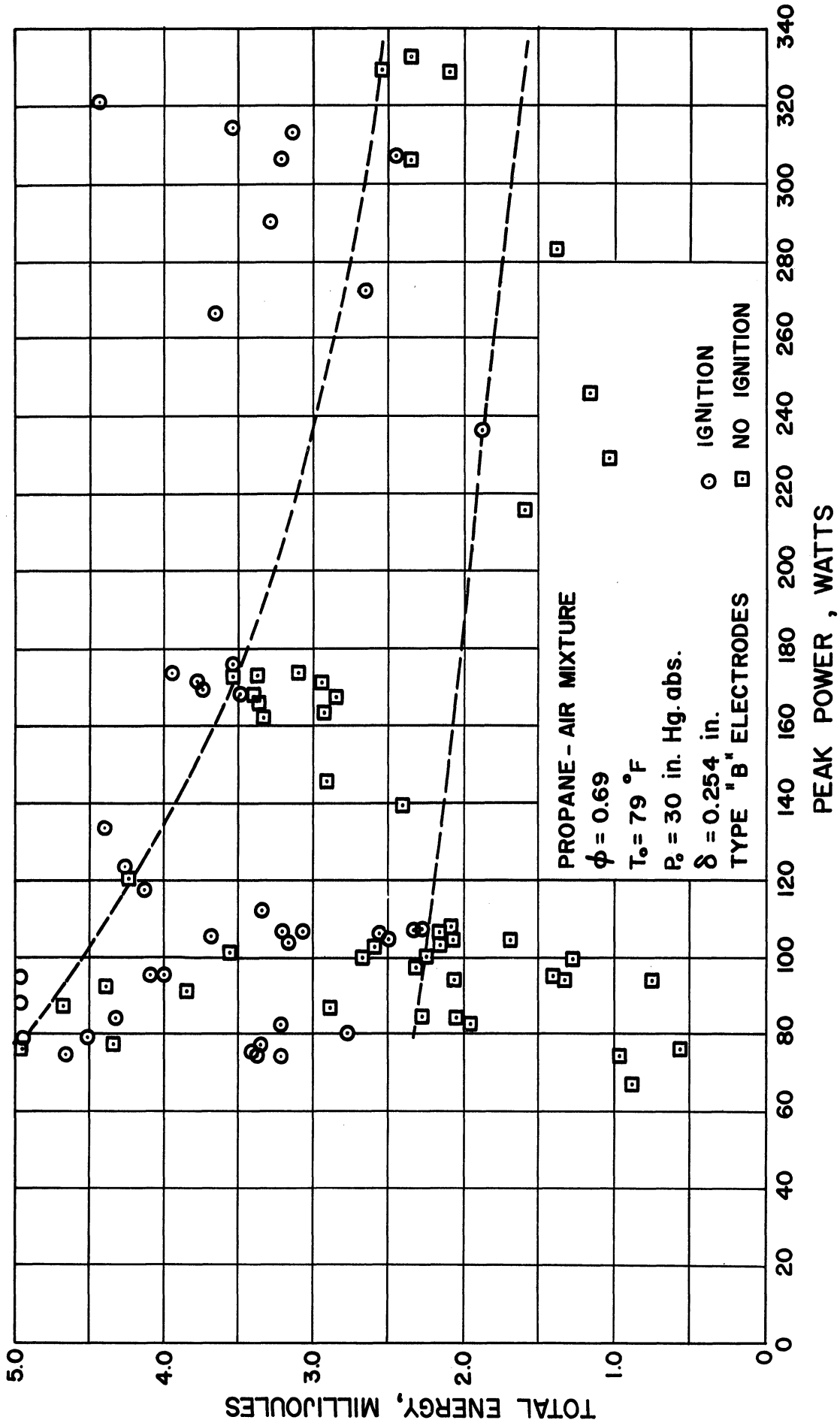

Figure 7.5. Effect of Peak Power Upon Minimum Ignition Energy.

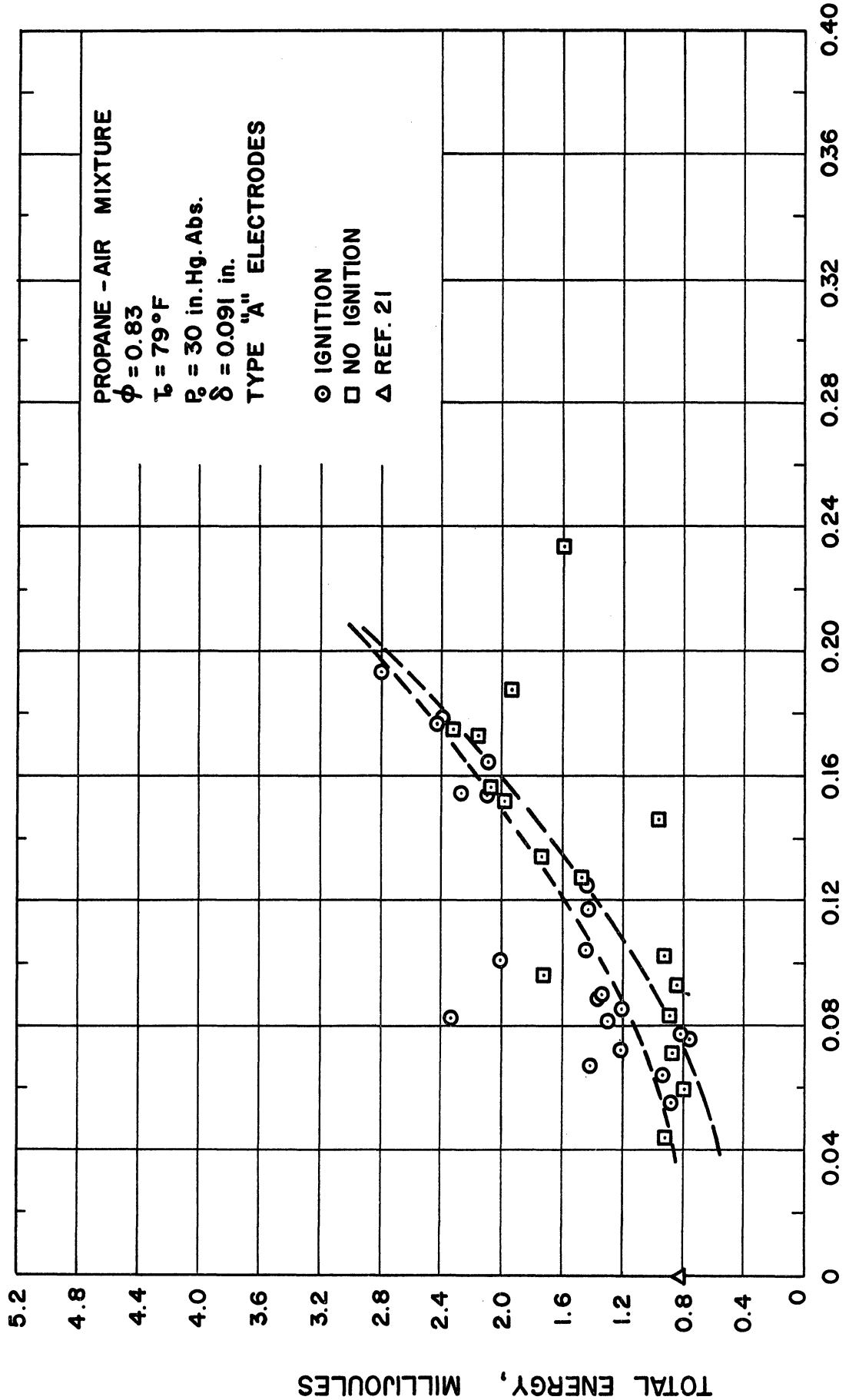

Figure 7.6. Effect of Rates of Energy Input Upon Minimum Ignition Energy for δ Less than Quench Distance.

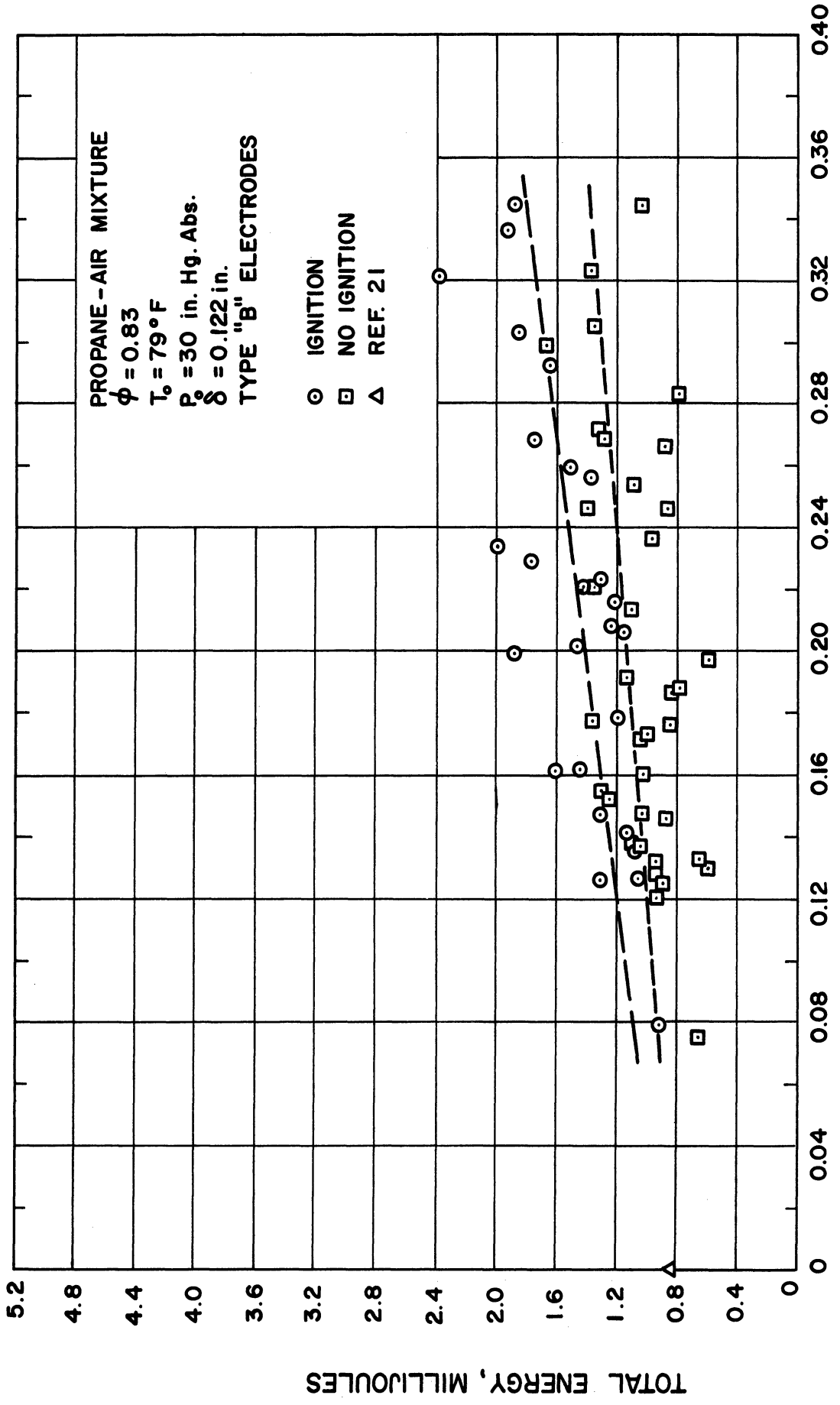

Figure 7.7. Effect of Rates of Energy Input Upon Minimum Ignition Energy.

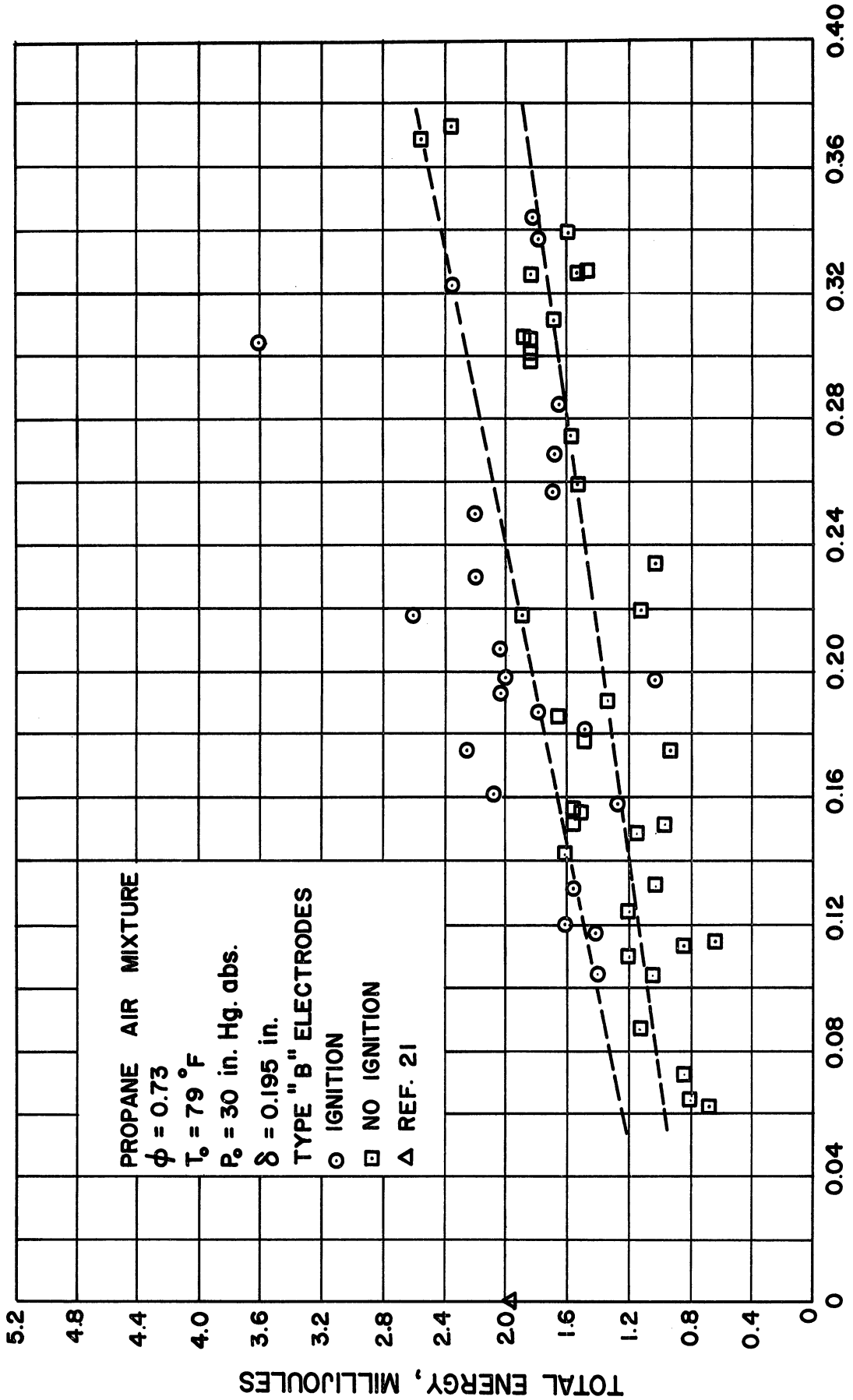

Figure 7.8. Effect of Rates of Energy Input Upon Minimum Ignition Energy.

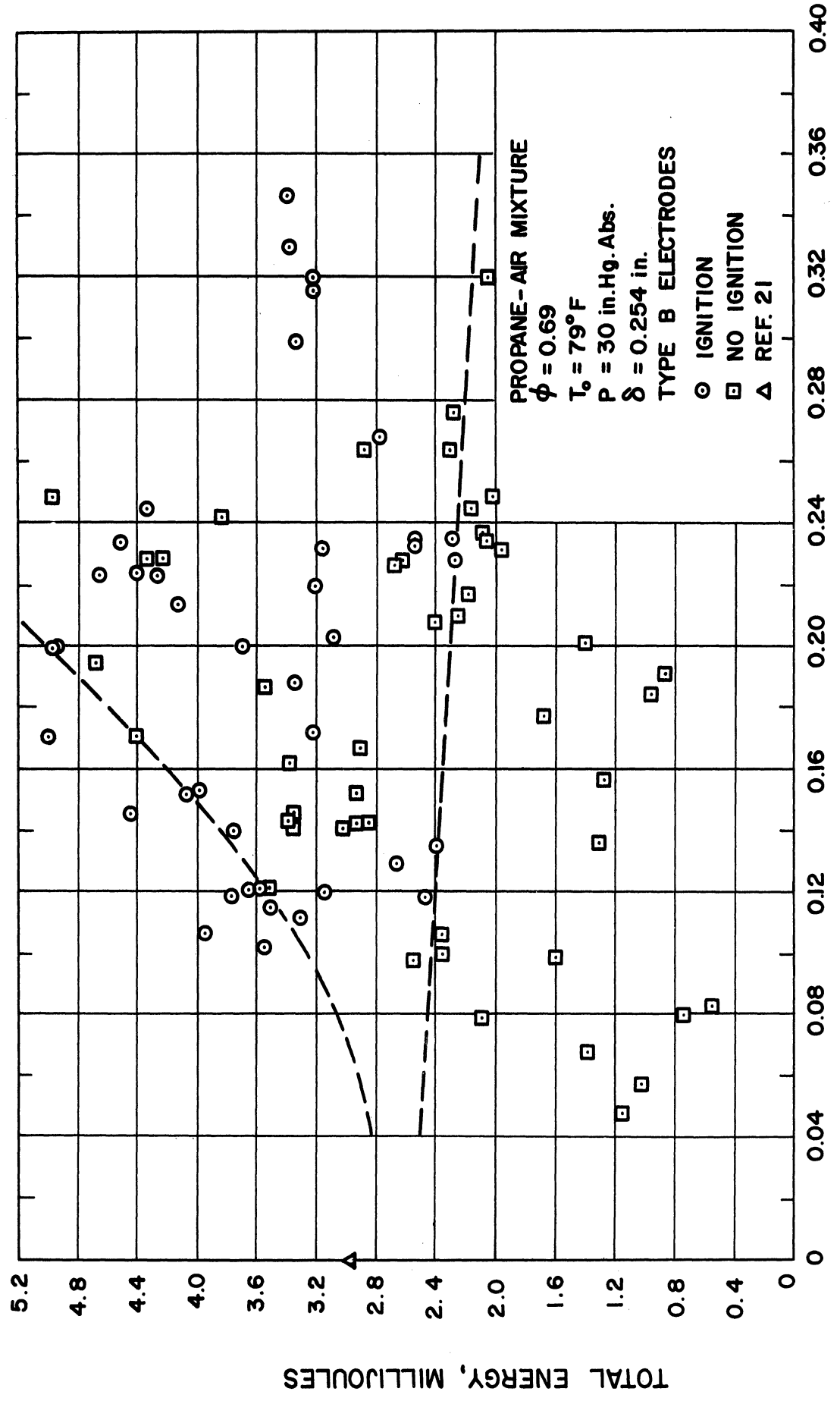

Figure 7.9. Effect of Rates of Energy Input Upon Minimum Ignition Energy.

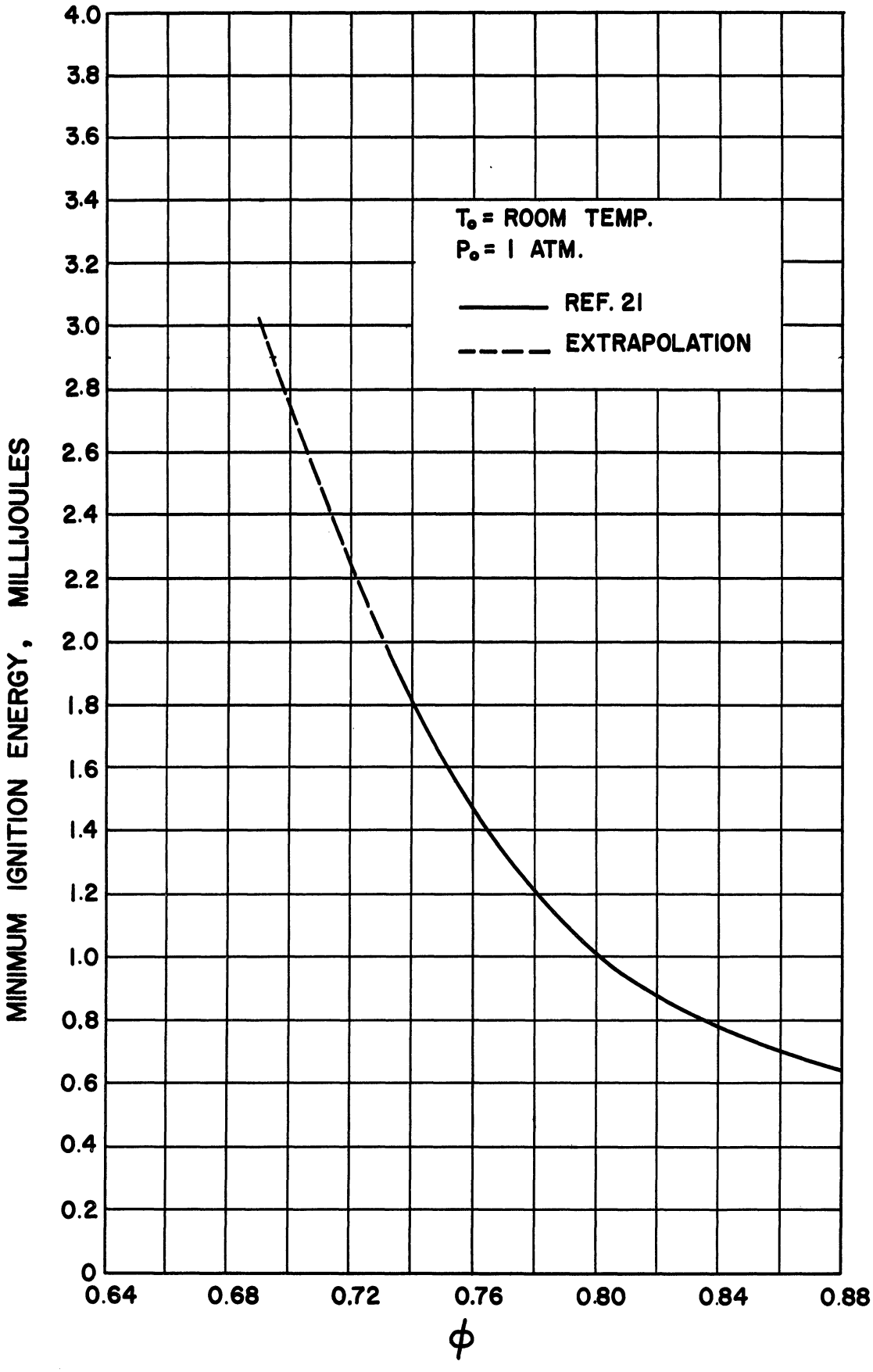

Figure 7.10. Minimum Ignition Energy vs ϕ for Propane-Air Mixtures.

be run with gaps larger than the quench distance, larger values than those reported by Harris[28] were used.

Type "B" electrodes were used for ignition energy measuremnets where the electrode spacings were larger than the quench distance. These electrodes were used because modified type "A" electrodes require large breakdown voltages causing improper operation of the control circuit with no spark formation. An aluminum cathode was used in all cases to reduce the work function of the cathode surface. This is discussed in Chapter III.

The upper dashed curves in Figures 7.2 through 7.9 were drawn through the non-ignition points representing the largest energies while the lower dashed curves were drawn through the ignition points having the smallest energies. The area between the two curves is a transition region between non-ignition and ignition. Spark energies which are smaller than the values defined by the lower curves would not possess enough energy to cause ignition. On the other hand, energies which fall above the upper curves would be expected to cause ignition. Therefore, the upper dashed curves in Figures 7.2 through 7.5 show the minimum ignition energy as a function of peak power P_p. In Figures 7.6 through 7.9 the upper dashed curve shows the minimum ignition energy as a function of the ratio P_{LA}/P_{HA}.

Consider the curves for minimum ignition energy versus peak power shown in Figures 7.2 through 7.5. In each figure, the minimum ignition energy decreases as the peak power is increased. It was found that this relationship can be expressed by an empirical equation of the following form:

$$E_{MIN} = F \frac{1}{P_p^{\nu}} \quad \text{or} \quad E_{MIN} P_p^{\nu} = F \tag{7.1}$$

where

F = constant

ν = constant

If a log-log plot of E_{MIN} versus P_p is a straight line, the slope of this line defines the value of the constant ν. The minimum ignition energy curves of Figures 7.2 through 7.5 are replotted on a log-log plot in Figure 7.11. Straight lines closely approximate the data and the values of the slopes ν are listed in Table II. The corresponding values of F are also shown in the table. Each F was calculated according to Equation (7.1) using the graphically determined constant ν.

The negative slope ν is largest for the case where the electrode spacing is smaller than the quench distance.

For electrode spacings larger than the quench distance, the slope ν increases as the equivalence ratio is decreased. In other words, the peak power has a greater effect upon the minimum ignition energy at smaller equivalence ratios. It appears that this is due to greater quenching of the initial flame volume by the mixture surrounding it which may be due to chain breaking rather than thermal processes.

TABLE II

EMPIRICAL CONSTANTS FOR ENERGY EQUATION

ϕ	δ	d_q	F	ν
0.83	0.091	0.114	52.1	.738
0.83	0.122	0.114	6.61	.348
0.73	0.195	0.183	15.1	.427
0.69	0.254	0.242	37.5	.463

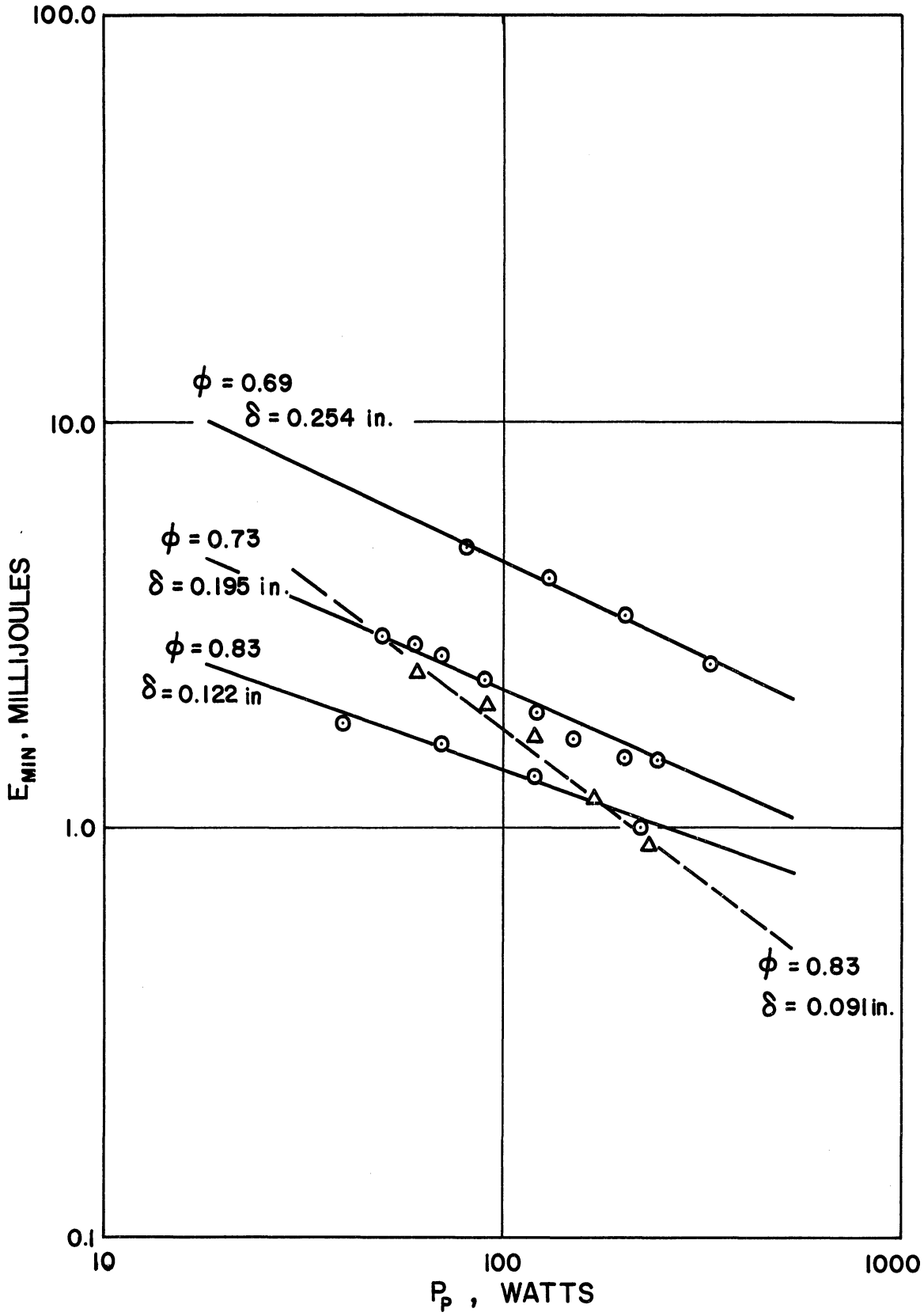

Figure 7.11. Determination of ν .

It would be of interest to see if any relationship exists between Equation (7.1) and Equations (4.25) and (4.26) of Chapter IV. Recall that Equations (4.25) and (4.26) were derived for the case where heat is transferred to the mixture from a source at temperature T_s. This temperature is proportional to the rate of heat transfer q. Since q is really a power term, the relationship between Equation (7.1) and Equation (4.25) or (4.26) is easily seen. The relevant difference between q and P_p is that q is constant over a period of time while P_p is an instantaneous peak value.

Another difference exists between Equations (4.25) and (7.1) Yang indicates that $(\Omega-1)$ should be large if the approximation in Equation (4.27) is to hold. The corresponding values of ν found in this investigation are all smaller than unity. Nevertheless, the basic forms of the equations are the same.

The shapes of the instantaneous power versus time curves for two sparks may be different and yet the peak powers P_p may be the same in each case. Consider the two curves shown in Figure 7.12. The area under curve b is larger than the area under curve a. If the energy for curve b is just adequate for ignition of a given mixture, the energy of curve a would be inadequate. The overall time duration of spark a would have to be increased as shown by the dashed curve to cause ignition. Thus, it can be seen that the peak power P_p does not thoroughly describe the spark requirement for ignition. To alleviate this, a plot of the total energy versus the ratio P_{LA}/P_{HA} was chosen where P_{LA} and P_{HA} were described in Section A. The two sparks in

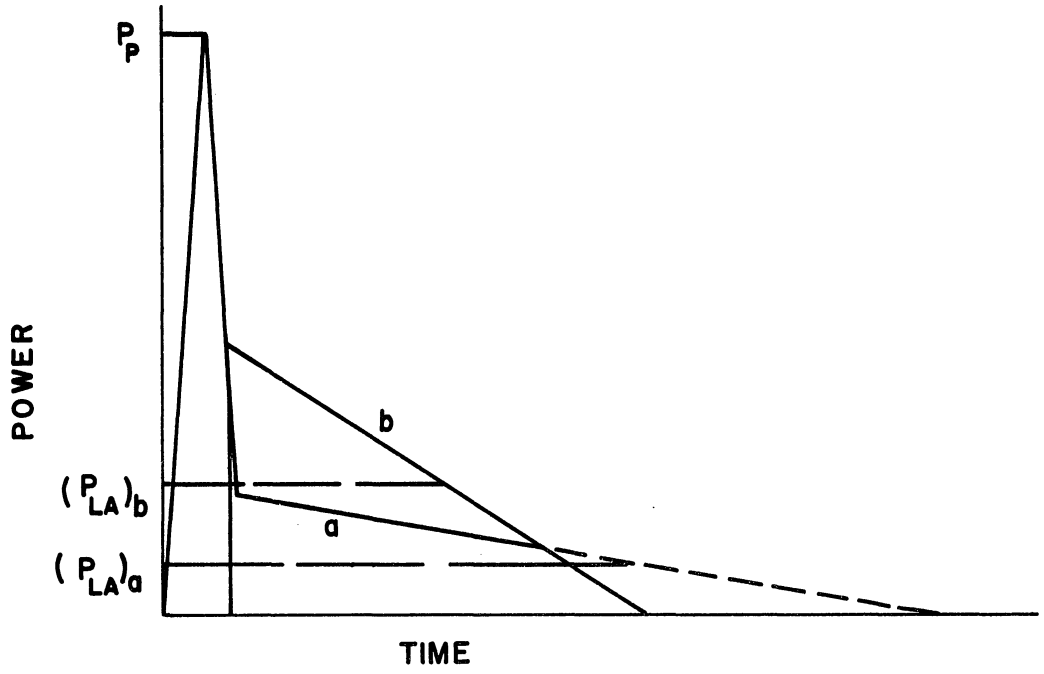

Figure 7.12. Power vs Time for Two Different Sparks.

Figure 7.12 would have nearly the same P_{HA}, but the respective values of P_{LA} would be different. Consequently, P_{LA}/P_{HA} would be different for the two sparks. The results plotted in Figures 7.6 through 7.9 show that the minimum ignition energy decreases as the ratio P_{LA}/P_{HA} decreases. At $P_{LA}/P_{HA} = 0$, corresponding to pure capacitive sparks, the data extrapolates to values close to those reported by Lewis and von Elbe[21] for capacitive sparks. Similar comparisons at all equivalence ratios show that the largest difference if for an equivalence ratio of 0.73 illustrated in Figure 7.8.

At all equivalence ratios, the width of the transition region increases with decrease in the peak power or increase in the ratio P_{LA}/P_{HA}. In other words, the transition region increases in width as the rate of energy input decreases. In addition, the band is wider for the leaner mixtures. Ignition seemed to occur at random within this region. Lewis and von Elbe[12,21] also noticed a randomness of ignition with hydrocarbons such as propane and higher. In addition, at the leaner mixtures they also noticed this randomness of ignition. There are several possible reasons for this. Lewis and von Elbe indicate that the cause may be due to the higher breakdown voltages encountered with leaner mixtures. That is, the quench distance increases with decrease in equivalence ratio whereas according to Paschen's Law as discussed in Chapter III the breakdown voltage increases. The higher resultant currents may cause a net mass flow between the electrodes due to electron wind resulting in a contraction of the reacting volume of gas after the discharge. Irregular movement of the initial flame kernel

toward the anode, a possible source of variation in the quench effect, has been photographed by Lewis and von Elbe.[12] They also suggest that because of the non-uniform potential distribution between the electrodes during breakdown, that the energy discharged in the spark may not be uniformly distributed. Variations from spark to spark would result in irregular ignition patterns. The present investigation has shown that at electrode spacings of 0.122 inches or less the discharge path of the spark is nearly the same for a series of sparks and the breakdown voltage is more uniform than for larger electrode spacings. Figure 7.13 shows a typical photograph of a spark at an electrode spacing of 0.122 inches. At an electrode spacing of 0.254 inches, extreme differences occur in the discharge path from spark to spark. This is illustrated by Figures 7.14 and 7.15. Certainly, the distribution of energy along the discharge path is different for each of these sparks. This may be a reason for the randomness of ignition at the larger electrode spacings shown in Figures 7.5 and 7.9. However, no correlation has as yet been made between the spark path and ignition. Another phenomenon was noticed in the photographs of the sparks. At large electrode spacings the spark discharge did not always start at the tip of the cathode. In many cases it started on the side of the cathode about 1/16 inch back from the tip. This could also cause random distributions of the energy between sparks. Type "C" electrodes were used in several runs to see if the irregular spark path and discharge from the side of the cathode might be improved with a pointed cathode. No difference was noted.

Determination of the exact cause for the spread in the data would require a very extensive study involving a systematic variation of all of the parameters. Even with the wide transition band, the results show that increasing the rate of energy input results in a decrease of the minimum ignition energy.

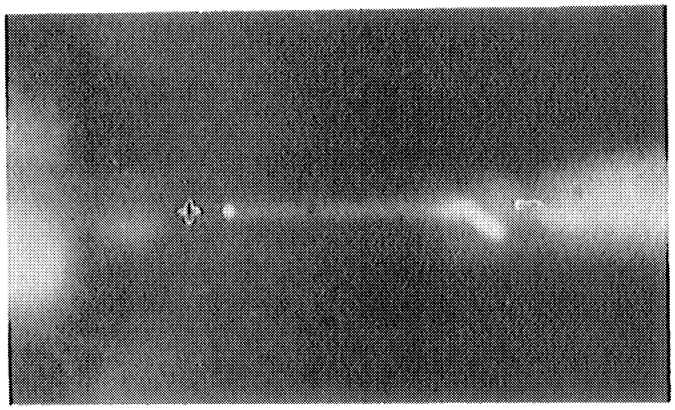

Figure 7.13. Spark Discharge; 0.122 Inch Gap, Type "B" Electrodes, Magnification = 10.

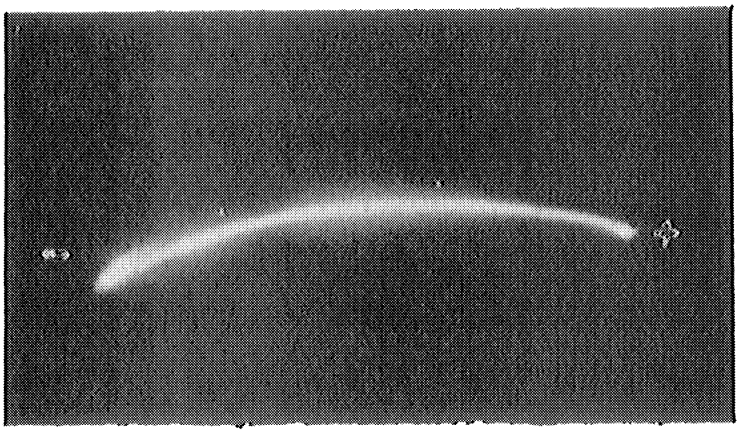

Figure 7.14. Spark Discharge; 0.254 Inch Gap, Type "B" Electrodes, Magnification = 10.

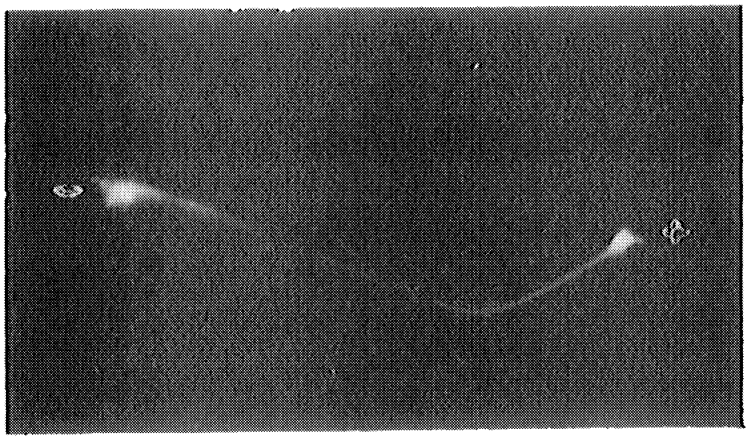

Figure 7.15. Spark Discharge; 0.254 Inch Gap, Type "C" Electrodes, Magnification = 10.

TABLE III.

RESULTS

Propane-Air Mixture
ϕ=0.83, T_o=79°F, P =30 in. Hg. Abs., δ =0.091 in.
Type "A" Electrodes

Run No.	E_T (Millijoules)	P_p Watts	$\frac{P_{LA}}{P_{HA}}$	Ignition
225001	.923	133.3	.102	No
212001	.881	110.8	.083	No
213001	1.474	118.8	.127	No
214001	1.703	107.7	.134	No
224001	1.732	113.2	.096	No
218001	2.016	111.0	.101	Yes
217001	2.354	133.3	.082	Yes
226001	.964	66.7	.146	No
227001	1.596	62.7	.233	No
228001	1.943	60.2	.187	No
229001	2.159	60.2	.172	No
249001	2.070	57.0	.156	No
250001	2.398	58.3	.178	Yes
245001	2.416	60.0	.177	Yes
241001	2.088	61.8	.153	Yes
230001	2.793	60.2	.193	Yes
237001	1.982	59.5	.152	No
247001	2.086	59.5	.164	Yes
232001	2.277	66.5	.154	Yes
238001	2.327	59.4	.175	No
258001	.794	193.3	.059	No
254001	.923	224.0	.044	No
263001	1.448	190.7	.125	Yes
260001	1.451	183.3	.104	Yes
251001	1.431	190.0	.117	Yes
264001	1.340	210.0	.09	Yes
266001	.873	206.7	.071	No
268001	.807	206.7	.077	Yes
255001	.843	200.0	.093	No
256001	.760	220.0	.075	Yes
267001	1.210	260.3	.085	Yes
253001	.878	220.0	.055	Yes
259001	1.211	221.0	.072	Yes
261001	1.314	210.0	.081	Yes
257001	.942	215.3	.064	Yes
262001	1.419	253.3	.067	Yes
265001	1.37	220.0	.088	Yes

TABLE IV.

RESULTS

Propane-Air Mixture
ϕ=0.83, T_o=79°F, P=30 in. Hg. Abs., δ=.122
Type "A" Electrodes

Run No.	E_T (Millijoules)	P_p Watts	$\frac{P_{LA}}{P_{HA}}$	Ignition
224005	.877	108.8	.146	No
225005	1.134	100.4	.191	No
226007	1.457	113.5	.201	Yes
227005	1.243	100.0	.208	Yes
228005	1.026	101.0	.172	No
229005	1.075	112.5	.137	No
230005	1.041	95.5	.344	No
231005	.789	91.9	.283	No
231105	.768	95.2	.147	No
232005	1.265	141.2	.152	No
233005	1.360	95.2	.177	No
234005	1.448	105.0	.162	Yes
235005	1.192	98.7	.178	Yes
236005	1.869	121.1	.199	Yes
237005	1.986	99.0	.234	Yes
204005	1.885	56.0	.345	Yes
205005	1.673	60.5	.299	No
206005	1.653	59.5	.292	Yes
207005	1.285	57.8	.269	No
209005	.864	50.4	.246	No
211005	1.096	53.0	.254	No
212005	.977	52.3	.236	No
213005	1.379	61.6	.256	Yes
214005	1.331	55.7	.271	No
216005	1.517	59.0	.259	Yes
217005	1.757	56.0	.268	Yes
218005	1.926	52.9	.336	Yes
219005	.881	52.0	.266	No
220005	1.358	56.5	.305	No
221005	1.374	49.4	.323	No
223005	.643	83.0	.133	No
225005	.937	151.0	.132	No
256005	1.062	158.7	.126	Yes
257005	.961	158.7	.128	No
258005	.918	189.0	.079	Yes
259005	.952	158.4	.121	No
261005	1.082	177.5	.136	Yes
263005	.893	175.5	.125	No
264005	1.046	201.7	.137	No

TABLE IV. (Cont'd)

Run No.	E_T (Millijoules)	P_p Watts	$\frac{P_{LA}}{P_{HA}}$	Ignition
265005	1.132	200.5	.141	Yes
266005	1.307	219.7	.126	Yes
267005	1.306	170.2	.147	Yes
180005	1.851	68.5	.303	Yes
181005	1.214	67.5	.216	Yes
183005	.784	80.0	.188	No
184005	.832	72.8	.187	No
186005	.587	57.5	.197	No
188005	.569	69.1	.130	No
189005	.655	105.6	.075	No
190005	1.309	75.6	.223	Yes
191005	1.155	70.5	.206	Yes
192005	.837	71.4	.176	No
193005	.999	78.4	.173	No
194005	1.025	96.	.147	No
195005	1.023	102.0	.160	No
196005	1.112	65.0	.213	No
197005	1.392	104.5	.246	No
198005	1.330	80.3	.221	No
199005	1.416	76.5	.221	Yes
200005	1.283	99.6	.155	No
201005	1.758	87.7	.229	Yes
202005	1.609	105.6	.161	Yes
203005	2.388	89.8	.321	Yes

TABLE V.

REULTS

Propane-Air Mixture
ϕ=0.73, T_o=79°F, P=30 in. Hg. Abs., δ=0.195

Run No.	E_T (Millijoules)	P_p Watts	$\frac{P_{LA}}{P_{HA}}$	Ignition
10014	1.832	71.9	.306	No
11014	1.808	63.8	.326	No
12014	1.825	62.0	.344	Yes
13014	1.653	60.6	.285	Yes
14014	1.787	61.3	.337	Yes
15014	1.688	72.6	.269	Yes
16014	1.697	67.9	.257	Yes
18014	1.661	70.6	.312	No
19014	1.561	71.9	.275	No
20014	1.190	78.4	.219	No
21014	.934	67.2	.175	No
22014	1.017	65.3	.234	No
24014	1.018	66.0	.197	Yes
28014	2.559	65.3	.369	No
29014	2.344	71.9	.322	Yes
30014	1.830	73.3	.298	No
32014	.624	107.7	.114	No
33014	.978	112.2	.152	No
34014	1.139	136.8	.132	No
35014	1.333	110.9	.191	No
36014	1.189	172.0	.124	No
37014	1.592	152.4	.142	No
38014	1.267	110.9	.158	Yes
39014	2.086	139.2	.161	Yes
40014	1.416	142.8	.117	Yes
41014	1.646	121.6	.186	No
42014	1.530	116.4	.152	No
43014	1.886	108.0	.218	No
44014	1.990	125.7	.198	Yes
45014	2.039	128.1	.207	Yes
46014	2.35	137.1	.193	Yes
47014	2.598	131.5	.218	Yes
48014	1.459	124.8	.178	No
49014	1.775	128.0	.187	Yes
50014	1.141	105.0	.149	No
51014	.835	101.6	.113	No
1014	3.604	84.0	.304	Yes
2014	2.329	90.0	.373	No
3014	1.866	98.1	.306	No

TABLE V. (Cont'd)

Run No.	E_T (Millijoules)	P_p Watts	$\frac{P_{LA}}{P_{HA}}$	Ignition
4014	1.808	99.7	.301	No
6014	2.187	108.8	.230	Yes
7014	2.189	92.4	.250	Yes
8014	1.480	60.7	.327	No
9014	1.58	64.5	.339	No
25014	1.531	65.3	.259	No
54014	.800	165.3	.065	No
55014	.651	162.7	.062	No
56014	1.037	185.8	.105	No
57014	1.112	192.7	.087	No
59014	1.399	202.4	.104	Yes
60014	1.564	189.3	.131	Yes
61014	1.469	127.5	.182	Yes
62014	2.250	186.7	.175	Yes
63014	1.526	165.0	.156	No
64014	1.604	186.7	.120	Yes
65014	1.19	195.5	.110	No
66014	.824	173.3	.073	No

TABLE VI.

RESULTS

Propane-Air Mixture
ϕ=.69, T_o=79°F, P=30 in. Hg. Abs., δ =.254
Type "A" Electrodes

Run No.	E_T (Millijoules)	P_p Watts	$\frac{P_{LA}}{P_{HA}}$	Ignition
31017	1.965	82.6	.232	No
32017	2.251	100.5	.210	No
33017	2.176	105.6	.217	No
34017	2.305	97.6	.264	No
35017	2.590	102.7	.228	No
36017	2.874	86.5	.264	No
37017	3.343	111.9	.188	Yes
38017	2.908	145.6	.167	No
39017	2.850	167.2	.142	No
40017	3.070	173.1	.141	No
41017	4.392	133.3	.224	Yes
42017	3.38	167.0	.143	No
43017	3.374	171.9	.162	No
44017	3.319	162.2	.146	No
45017	4.262	122.7	.223	Yes
46017	4.210	120.0	.229	No
48017	4.132	117.3	.214	Yes
49017	3.741	168.5	.140	Yes
50017	3.516	171.6	.121	No
51017	3.544	175.4	.121	Yes
52017	3.510	170.1	.115	Yes
53017	3.763	170.1	.119	Yes
54017	3.356	165.7	.140	No
55017	2.928	170.1	.142	No
56017	2.919	162.8	.152	No
57017	2.402	138.6	.208	No
59017	3.944	173.3	.107	Yes
60017	1.023	229.5	.057	No
61017	1.155	245.7	.048	No
62017	1.384	283.3	.068	No
63017	1.595	215.6	.099	No
64017	2.088	329.3	.079	No
65017	2.357	306.0	.100	No
66017	2.456	307.2	.118	Yes
67017	2.352	333.2	.106	No
68017	2.393	236.1	.135	Yes

TABLE VI. (Cont'd)

Run No.	E_T (Millijoules)	P_p Watts	$\frac{P_{LA}}{P_{HA}}$	Ignition
69017	3.224	306.0	.172	Yes
70017	2.657	272.3	.129	Yes
71017	3.135	312.6	.120	Yes
72017	3.309	290.1	.112	Yes
73017	3.544	313.5	.102	Yes
74017	3.638	266.0	.121	Yes
75017	4.438	321.0	.146	Yes
76017	2.552	329.9	.098	No
77017	2.025	93.8	.249	No
78017	2.070	107.0	.238	No
79017	2.160	103.0	.245	No
80017	2.270	85.0	.276	No
81017	2.540	107.4	.236	No
82017	2.660	100.0	.227	No
83017	3.20	106.0	.220	Yes
84017	3.070	106.0	.203	Yes
85017	3.150	103.0	.232	Yes
86017	3.316	77.4	.299	Yes
87017	3.370	74.7	.330	Yes
88017	3.37	75.0	.347	Yes
89017	3.214	81.8	.320	Yes
90017	2.525	105.7	.233	Yes
91017	2.268	107.1	.228	Yes
92017	2.280	107.1	.235	Yes
93017	2.060	104.1	.235	No
94017	2.038	84.3	.320	No
1017	4.980	95.4	.171	Yes
2017	4.660	86.8	.195	No
3017	6.743	107.3	.242	Yes
4017	4.652	74.8	.223	Yes
5017	4.929	79.3	.200	Yes
6017	4.943	88.0	.200	Yes
7017	4.961	76.9	.249	No
8017	4.318	77.3	.228	No
9017	4.387	93.00	.171	No
10017	3.975	94.70	.153	Yes
11017	4.066	95.20	.152	Yes
12017	4.499	78.70	.234	Yes
13017	3.823	91.3	.242	No
15017	4.323	83.8	.245	Yes
16017	3.536	100.3	.187	No
14017	3.684	105.6	.200	Yes
17017	2.759	80.0	.268	Yes
19017	3.197	74.0	.316	Yes

TABLE VI. (Cont'd)

Run No.	E_T (Millijoules)	P_p Watts	$\frac{P_{LA}}{P_{HA}}$	Ignition
20017	2.528	106.2	.235	Yes
21017	1.309	93.9	.136	No
22017	1.264	99.7	.156	No
23017	1.400	95.1	.201	No
24017	.862	67.2	.191	No
26017	.742	94.4	.08	No
27017	.955	73.5	.182	No
28017	.541	76.3	.083	No
30017	1.676	104.3	.177	No

VIII. CONCLUSIONS AND RECOMMENDATIONS

A. Conclusions

1. For the initial mixture conditions used in this study, minimum ignition energy decreases by approximately 40 percent as the rate of energy input increases by approximately 100 percent.
2. The minimum ignition energy can be correlated with the peak power according to the semi-empirical equation $E_{MIN} P_p^{\nu} = F$.
3. The value of ν increases with decrease in equivalence ratio.
4. The transition band between non-ignition and ignition becomes wider as the equivalence ratio decreases.
5. The transition band decreases in width as the rate of energy input increases.
6. Even under carefully controlled conditions in the constant volume bomb, variations in energy and rates of energy input requirements are appreciable.
7. Information derived from a plot of P_{LA}/P_{HA} versus total energy would be indicative of the adequacy of a conventional engine ignition system for lean mixtures.
8. A plot of P_{LA}/P_{HA} versus total energy can be used to obtain the minimum ignition energy for a pure capacitive spark.

B. Recommendations

1. Future Investigation

a. To determine the cause of the wide transition band, a complete study involving changes of all parameters should be undertaken.

Some of the more important parameters appear to be; fuel type, electrode shape, electrode material and electrode temperature.

b. It appears that experimental data on quench distances at high pressures is lacking in the literature. Therefore, quench distances for higher pressures (i.e., up to 150 psi) would be a contribution.

c. The effect of the electrode flange size upon quenching should be investigated.

d. Effects of the rate of energy input upon the minimum ignition energy should be studied at higher pressures and temperatures.

e. A study of the influence of diluents upon the relationship between the rate of energy input and minimum ignition energy should be made.

f. An exploratory investigation of the energy distribution and molecular makeup of the spark during ignition appears to be a fruitful area of investigation. One possibility would be the use of emission spectroscopy with photomultiplier detectors.

2. Equipment Modification

a. It appears that a decrease in the data reduction time can be accomplished through the use of a diode multiplier. This device could be used for multiplication of the voltage and current during the discharge to produce a power versus time

trace on the oscilloscope. Then the area under the trace on the photographic record could be measured with a planimeter to obtain the energy.

b. Improved data during the initial phase of the discharge could be obtained if two oscilloscopes are used simultaneously. One oscilloscope sweep rate could be set at a fast rate to record the initial phase of the high rate component and the other at a slow rate to record the low rate component.

c. Use of a storage type oscilloscope would reduce the quantity of photographic records during equipment development and data operation.

APPENDIX A

DERIVATION OF PRE-BREAKDOWN CURRENT EQUATIONS

1. Derivation of Equation (3.4), from Reference 59

Assume that a discharge is taking place at a constant applied voltage in Figure A.1.

Consider the differential element dx. Electrons will generate $n_-\alpha dx$ electrons and ions per second while passing through dx.

$$dn_- = \alpha n_- dx \tag{A-1}$$

and

$$n_- = n_o \qquad \text{when} \quad x = 0$$

Similarly

$$dn_+ = -\alpha n_- dx \tag{A-2}$$

where

$$n_+ = 0 \qquad \text{at} \quad x = \delta$$

Integrating Equations (A-1) and (A-2) and multiplying by the electron charge and electrode area gives

$$i_- = i_o e^{\alpha x} \tag{A-3}$$

$$i_+ = i_o (e^{\alpha\delta} - e^{\alpha x}) \tag{A-4}$$

The total current is expressed as follows:

$$i = i_- + i_+ \tag{A-5}$$

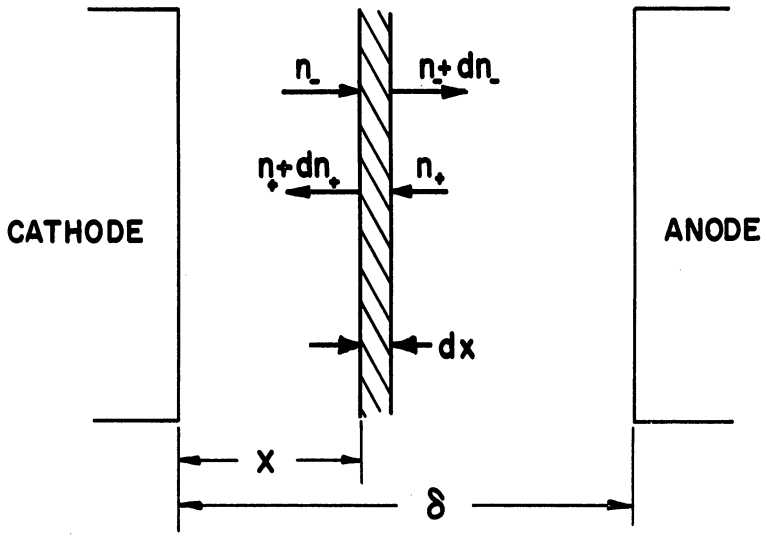

Figure A.1. Pre-Breakdown Current Model.

Therefore:

$$i = i\, e^{\alpha\delta} \tag{3.4}$$

2. Derivation of Equation (3.6) from Reference 59

According to Townsend, each electron produces α ions and electrons per centimeter of pathlength. Each positive ion produces β ions and electrons per centimeter of pathlength. Therefore, under steady conditions of Figure A.1 the following equations apply.

$$dn_- = (\alpha n_- + \beta n_+)dx \tag{A-6}$$

or

$$\frac{dn_-}{dx} = \alpha n_- + \beta n_+$$

also

$$-\frac{dn_+}{dx} = \alpha n_- + \beta n_+ \tag{A-7}$$

Therefore:

$$\frac{dn_-}{dx} + \frac{dn_+}{dx} = 0$$

Since

$$n = n_- + n_+$$

$$\frac{dn_-}{dx} = (\alpha-\beta)n_- + \beta n \tag{A-8}$$

Upon integration of Equation (A-8):

$$n_- = -\frac{\beta}{\alpha-\beta} n + De^{(\alpha-\beta)x} \tag{A-9}$$

Here again

$$n_- = n_o \qquad \text{at} \qquad x = 0$$

Therefore:

$$D = n_o + \frac{\beta}{\alpha-\beta} n \tag{A-10}$$

Also since $n = n_- + n_+$

$$n_+ = \frac{\alpha}{\alpha-\beta} n - D\, e^{(\alpha-\beta)x} \tag{A-11}$$

and

$$n_+ = 0 \qquad \text{at} \qquad x = \delta$$

Thus:

$$D\, e^{(\alpha-\beta)\delta} = \frac{\alpha}{\alpha-\beta} n \tag{A-12}$$

Substitution of Equation (A-10) into Equation (A-12) and multiplying by the electron charge and electrode area yields Equation (3.6)

$$i = i_o \frac{(\alpha-\beta)\, e^{(\alpha-\beta)\delta}}{\alpha-\beta\, e^{(\alpha-\beta)\delta}} \tag{3.6}$$

3. Derivation of Equation (3.8) from Reference 49

Current at the anode is expressed as:

$$i = (i_o + i^+)\, e^{\alpha\delta} \tag{A-13}$$

where i_o is the photocurrent and i^+ is the number of electrons ejected from the cathode due to positive ion bombardment and is expressed as follows:

$$i^+ = \gamma \left[i - (i_o + i^+) \right] \tag{A-14}$$

γ is the number of secondary electrons generated per primary electron which causes an avalanche in the gap.

Elimination of i^+ in Equation (A-13) and (A-14) gives:

$$i = i \frac{e^{\alpha\delta}}{1 - \gamma(e^{\alpha\delta} - 1)} \tag{3.8}$$

4. Derivation of Equation (3.9) from References 64 and 65

The total number of electrons emitted at the cathode is:

$$n' = n_o + \eta z \tag{A-15}$$

where n_o is the number of electrons emitted per second due to photons impinging from outside the system. Z is the number of photons generated in the gas by electrons. η is the fraction of photons which produce electrons which leave the cathode. Therefore, the number of photons produced in an element dx at a distance x from the cathode and available at the cathode is:

$$dz = (n' + n_c)\, g\theta\, e^{-\mu x}\, dx \tag{A-16}$$

where n_c is the number of new electrons created by collision between the cathode and element dx . θ is the number of photons produced by an electron per centimeter of path length in the field direction. μ is the average absorption coefficient of the photons by the gas. g is the geometric factor which represents the fraction of photons which reach the cathode.

The number of new electrons produced in the element dx by collision is:

$$dn_c = (n' + n_c)\, \alpha dx \tag{A-17}$$

where α is the number of ions produced per centimeter of travel, and

$$n_c = n' \quad \text{at} \quad x = 0$$

By integration of Equation (A-17) the following result is obtained:

$$n_c = n'(e^{ax} - 1) \tag{A-18}$$

Then

$$dz = n'g\,\Theta\, e^{(\alpha-\mu)x}\, dx \tag{A-19}$$

In this case

$$Z = 0 \quad \text{at} \quad x = 0$$

Upon integration of Equation (A-19), the number of photons generated in the gas by electrons is expressed as follows:

$$z = \frac{n'g\Theta}{\alpha-\mu}\left[e^{(\alpha-\mu)x} - 1\right] \tag{A-20}$$

By substitution of Equation (A-20) into Equation (A-15), the total number of electrons emitted at the cathode is expressed by the following:

$$n' = \frac{n_o}{1 - \frac{\eta\Theta g}{\alpha-\mu}\left[e^{(\alpha-\mu)x} - 1\right]} \tag{A-21}$$

The number of electrons which reach the element dx at steady state are:

$$n = n' + n_c \tag{A-22}$$

Substitution of Equation (A-18) into Equation (A-22) gives:

$$n = n'\, e^{\alpha x} \tag{A-23}$$

Finally by substitution of (A-21) into (A-23) gives:

$$n = n_o \frac{(\alpha-\mu)e^{\alpha x}}{(\alpha-\mu) - \eta\theta g \left[e^{(\alpha-\mu)x}\right]} \tag{3.9}$$

which is Equation (3.9) when n and n_o are both multiplied by the electron charge and electrode area.

APPENDIX B

DETERMINATION OF INTERELECTRODE CAPACITANCE OF A COIL

Stout[86] discusses a technique which he feels is the most reliable for the determination of the capacitance of a coil such as is shown in Figure B.1.

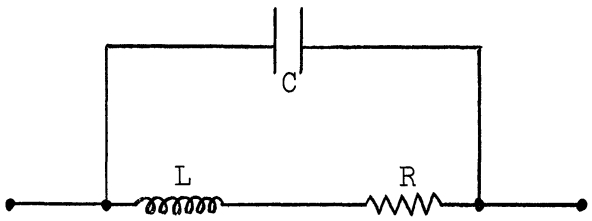

Figure B.1. Equivalent Circuit of a Coil.

It can be shown that the following equation applies to this circuit.

$$\frac{1}{L_e} = \frac{1}{L} - \omega^2 C \qquad \text{(B-1)}$$

where

L_e = equivalent inductance

L = zero frequency inductance

ω = $2\pi f$

f = frequency

C = capacitance

The procedure for obtaining C is to measure L_e as a function of ω using an alternating current bridge. Then plot $\frac{1}{L_e}$ versus ω^2 and the slope of the resultant straight line is equal to

the interelectrode capacitance of the coil. The zero frequency inductance is determined by the $\frac{1}{L_e}$ intercept of the straight line at zero frequency. Tables VII and VIII respectively include the data taken for the secondaries of the Mallory and Delco coils. Figure B.2 is a plot of the data. The results are as follows along with resistances of the secondary coils.

Mallory: $C = 53.5$ pf; $L_o = 55$ henry

$R = 8600$ ohms

Delco: $C = 29.1$ pf; $L_o = 53.6$ henry

$R = 9900$ ohms

The following is a derivation of Equation (B-1). The equivalent impedance is

$$\frac{1}{Z_e} = \frac{1}{R+jX_L} + \frac{1}{-jX_c} = \frac{-jX_c+R+jX_L}{-jX_c(R+jX_L)} \tag{B-2}$$

which can be reduced to the following

$$Z_e = \frac{R+j\left[\omega L(1-\omega^2LC)-R^2C\right]}{\omega^2R^2C^2+(1-\omega^2LC)^2} \tag{B-3}$$

Then taking the imaginary part for the capacitive reactance

$$X_e = \frac{\omega L(1-\omega^2LC)-R^2C}{\omega^2R^2C^2+(1-\omega^2LC)^2} \tag{B-4}$$

Since $R^2C \ll L$, neglect R^2C terms then

$$X_e = \frac{\omega L(1-\omega^2LC)}{(1-\omega^2LC)^2} \tag{B-5}$$

And

$$L_e \approx \frac{L}{1 - \omega^2 LC} \tag{B-6}$$

Finally,

$$\frac{1}{L_e} = \frac{1}{L} - \omega^2 C \ . \tag{B-1}$$

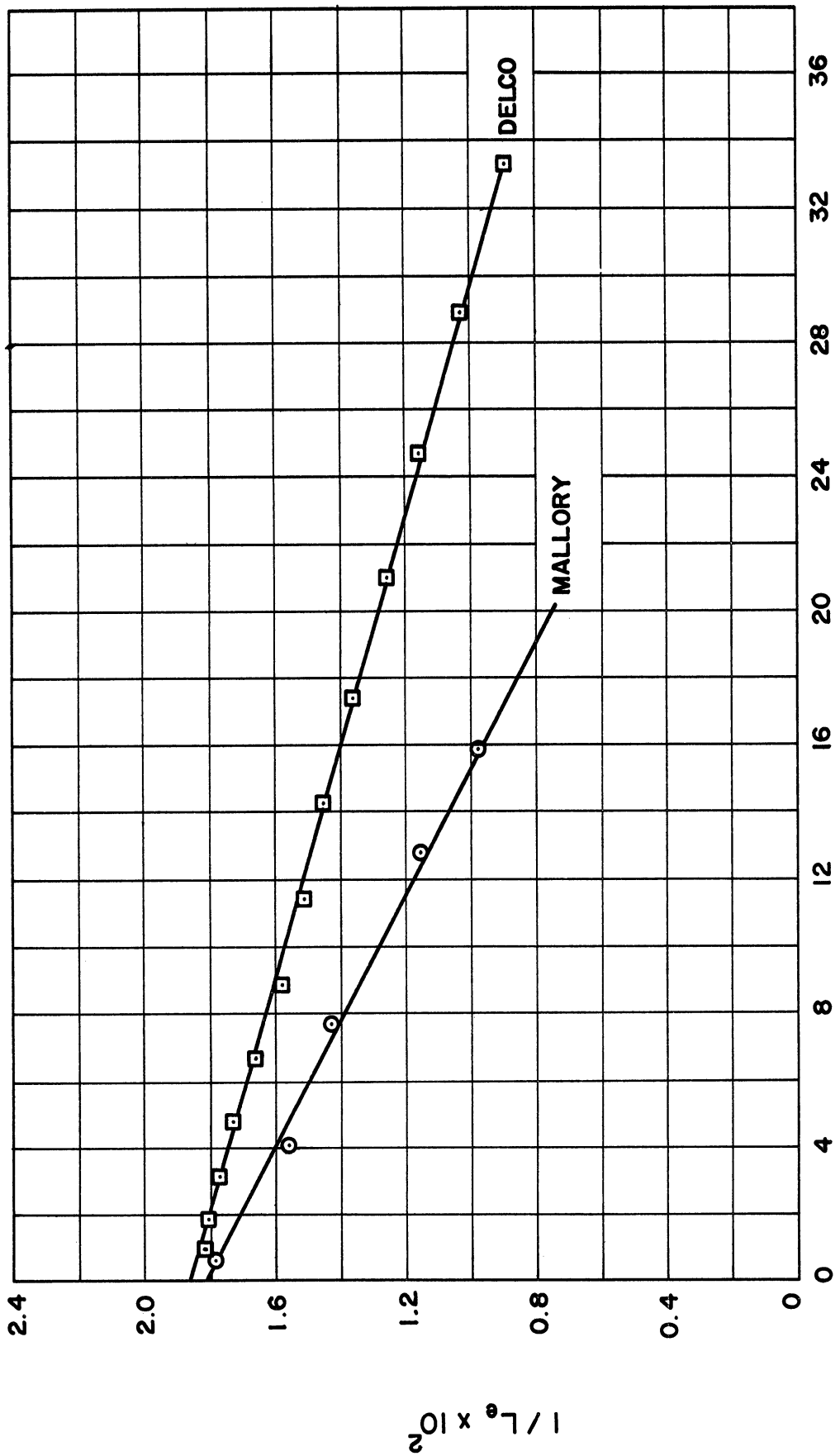

Figure B.2. Determination of Coil Capacitance.

APPENDIX C

DESIGN REQUIREMENT FOR A VOLTAGE DIVIDER

Reference 87 describes a method of construction of a voltage divider for high voltages. If the voltage divider is to operate properly at high frequencies, the divider must be frequency compensated. The following equation must be satisfied if a voltage divider is properly frequency compensated where the distributed capacitance C_1' of the high voltage section is neglected.

$$R_1C_1 = R_eC_e \tag{C-1}$$

where

R_e = equivalent resistance of the low voltage section

C_e = equivalent capacitance of the low voltage section

Derivation of Equation (C-1) follows.

The capacitive reactance is expressed by the following equation

$$X_c = \frac{1}{2\pi fc} \tag{C-2}$$

Therefore:

$$X_{1c} = \frac{1}{2\pi fc_1} \tag{C-3}$$

$$X_{2c} = \frac{1}{2\pi fc_2} \tag{C-4}$$

$$X_{oc} = \frac{1}{2\pi fc} \tag{C-5}$$

The equivalent impedances are

$$\frac{1}{Z_1} = \frac{1}{R_1} + \frac{j}{X_{1c}} \tag{C-6}$$

$$\frac{1}{Z_2} = \frac{1}{R_2} + \frac{j}{X_{2c}} \tag{C-7}$$

$$\frac{1}{Z_o} = \frac{1}{R_o} + \frac{j}{X_{oc}} \tag{C-8}$$

and

$$\frac{1}{Z_e} = \frac{1}{R_2} + \frac{1}{R_o} + j\left(\frac{1}{X_{2c}} + \frac{1}{X_{oc}}\right) \tag{C-9}$$

Therefore:

$$R_e = \frac{R_o R_2}{R_o + R_2} \tag{C-10}$$

and

$$X_{ec} = \frac{1}{2\pi f(C_2+C_o)} \tag{C-11}$$

or

$$C_e = C_o + C_2 \tag{C-12}$$

The current in both parts of the voltage divider must have the same magnitude and phase angle if the output is to be a fixed proportion of the input signal. The necessary condition is that the phase angles in the two parts of the circuit be equal. That is,

$$\tan \theta_e = \tan \theta_1 = \frac{X_{1c}}{R_1} = \frac{X_{ec}}{R_e} \tag{C-13}$$

Substitution of Equation (C-11) and (C-10) into (C-13) and solving:

$$R_1C_1 = R_eC_e = \frac{R_2 R_o}{R_2+R_o}(C_2 + C_o) \qquad (C\text{-}14)$$

Therefore, the capacitor C_2 is made adjustable for frequency compensation. Correct adjustment of C_2 is accomplished by applying a square wave signal to the input, viewing the oscilloscope output, and then adjusting until the output waveform is a square wave.

In voltage dividers which have large attenuation ratios the resistor R_1 will have an appreciable amount of stray capacitance C_1' distributed along its length as shown in Figure C.1. The resultant output waveform after compensation is like that shown in Figure C.2 due to the distributed capacitance for which compensation has not been made.

Compensation for this stray capacitance is a most difficult problem and involves a trial and error procedure. Usually addition of a compensation capacitance between R_1 and point a as shown by C_1'' in Figure C.1 will yield satisfactory results. This final compensation should cause the output waveform to be a perfect square wave.

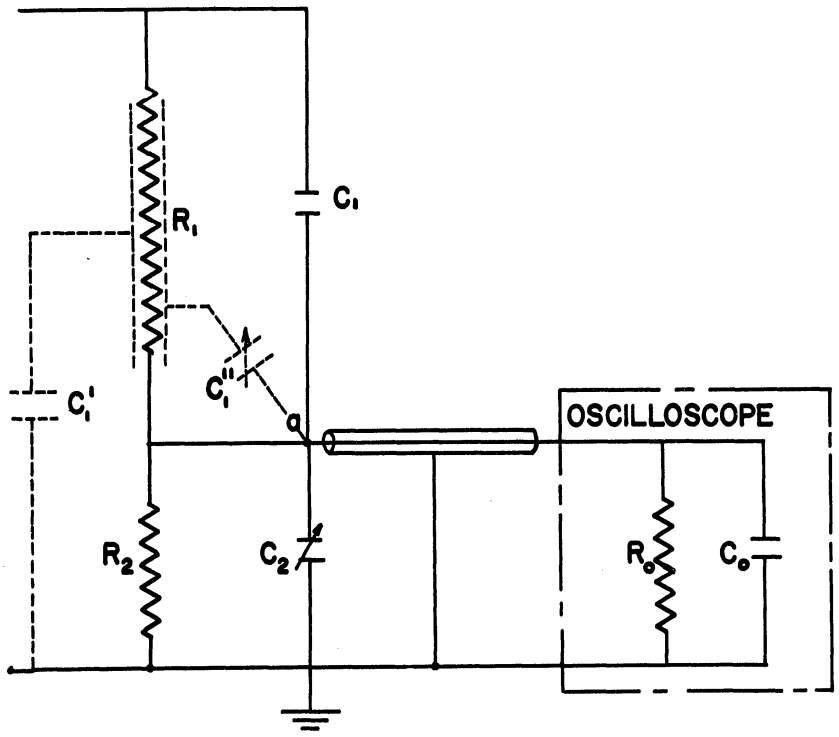

Figure C.1. Voltage Divider Circuit.

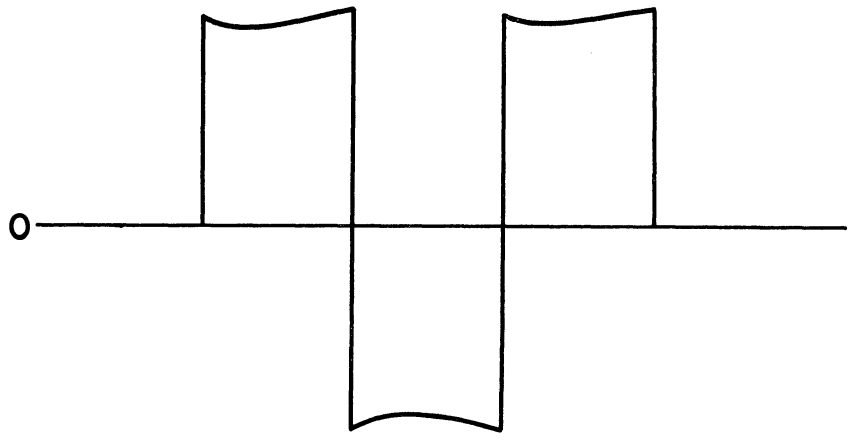

Figure C.2. Voltage Divider Output Incompletely Compensated for Distributed Capacitance.

APPENDIX D

CIRCUIT AND CALIBRATION DATA

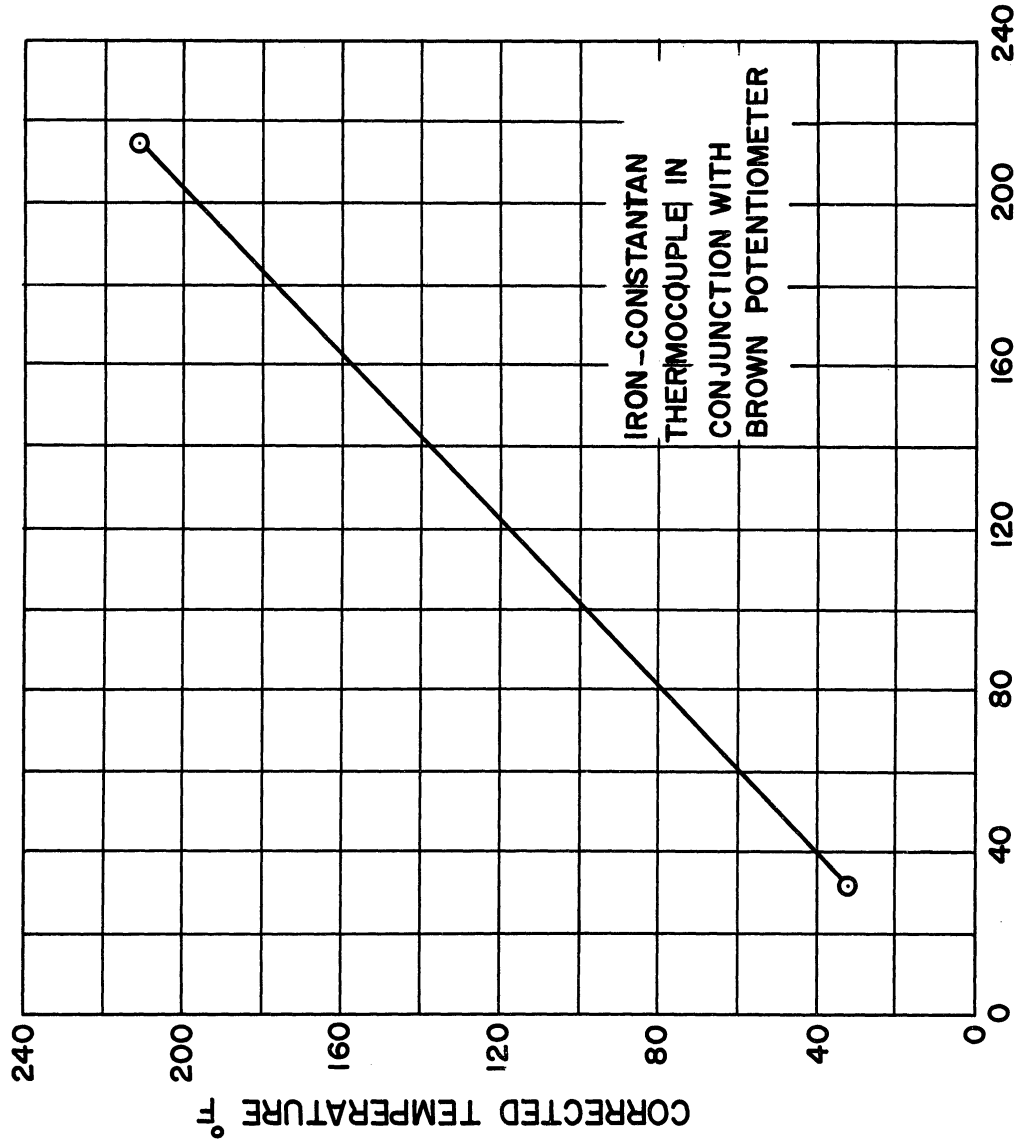

Figure D.1. Thermocouple Calibration Curve.

TABLE VII

SECONDARY CAPACITANCE DATA FOR MALLORY COIL

Model F-12T Coil, Primary Open

f cps	ω X10^{-3}	ω^2 X10^{-7}	L_e (henry)	$1/L_e$ X10^{+2}
400	2.51	.63	55.8	1.79
1000	6.38	4.07	64.0	1.56
1400	8.80	7.75	70.0	1.43
1800	11.30	12.80	87.1	1.15
2000	12.60	15.90	102.0	.98

TABLE VIII

SECONDARY CAPACITANCE DATA FOR DELCO COIL

Model 115251 Coil, Primary Open

f cps	ω X10^{-3}	ω^2 X10^{-7}	L_e (henry)	$1/L_e$ X10^{+2}
500	3.15	.982	55.2	1.81
700	4.40	1.940	55.5	1.80
900	5.66	3.200	56.5	1.77
1100	6.91	4.780	57.8	1.73
1300	8.18	6.690	60.2	1.66
1500	9.43	8.900	63.1	1.58
1700	10.70	11.450	66.4	1.51
1900	11.95	14.300	69.0	1.45
2100	13.20	17.430	73.7	1.36
2300	14.50	21.000	79.2	1.26
2500	15.72	24.700	86.9	1.16
2700	17.00	28.900	97.3	1.03
2900	18.24	33.30	112.2	0.89

TABLE IX

SPARK CONTROL CIRCUIT DATA

R_{1A} = 50Ω, 5w

R_{1B} = 130Ω, 10w

R_2 = 820Ω, 0.5w

R_3 = 0-5K, 10 turn precision pot.

R_4 = 5K, 0.5w

R_5 = 60Ω, 1w

R_6 = 50Ω, 0.5w

R_7 = 1M, 0.5w

R_8 = 3.3K, 0.5w

R_{9A} = 60Ω, 10w

R_{9B} = 60Ω, 10w

R_{10A} = R_{10B} = 30, 10w

R_{11} = 680Ω, 0.5w

R_{12} = 2.7Ω, 2w

R_{13} = 0-6Ω, 10w

R_{14} = 0-4Ω, 125w

R_{15} = 0-4Ω, 125w

R_{16} = variable resistance

R_{17} = 150Ω, ± 1%, 1w

C_1 = 0.005μf

C_2 = 0.01μf

C_{3A} = 1.0μf

C_{3B} = 2.0μf

C_4 = 1.0μf

C_5 = variable capacitance

D_{1A} = D_{1B} = Type 1N100

Q_1 = Q_2 = Type 2N1481

Q_{3A} = Q_{3B} = Type 2N1099

Q_4 = Type 2N1183B

Z_1 = Type 1N3008B

T_1 = Type TA-7 (Stancor)

V_1 = 12 volts

V_2 = 6 volts

V_{3a} = V_{3b} = 3 volts

V_4 = 6 volts

TABLE X

COUNTER CALIBRATION DATA

ERIE MODEL 400 COUNTER

Counting Time Interval (Minutes)	Counter Reading	Correct Reading	Percentage Error
40	2399×10^5	2400×10^5	0.04
40	2400×10^5	2400×10^5	0
45	26998×10^4	27000×10^4	0.0074
5	3000×10^4	3000×10^4	0
5	29987×10^3	30000×10^3	0.04
5	30005×10^3	30000×10^3	0.016
5	29999×10^3	30000×10^3	0.003

TABLE XI.

OSCILLOSCOPE SWEEP RATE DATA

Time Marker Output	Oscilloscope Sweep Rate Setting	Actual Horizontal Deflection	Actual Corrected Sweep Rate
1 msec./cm.	1 msec./cm.	1.00 cm.	1. msec./cm.
1 msec./cm.	0.5 msec./cm.	1.87 cm.	53.5 μsec./cm.
1 msec./cm.	0.2 msec./cm.	4.85 cm.	20.5 μsec./cm.
100 μsec./cm.	100 μsec./cm.	1.00 cm.	100.0 μsec./cm.
100 μsec./cm.	50 μsec./cm.X2 Mag.	1.87 cm.	53.5 μsec./cm.
100 μsec./cm.	50 μsec./cm.	3.73 cm.	21.1 μsec./cm.
100 μsec./cm.	20 μsec./cm.	4.86 cm.	20.5 μsec./cm.
10 μsec./cm.	10 μsec./cm.	1.00 cm.	10.0 μsec./cm.
10 μsec./cm.	20 μsec./cm.X2 Mag.	0.96 cm.	10.4 μsec./cm.

TABLE XII.

PRESSURE GAGE CALIBRATION DATA

Correct psi	Gage Reading Psi (Pressure Decreasing)	Gage Reading Psi (Pressure Increasing)	Average Gage Reading psi	Average Deviation psi (ΔP)
C. L. 01, U. S. Gauge Co., 10861, Supergauge 0-100 psi, 1 psi increments				
5.0	5.2	5.0	5.1	+ 0.1
10.0	10.0	9.7	9.85	- 0.15
15.0	15.2	14.6	14.90	- 0.10
20.0	20.2	19.7	19.95	- 0.05
25.0	25.2	24.5	24.85	- 0.15
30.0	30.3	29.7	30.00	0.00
35.0	35.3	34.7	35.00	0.00
40.0	40.4	39.7	40.05	+ 0.05
45.0	45.4	44.8	45.10	+ 0.10
50.0	50.3	49.8	50.05	+ 0.05
55.0	55.4	54.8	55.10	+ 0.10
60.0	60.3	59.8	60.05	+ 0.05
65.0	65.2	64.8	65.00	0.00
70.0	70.2	69.8	70.00	0.00
75.0	75.3	74.8	75.05	+ 0.05
80.0	80.2	79.8	80.00	0.00
85.0	85.1	84.8	84.95	- 0.05
90.0	90.0	89.8	89.90	- 0.10
95.0	95.2	94.8	95.00	0.00
100.0	99.9	99.7	99.80	- 0.20
C. L. 02, Lonergan Maximon Gauge, 0-300 psi, 5 psi/div.				
15.0	16.5	16.0	16.25	+ 1.25
20.0	21.5	21.0	21.25	+ 1.25
25.0	26.0	25.5	25.75	+ 0.75
30.0	31.0	30.0	30.50	+ 0.50
35.0	35.5	34.5	35.00	0.00
40.0	40.0	39.0	39.75	- 0.25
45.0	45.0	44.0	44.5	- 0.50
50.0	49.0	49.0	48.25	- 0.75
55.0	54.0	54.0	54.0	- 1.00
60.0	59.0	58.5	58.75	- 1.25
65.0	64.5	64.0	64.25	- 0.75
70.0	69.0	68.0	68.50	- 1.50
75.0	74.0	74.0	74.00	- 1.00
80.0	78.5	78.5	78.50	- 1.50
85.0	83.5	83.0	83.25	- 1.75
90.0	88.0	88.5	88.25	- 1.75
95.0	93.0	93.5	93.25	- 1.75

TABLE XII. (Cont'd)

Correct psi	Gage Reading Psi (Pressure Decreasing)	Gage Reading Psi (Pressure Increasing)	Average Gage Reading psi	Average Deviation psi (ΔP)
100.0	98.0	98.0	98.00	- 2.00
105.0	102.5	102.5	102.50	- 2.50
115.0	112.5	112.5	112.50	- 2.50
120.0	117.5	117.5	117.50	- 2.50
125.0	122.5	123.0	122.75	- 2.25
130.0	127.0	127.5	127.25	- 2.75
135.0	132.0	132.0	132.00	- 3.00
140.0	137.0	137.0	137.00	- 3.00
145.0	142.0	142.0	142.00	- 3.00
150.0	147.0	147.0	147.00	- 3.00
155.0	152.0	152.0	152.00	- 3.00
160.0	157.5	157.5	157.50	- 2.50
165.0	162.0	162.5	162.25	- 2.75
170.0	167.0	167.5	167.25	- 2.75
175.0	172.0	172.0	172.00	- 3.00
180.0	177.0	177.0	177.00	- 3.00
185.0	182.0	182.0	182.00	- 3.00
190.0	187.0	187.0	187.00	- 3.00
195.0	192.0	192.0	192.00	- 3.00
200.0	197.0	197.0	197.00	- 3.00
205.0	202.5	202.5	202.50	- 2.50
210.0	207.5	207.5	207.50	- 2.50
215.0	212.5	212.5	212.50	- 2.50
220.0	217.5	217.0	217.25	- 2.50
225.0	223.0	223.0	223.00	- 2.00
230.0	228.0	228.0	228.00	- 2.00
235.0	233.0	233.0	233.00	- 2.00
240.0	238.0	238.0	238.00	- 2.00
245.0	243.0	243.0	243.00	- 2.00
250.0	248.0	248.0	248.00	- 2.00
255.0	253.0	253.0	253.00	- 2.00
260.0	258.0	258.0	258.00	- 2.00
265.0	263.5	263.5	263.50	- 1.50
270.0	268.5	268.5	268.50	- 1.50
275.0	274.0	274.0	274.00	- 1.00
280.0	279.0	279.0	279.00	- 1.00
285.0	284.0	284.0	284.00	- 1.00
290.0	289.5	289.5	289.50	- 0.50
295.0	295.0	295.0	295.00	0.00

TABLE XIII.

FUEL-AIR MIXING INFORMATION

* Lean Limit Ref. 26

ø	A/F (By Vol.)	A/F (By Wt.)	F/A (By Vol.)	F/A (By Wt.)	η in Percent	$\frac{P_f}{P_T}$	P_f in.Hg. for P_T=200psia
1.00	23.80	15.66	.0420	.0639	100.0	.0403	16.46
0.98	24.30	15.98	.0411	.0626	102.0	.0395	16.10
0.96	24.80	16.30	.0403	.0613	104.1	.0388	15.84
0.94	25.30	16.65	.0395	.0600	106.3	.0380	15.50
0.92	25.86	17.00	.0386	.0588	108.7	.0372	15.18
0.90	26.45	17.40	.0378	.0575	111.0	.0365	14.90
0.88	27.04	17.78	.0370	.0563	113.6	.0357	14.57
0.86	27.68	18.20	.0361	.0550	116.2	.0349	14.25
0.84	28.35	18.63	.0353	.0536	119.0	.0341	13.92
0.82	29.00	19.10	.0345	.0523	122.0	.0333	13.60
0.80	29.75	19.57	.0336	.0511	125.0	.0325	13.26
0.78	30.52	20.05	.0328	.0499	128.2	.0318	13.00
0.76	31.32	20.60	.0319	.0485	131.6	.0310	12.66
0.74	32.20	21.15	.0311	.0473	135.0	.0302	12.33
0.72	33.05	21.73	.0325	.0460	139.0	.0293	11.96
0.70	34.00	22.35	.0294	.0448	143.0	.0285	11.63
0.68	35.00	23.00	.0286	.0435	147.0	.0278	11.36
0.66	36.05	23.70	.0278	.0422	151.5	.0270	11.00
0.64	37.20	24.45	.0269	.0409	156.2	.0262	10.70
0.62	38.40	25.25	.0260	.0396	161.2	.0254	10.37
0.60	39.70	26.10	.0252	.0383	166.6	.0246	10.05
0.58	41.00	27.00	.0244	.0370	172.4	.0238	9.72
0.56	42.50	27.95	.0235	.0358	178.6	.0230	9.39
0.54	44.06	29.00	.0227	.0345	135.0	.0222	9.08
0.538	44.20	29.10	.0226	.0344	186.0	.0221	9.01 *
0.52	45.80	30.01	.0218	.0333	192.3	.0214	8.74

APPENDIX E

ORIGINAL DATA

TABLE XIV.

EXPERIMENTAL MIXTURE DATA

Mix No. Tank No.	ø Nominal	Barometer in. Hg.	Barometer ^{o}F	Corr. Barometer in. Hg.	Corr. Barometer psia	P_f in Hg.	P_T psig	Tank Evacuation Pressure Micron Hg.	T ^{o}F Fuel	T ^{o}F Mix	P_T psig Corrected	P_T psia Actual	$\frac{P_f}{P_T}$ Actual	ø Actual
1 A	0.84	29.29	71	29.17	14.33	14.88	200.	125	67.0	69.5	202.5	216.8	.0336	0.83
5 A	0.84	28.95	72	28.83	14.12	13.92	185.9	115	70.0	72.2	188.9	203.0	.0336	0.83
14 A	0.74	29.09	82	28.84	14.14	12.33	185.9	200	79.6	82.4	188.9	203.0	.0297	0.73
17 A	0.70	29.28	75	29.15	14.3	11.63	185.7	50	73.2	75.6	188.7	203.0	.0281	0.69

TABLE XV.

EXPERIMENTAL IGNITION DATA

$\phi = 0.83, \delta = 0.091$ inches

Run No.	Barometer in.Hg.	Barometer Temp °F	Evac. Press.	P_o in. Hg.	T_o °F	I_o Amps.	Scope Settings Kv. cm.	Scope Settings Sw.Rate μ sec. cm.	Scope Settings I v. cm.	Time Constant Settings R	Time Constant Settings C	Ignition
Mallory Coil + 174 K ohms and 50 Pf added through 77 K ohms												
226001	29.55	72	130	30	80	5.0	5.0	53.5	5.0	0.5	1.0	No
227001	29.55	72	130	30	80	5.0	5.0	53.5	5.0	0.75	1.0	No
228001	29.55	72	105	30	80	5.0	5.0	100.0	5.0	1.00	1.0	No
229001	29.55	72	120	30	80	5.0	5.0	100.0	5.0	1.25	1.0	No
230001	29.55	72	110	30	80	5.0	5.0	100.0	5.0	1.50	1.0	Yes
232001	29.55	72	110	30	80	5.0	5.0	100.0	5.0	1.35	1.0	Yes
237001	29.55	72	130	30	80	5.0	5.0	100.0	5.0	1.30	1.0	No
238001	29.55	72	130	30	80	5.0	5.0	100.0	5.0	1.35	1.0	No
241001	29.55	72	130	30	80	5.0	5.0	100.0	5.0	1.40	1.0	Yes
245001	29.51	76	150	30	80	5.0	5.0	100.0	5.0	1.35	1.0	Yes
247001	29.51	76	150	30	80	5.0	5.0	100.0	5.0	1.30	1.0	Yes
249001	29.51	76	135	30	80	5.0	5.0	100.0	5.0	1.30	1.0	No
250001	29.51	76	140	30	80	5.0	5.0	100.0	5.0	1.35	1.0	Yes
Mallory Coil + 174 K ohm and 50 Pf added through 43.5 K ohm												
212001	29.54	72	110	30	80	5.0	5.0	53.5	10.0	0.5	1.0	No
213001	29.54	72	120	30	80	5.0	5.0	53.5	10.0	0.75	1.0	No
214001	29.52	72	110	30	80	5.0	5.0	100.0	10.0	1.00	1.0	No
216001	29.52	72	130	30	80	5.0	5.0	100.0	10.0	1.25	1.0	Yes
217001	29.52	72	125	30	80	5.0	5.0	100.0	10.0	1.25	1.0	Yes
218001	29.52	72	120	30	80	5.0	5.0	100.0	10.0	1.125	1.0	Yes
224001	29.52	72	125	30	80	5.0	5.0	100.0	10.0	1.06	1.0	No
225001	29.52	72	125	30	80	5.0	5.0	100.0	10.0	0.30	1.0	No

TABLE XV. (Cont'd)

Run No.	Barometer in.Hg.	Barometer Temp. °F	Evac. Press. in. Hg.	T_o °F	I_o Amps.	Scope Settings V Kv. cm.	Scope Settings Sw.Rate μ sec. cm.	Scope Settings I v. cm.	Time Constant Settings R	Time Constant Settings C	Ignition
Mallory Coil + 174 K ohm and 50 Pf added through 18 K ohm											
251001	29.41	76	130	30	80	5.0	5.0	53.5	10.0	0.5	1.0	Yes
253001	29.41	76	140	30	80	5.0	5.0	53.5	10.0	0.3	1.0	Yes
254001	29.51	76	140	30	80	5.0	5.0	53.5	10.0	0.25	1.0	No
255001	29.41	76	140	30	80	5.0	5.0	53.5	10.0	0.30	1.0	No
256001	29.41	76	145	30	80	5.0	5.0	53.5	10.0	0.30	1.0	Yes
257001	29.41	76	150	30	80	5.0	5.0	53.5	10.0	0.20	1.0	Yes
258001	29.41	76	150	30	80	5.0	5.0	53.5	10.0	0.18	1.0	No
259001	29.41	76	150	30	80	5.0	5.0	53.5	10.0	0.30	1.0	Yes
260001	29.41	76	150	30	80	5.0	5.0	53.5	10.0	0.40	1.0	Yes
261001	29.41	76	150	30	80	5.0	5.0	53.5	10.0	0.35	1.0	Yes
263001	29.40	76	150	30	80	5.0	5.0	53.5	10.0	0.35	1.0	Yes
264001	29.40	76	150	30	80	5.0	5.0	53.5	10.0	0.30	1.0	Yes
266001	29.40	76	155	30	80	5.0	5.0	53.5	10.0	0.30	1.0	No
267001	29.40	76	150	30	80	5.0	5.0	53.5	10.0	0.35	1.0	Yes
268001	29.40	76	150	30	80	5.0	5.0	53.5	10.0	0.18	1.0	Yes

TABLE XVI.

EXPERIMENTAL IGNITION DATA

$\phi = 0.83$; $\delta = 0.122$ inches

Run No.	Barometer in.Hg.	Barometer Temp. °F	Evac. Press. in. Hg.	T_o °F	I_o Amps.	Scope Settings V Kv/cm.	Scope Settings Sw.Rate μsec./cm.	Scope Settings I v./cm.	Time Constant Settings R	Time Constant Settings C	Ignition
Mallory Coil + 174 K ohm											
180005	29.04	73	135	30	81	5.0	2.0	100.0	2.0	0.4	1.0	Yes
181005	29.04	73	130	30	80	5.0	2.0	53.5	2.0	0.3	1.0	Yes
182005	29.04	73	135	30	80	5.0	2.0	20.5	2.0	0.2	1.0	No
183005	29.05	75	135	30	80	5.0	2.0	20.5	2.0	0.2	1.0	No
184005	29.05	75	140	30	80	5.0	2.0	20.5	2.0	0.2	1.0	No
186005	29.05	74	150	30	80	5.0	2.0	20.5	2.0	0.15	1.0	No
188005	29.05	74	135	30	80	5.0	2.0	20.5	2.0	0.15	1.0	No
189005	29.05	74	135	30	80	5.0	2.0	20.5	2.0	0.2	1.0	No
190005	29.05	75	140	30	80	5.0	2.0	20.5	2.0	0.3	1.0	Yes
191005	29.05	75	150	30	80	5.0	2.0	20.5	2.0	0.25	1.0	Yes
192005	29.05	75	135	30	80	5.0	2.0	20.5	2.0	0.22	1.0	No
193005	29.05	75	145	30	80	5.0	2.0	20.5	2.0	0.23	1.0	No
194005	29.05	75	150	30	80	5.0	2.0	20.5	2.0	0.24	1.0	No
195005	29.05	75	145	30	80	5.0	2.0	20.5	2.0	0.25	1.0	No
196005	29.05	75	150	30	80	5.0	2.0	20.5	2.0	0.27	1.0	No
197005	29.13	75	150	30	80	5.0	2.0	20.5	2.0	0.30	1.0	No
198005	29.13	75	145	30	80	5.0	2.0	20.5	2.0	0.35	1.0	No
199005	29.13	75	140	30	80	5.0	2.0	20.5	2.0	0.4	1.0	Yes
200005	29.13	75	135	30	80	5.0	2.0	20.5	2.0	0.3	1.0	No
201005	29.13	75	135	30	80	5.0	2.0	20.5	2.0	0.5	1.0	Yes
202005	29.13	75	135	30	80	5.0	2.0	20.5	2.0	0.45	1.0	Yes
203005	29.13	75	135	30	80	5.0	2.0	53.5	2.0	0.6	1.0	Yes

TABLE XVI. (Cont'd)

Run No.	Barometer in.Hg.	Barometer Temp. °F	Evac. Press.	in. Hg.	T_o °F	I_o Amps.	Scope Settings V Kv / cm.	Scope Settings Sw.Rate μsec. / cm.	Scope Settings I v. / cm.	Time Constant Settings R	Time Constant Settings C	Ignition
Mallory Coil + 256 K ohm * 25 Pf added through 125 K ohm												
204005	29.29	74	120	30	80	5.0	2.0	20.5	2.0	0.5	1.0	Yes
205005	29.29	74	125	30	80	5.0	2.0	20.5	2.0	0.4	1.0	No
206005	29.29	74	125	30	80	5.0	2.0	20.5	2.0	0.4	1.0	Yes
207005	29.29	74	130	30	80	5.0	2.0	20.5	2.0	0.3	1.0	No
209005	29.29	74	135	30	80	5.0	2.0	20.5	2.0	0.2	1.0	No
211005	29.29	74	160	30	80	5.0	2.0	20.5	2.0	0.25	1.0	No
212005	29.29	77	145	30	80	5.0	2.0	20.5	2.0	0.25	1.0	No
213005	29.42	69	95	30	80	5.0	2.0	20.5	2.0	0.35	1.0	Yes
214005	29.42	70	98	30	80	5.0	2.0	20.5	2.0	0.3	1.0	No
215005	29.42	70	115	30	80	5.0	2.0	20.5	2.0	0.4	1.0	No
216005	29.42	70	115	30	80	5.0	2.0	20.5	2.0	0.4	1.0	Yes
217005	29.42	70	125	30	80	5.0	2.0	20.5	2.0	0.45	1.0	Yes
218005	29.42	70	120	30	80	5.0	2.0	53.3	2.0	0.55	1.0	Yes
219005	29.41	73	120	30	80	5.0	2.0	20.5	2.0	0.2	1.0	No
220005	29.41	73	125	30	80	5.0	2.0	20.5	2.0	0.3	1.0	No
221005	29.41	73	125	30	80	5.0	2.0	20.5	2.0	0.35	1.0	No
223005	29.40	74	140	30	80	5.0	2.0	20.5	2.0	0.18	1.0	No*
Mallory Coil + 256 K ohm and 50 Pf added through 125 K ohm												
224005	29.40	74	135	30	80	5.0	2.0	20.5	2.0	0.2	1.0	No
225005	29.40	74	135	30	81	5.0	2.0	20.5	2.0	0.25	1.0	No
226005	29.40	74	135	30	80	5.0	2.0	20.5	2.0	0.30	1.0	Yes
227005	29.40	74	140	30	80	5.0	2.0	20.5	2.0	0.25	1.0	Yes
228005	29.40	74	150	30	79	5.0	2.0	20.5	2.0	0.22	1.0	No
229005	29.40	74	150	30	80	5.0	2.0	20.5	2.0	0.22	1.0	No

TABLE XVI. (Cont'd)

Run No.	Barometer in.Hg.	Barometer Temp. °F	Evac. Press.	in Hg.	T_o °F	I_o Amps.	Scope Settings V Kv/cm.	Scope Settings Sw.Rate μsec./cm.	Scope Settings I v./cm.	Time Constant Settings R	Time Constant Settings C	Ignition
Mallory Coil + 256 K ohm and 50 Pf added through 125 K ohm												
230005	29.40	74	140	30	80	5.0	2.0	20.5	2.0	0.20	1.0	No
231005	29.40	74	140	30	80	5.0	2.0	20.5	2.0	0.18	1.0	No
231105	29.40	74	140	30	80	5.0	2.0	20.5	2.0	0.18	1.0	No
232005	29.40	74	145	30	80	5.0	2.0	20.5	2.0	0.27	1.0	No
233005	29.40	74	145	30	80	5.0	2.0	20.5	2.0	0.27	1.0	No
234005	29.40	77	150	30	80	5.0	2.0	20.5	2.0	0.30	1.0	Yes
235005	29.40	77	150	30	80	5.0	2.0	20.5	2.0	0.35	1.0	Yes
236005	29.40	77	150	30	80	5.0	2.0	20.5	2.0	0.4	1.0	Yes
237005	29.40	77	155	30	80	5.0	2.0	53.5	2.0	0.5	1.0	Yes
Mallory Coil + 256 K ohm and 25 Pf added through 25.5 K ohm												
255005	29.55	70	100	30	80	5.0	2.0	20.5	5.0	0.36	1.0	No
256005	29.55	78	140	30	80	5.0	2.0	20.5	5.0	0.40	1.0	Yes
257005	29.55	78	150	30	80	5.0	2.0	20.5	5.0	0.36	1.0	No
258005	29.55	78	155	30	80	5.0	2.0	20.5	5.0	0.38	1.0	Yes
259005	29.55	78	155	30	80	5.0	2.0	20.5	5.0	0.36	1.0	No
261005	29.55	80	170	30	80	5.0	2.0	20.5	5.0	0.40	1.0	Yes
263005	29.52	82	195	30	80	5.0	2.0	20.5	5.0	0.40	1.0	No
264005	29.48	82	200	30	80	5.0	2.0	20.5	5.0	0.43	1.0	No
265005	29.48	82	200	30	80	5.0	2.0	20.5	5.0	0.45	1.0	Yes
266005	29.48	82	200	30	80	5.0	2.0	20.5	5.0	0.50	1.0	Yes
267005	29.48	82	200	30	80	5.0	2.0	20.5	5.0	0.50	1.0	Yes

TABLE XVII.

EXPERIMENTAL IGNITION DATA

$\phi = 0.73$; $\delta = 0.195$ inches

Run No.	Barometer in.Hg.	Barometer Temp. °F	Evac. Press.	in. Hg.	T_o °F	I_o Amps.	Scope Settings V Kv/cm.	Scope Settings Sw.Rate μsec./cm.	Scope Settings I v./cm.	Time Constant Settings R	Time Constant Settings C	Ignition
Delco Coil + 249.5 K ohm												
10014	29.20	75	120	30	80	4.6	5.0	100.0	5.0	1.0	1.0	Yes
20014	29.20	75	125	30	80	4.6	5.0	53.5	5.0	0.5	1.0	No
30014	29.20	79	130	30	80	4.6	2.0	53.5	2.0	0.5	1.0	No
40014	29.20	79	130	30	80	4.6	2.0	53.5	2.0	0.5	1.0	No
60014	29.20	79	140	30	80	4.6	2.0	53.5	2.0	0.70	1.0	Yes
70014	29.20	79	130	30	80	4.6	2.0	53.5	2.0	0.70	1.0	Yes
80014	29.23	81	150	30	80	4.6	2.0	53.5	2.0	0.70	1.0	No
90014	29.23	81	135	30	80	4.6	2.0	53.5	2.0	0.70	1.0	No
100014	29.23	81	75	30	80	4.6	2.0	53.5	2.0	0.8	1.0	No
110014	29.23	81	100	30	80	4.6	2.0	53.5	2.0	0.8	1.0	No
120014	29.23	81	150	30	80	4.6	2.0	53.5	2.0	0.85	1.0	Yes
130014	29.23	81	145	30	80	4.6	2.0	53.5	2.0	0.85	1.0	Yes
140014	29.23	81	120	30	80	4.6	2.0	53.5	2.0	0.85	1.0	Yes
150014	29.23	81	145	30	80	4.6	2.0	53.5	2.0	0.80	1.0	Yes
160014	29.23	81	125	30	80	4.6	2.0	53.5	2.0	0.80	1.0	Yes
180014	29.23	81	150	30	80	4.6	2.0	53.5	2.0	0.75	1.0	No
190014	29.23	81	130	30	80	4.6	2.0	53.5	2.0	0.75	1.0	No
200014	29.23	81	170	30	80	4.6	2.0	53.5	2.0	0.60	1.0	No
210014	29.23	81	125	30	80	4.6	2.0	53.5	2.0	0.5	1.0	No
220014	29.23	81	150	30	80	4.6	2.0	53.5	2.0	0.5	1.0	No
240014	29.23	81	160	30	80	4.6	2.0	53.5	2.0	0.8	1.0	Yes
250014	29.23	81	150	30	80	4.6	2.0	53.5	2.0	0.9	1.0	Yes
280014	29.23	81	130	30	80	4.6	2.0	53.5	2.0	1.0	1.0	No

TABLE XVII. (Cont'd)

Run No.	Barometer in.Hg.	Barometer Temp. °F	Evac. Press.	T_o in. Hg.	T_o °F	I_o Amps.	Scope Settings V Kv/cm.	Scope Settings Sw.Rate μsec./cm.	Scope Settings I v./cm.	Time Constant Settings R	Time Constant Settings C	Ignition
Delco Coil + 249.5 K ohm												
290014	29.23	81	140	30	80	4.6	2.0	53.5	2.0	1.0	1.0	Yes
300014	29.23	81	175	30	80	4.6	2.0	53.5	2.0	0.8	1.0	No
Delco Coil + 249.5 K ohm and 25 Pf added through 118 K ohm												
320014	29.23	76	105	30	80	5.0	2.0	20.5	2.0	0.4	1.0	No
330014	29.23	76	140	30	80	5.0	2.0	20.5	2.0	0.5	1.0	No
340014	29.23	76	120	30	80	5.0	2.0	20.5	2.0	0.5	1.0	No
350014	29.23	76	140	30	80	5.0	2.0	20.5	2.0	0.6	1.0	No
360014	29.23	76	100	30	80	5.0	2.0	20.5	2.0	0.6	1.0	No
370014	29.23	76	130	30	80	5.0	2.0	53.5	2.0	0.7	1.0	No
380014	29.23	76	125	30	80	5.0	2.0	53.5	2.0	0.8	1.0	Yes
390014	29.23	76	105	30	80	5.0	2.0	53.5	2.0	0.7	1.0	Yes
400014	29.23	76	130	30	80	5.0	2.0	53.5	2.0	0.6	1.0	Yes
410014	29.23	76	125	30	80	5.0	2.0	53.5	2.0	0.6	1.0	No
420014	29.23	75	135	30	80	5.0	2.0	53.5	2.0	0.55	1.0	No
430014	29.23	75	105	30	80	5.0	2.0	53.5	2.0	0.8	1.0	No
440014	29.23	75	90	30	80	5.0	2.0	53.5	2.0	0.8	1.0	Yes
450014	29.23	75	85	30	80	5.0	2.0	53.5	2.0	0.9	1.0	Yes
460014	29.23	75	100	30	80	5.0	2.0	53.5	2.0	1.0	1.0	Yes
470014	29.23	75	110	30	80	5.0	2.0	53.5	2.0	1.1	1.0	Yes
480014	29.23	75	80	30	80	5.0	2.0	53.5	2.0	0.7	1.0	No
490014	29.23	75	80	30	80	5.0	2.0	53.5	2.0	0.8	1.0	Yes
500014	29.23	75	160	30	80	5.0	2.0	53.5	2.0	0.5	1.0	No
510014	29.23	72	85	30	80	5.0	2.0	53.5	2.0	0.4	1.0	No

TABLE XVII (Cont'd)

Run No.	Barometer in.Hg.	Barometer Temp. °F	Evac. Press.	in. Hg.	T_o °F	I_o Amps.	Scope Settings V Kv/cm.	Scope Settings Sw.Rate μ sec./cm.	Scope Settings I v./cm.	Time Constant Settings R	Time Constant Settings C	Ignition
Delco Coil & 249.5 K ohm and 25 pf added through 52 K ohm												
540014	29.23	72	95	30	80	5.0	2.0	20.5	5.0	0.40	1.0	No
550014	29.24	76	160	30	80	5.0	2.0	20.5	5.0	0.40	1.0	No
560014	29.24	76	90	30	80	5.0	2.0	20.5	5.0	0.5	1.0	No
570014	29.24	76	95	30	80	5.0	2.0	20.5	5.0	0.5	1.0	No
580014	29.24	76	100	30	80	5.0	2.0	20.5	5.0	0.6	1.0	No
590014	29.24	74	105	30	80	5.0	2.0	20.5	5.0	0.6	1.0	Yes
600014	29.24	74	70	30	80	5.0	2.0	53.5	5.0	0.7	1.0	Yes
610014	29.24	74	100	30	80	5.0	2.0	53.5	5.0	0.8	1.0	Yes
620014	29.24	74	75	30	80	5.0	2.0	53.5	5.0	0.9	1.0	Yes
630014	29.24	74	120	30	80	5.0	2.0	53.5	5.0	0.75	1.0	No
640014	29.24	74	90	30	80	5.0	2.0	53.5	5.0	0.65	1.0	Yes
650014	29.24	74	80	30	80	5.0	2.0	20.5	5.0	0.55	1.0	No
660014	29.24	74	95	30	80	5.0	2.0	20.5	5.0	0.45	1.0	No

TABLE XVIII.

EXPERIMENTAL IGNITION DATA

$\phi = 0.69$; $\delta = 0.254$ inches

Run No.	Barometer in.Hg.	Barometer Temp. °F	Evac. Press.	T_o in. Hg.	T_o °F	I_o Amps.	Scope Settings V Kv/cm.	Scope Settings Sw.Rate μ sec./cm.	Scope Settings I v./cm.	Time Constant Settings R	Time Constant Settings C	Ignition
Delco Coil + 249.5 K ohm												
10017	29.42	80	55	30	80	5.0	2.0	100.0	5.0	3.0	1.0	Yes
20017	29.42	80	60	30	80	5.0	2.0	100.0	2.0	3.0	1.0	No
30017	29.42	80	70	30	80	5.0	2.0	100.0	2.0	3.5	1.0	Yes
40017	29.42	80	73	30	80	5.0	2.0	100.0	2.0	3.5	1.0	Yes
50017	29.42	80	70	30	80	5.0	2.0	100.0	2.0	3.0	1.0	Yes
60017	29.42	80	70	30	80	5.0	2.0	100.0	2.0	2.5	1.0	Yes
70017	29.42	80	75	30	80	5.0	2.0	100.0	2.0	2.0	1.0	No
80017	29.42	80	85	30	80	5.0	2.0	100.0	2.0	2.0	1.0	No
90017	29.42	80	85	30	80	5.0	2.0	100.0	2.0	2.25	1.0	No
100017	29.42	80	85	30	80	5.0	2.0	100.0	2.0	2.25	1.0	Yes
110017	29.42	80	85	30	80	5.0	2.0	100.0	2.0	2.25	1.0	Yes
120017	29.41	85	90	30	80	5.0	2.0	100.0	2.0	2.00	1.0	Yes
130017	29.41	85	90	30	80	5.0	2.0	100.0	2.0	1.50	1.0	No
140017	29.41	85	90	30	80	5.0	2.0	100.0	2.0	1.50	1.0	No
150017	29.41	85	95	30	80	5.0	2.0	100.0	2.0	1.75	1.0	Yes
160017	29.41	85	95	30	80	5.0	2.0	100.0	2.0	1.50	1.0	Yes
170017	29.41	85	95	30	80	5.0	2.0	100.0	2.0	1.25	1.0	Yes
190017	29.41	85	95	30	80	5.0	2.0	53.5	2.0	1.25	1.0	Yes
200017	29.41	85	100	30	80	5.0	2.0	53.5	2.0	1.0	1.0	Yes
210017	29.41	85	95	30	80	5.0	2.0	53.5	2.0	0.5	1.0	No
220017	29.41	85	100	30	80	5.0	2.0	20.5	2.0	0.5	1.0	No
230017	29.41	85	95	30	80	5.0	2.0	20.5	2.0	0.5	1.0	No
240017	29.41	82	95	30	80	5.0	2.0	20.5	2.0	0.4	1.0	No

TABLE XVIII. (Cont'd)

Run No.	Barometer in.Hg.	Barometer Temp. °F	Evac. Press.	in. Hg.	T_o °F	I_o Amps.	Scope Settings V Kv/cm.	Scope Settings Sw.Rate μsec./cm.	Scope Settings I v./cm.	Time Constant Settings R	Time Constant Settings C	Ignition
Delco Coil + 249.5 K ohm												
260017	29.41	82	85	30	80	5.0	2.0	20.5	2.0	0.4	1.0	No
270017	29.41	82	80	30	80	5.0	2.0	20.5	2.0	0.4	1.0	No
280017	29.41	82	90	30	80	5.0	2.0	20.5	2.0	0.3	1.0	No
300017	29.41	80	90	30	80	5.0	2.0	53.5	2.0	0.6	1.0	No
310017	29.41	80	85	30	80	5.0	2.0	53.5	2.0	0.7	1.0	No
320017	29.41	80	70	30	80	5.0	2.0	53.5	2.0	0.8	1.0	No
330017	29.41	80	70	30	80	5.0	2.0	53.5	2.0	0.8	1.0	No
340017	29.41	80	100	30	80	5.0	2.0	53.5	2.0	0.8	1.0	No
350017	29.41	80	65	30	80	5.0	2.0	53.5	2.0	1.0	1.0	No
360017	29.41	80	80	30	80	5.0	2.0	53.5	2.0	1.10	1.0	No
370017	29.41	80	90	30	80	5.0	2.0	53.5	2.0	1.20	1.0	Yes
Delco Coil + 249.5 K ohm and 25 Pf added through 149.5 K ohm												
380017	29.41	77	85	30	80	5.0	2.0	53.5	2.0	1.20	1.0	No
390017	29.41	77	70	30	80	5.0	2.0	53.5	2.0	1.30	1.0	No
400017	29.41	77	70	30	80	5.0	2.0	53.5	2.0	1.30	1.0	No
410017	29.41	77	70	30	80	5.0	2.0	53.5	2.0	1.40	1.0	Yes
420017	29.41	77	65	30	80	5.0	2.0	53.5	2.0	1.50	1.0	No
430017	29.41	77	65	30	80	5.0	2.0	53.5	2.0	1.50	1.0	No
440017	29.41	77	65	30	80	5.0	2.0	53.5	2.0	1.60	1.0	No
450017	29.41	77	60	30	80	5.0	2.0	53.5	2.0	1.70	1.0	Yes
460017	29.41	77	70	30	80	5.0	2.0	53.5	2.0	1.70	1.0	No
480017	29.41	77	80	30	80	5.0	2.0	53.5	2.0	1.80	1.0	Yes
490017	29.41	79	75	30	80	5.0	2.0	53.5	2.0	1.90	1.0	Yes
500017	29.41	79	70	30	80	5.0	2.0	53.5	2.0	2.00	1.0	No

TABLE XVIII. (Cont'd)

Run No.	Barometer in.Hg.	Barometer Temp. °F	Evac. Press.	in. Hg.	T_o °F	I_o Amps.	Scope Settings V Kv/cm.	Scope Settings Sw.Rate μ sec./cm.	Scope Settings I v./cm.	Time Constant Settings R	Time Constant Settings C	Ignition
Delco Coil + 249.5 K ohm and 25 Pf added through 149.5 K ohm												
510017	29.41	79	70	30	80	5.0	2.0	53.5	2.0	2.0	1.0	Yes
520017	29.41	79	70	30	80	5.0	2.0	53.5	2.0	2.0	1.0	Yes
530017	29.41	79	80	30	80	5.0	2.0	53.5	2.0	2.2	1.0	Yes
540017	29.41	79	100	30	80	5.0	2.0	53.5	2.0	1.8	1.0	No
550017	29.41	79	90	30	80	5.0	2.0	53.5	2.0	1.4	1.0	No
560017	29.47	80	70	30	80	5.0	2.0	53.5	2.0	1.4	1.0	No
570017	29.47	80	80	30	80	5.0	2.0	53.5	2.0	1.0	1.0	No
590017	29.47	80	100	30	80	5.0	2.0	53.5	2.0	2.4	1.0	Yes
Delco Coil + 249.5 K ohm and 25 Pf added through 49.5 K ohm												
600017	29.43	81	95	30	80	5.0	2.0	20.5	5.0	0.5	1.0	No
610017	29.43	81	100	30	80	5.0	2.0	20.5	5.0	0.5	1.0	No
620017	29.43	81	125	30	80	5.0	2.0	20.5	5.0	0.6	1.0	No
630017	29.43	81	100	30	80	5.0	2.0	20.5	5.0	0.7	1.0	No
640017	29.43	81	100	30	80	5.0	2.0	20.5	5.0	0.8	1.0	No
650017	29.43	81	90	30	80	5.0	2.0	53.5	5.0	0.9	1.0	No
660017	29.43	81	95	30	80	5.0	2.0	53.5	5.0	1.0	1.0	Yes
670017	29.43	81	90	30	80	5.0	2.0	53.5	5.0	0.9	1.0	No
680017	29.43	81	85	30	80	5.0	2.0	53.5	5.0	1.0	1.0	Yes
690017	29.43	81	100	30	80	5.0	2.0	53.5	5.0	1.1	1.0	Yes
700017	29.43	81	85	30	80	5.0	2.0	53.5	5.0	1.2	1.0	Yes
710017	29.43	81	100	30	80	5.0	2.0	53.5	5.0	1.3	1.0	Yes
720017	29.43	81	100	30	80	5.0	2.0	53.5	5.0	1.4	1.0	Yes
730017	29.43	81	90	30	80	5.0	2.0	53.5	5.0	1.5	1.0	Yes
740017	29.43	81	90	30	80	5.0	2.0	53.5	5.0	1.6	1.0	Yes

TABLE XVIII (Cont'd)

Run No.	Barometer in.Hg.	Barometer Temp. °F	Evac. Press.	in. Hg.	T_o °F	I_o Amps.	Scope Settings V Kv/cm.	Scope Settings Sw.Rate μ sec./cm.	Scope Settings I v./cm.	Time Constant Settings R	Time Constant Settings C	Ignition
Delco Coil + 249.5 K ohm and 25 Pf added through 49.5 K ohm												
750017	29.43	81	100	30	80	5.0	2.0	53.5	5.0	1.7	1.0	Yes
760017	29.43	81	100	30	80	5.0	2.0	53.5	5.0	0.95	1.0	No
Delco Coil + 249.5 K ohm												
770017	29.43	81	90	30	80	5.0	2.0	20.5	2.0	0.7	1.0	No
780017	29.43	81	100	30	80	5.0	2.0	20.5	2.0	0.8	1.0	No
790017	29.43	81	90	30	80	5.0	2.0	20.5	2.0	0.9	1.0	No
800017	29.43	81	105	30	80	5.0	2.0	20.5	2.0	1.0	1.0	No
810017	29.43	81	90	30	80	5.0	2.0	53.5	2.0	1.1	1.0	No
820017	29.43	81	120	30	80	5.0	2.0	53.5	2.0	1.3	1.0	No
830017	29.43	81	85	30	80	5.0	2.0	53.5	2.0	1.5	1.0	Yes
840017	29.43	81	100	30	80	5.0	2.0	53.5	2.0	1.5	1.0	Yes
850017	29.43	81	95	30	80	5.0	2.0	53.5	2.0	1.4	1.0	Yes
860017	29.43	81	100	30	80	5.0	2.0	53.5	2.0	1.35	1.0	Yes
870017	29.43	81	105	30	80	5.0	2.0	53.5	2.0	1.3	1.0	Yes
880017	29.43	81	90	30	80	5.0	2.0	53.5	2.0	1.2	1.0	Yes
890017	29.43	81	95	30	80	5.0	2.0	53.5	2.0	1.1	1.0	Yes
900017	29.43	80	105	30	80	5.0	2.0	53.5	2.0	1.0	1.0	Yes
910017	29.43	80	90	30	80	5.0	2.0	53.5	2.0	0.9	1.0	Yes
920017	29.43	80	95	30	80	5.0	2.0	53.5	2.0	0.9	1.0	Yes
930017	29.43	80	95	30	80	5.0	2.0	53.5	2.0	0.8	1.0	No
940017	29.43	80	105	30	80	5.0	2.0	53.5	2.0	0.7	1.0	No

APPENDIX F

DATA REDUCTION

Data for each spark consists of the photograph of the voltage and current traces and the corresponding initial temperature and pressure readings, etc., which are listed in Tables XIV through XVIII. A typical photograph is shown in Figure F.1. The traces shown on the photograph were broken up into small time increments such that the curves could be closely approximated by straight segments. Values of voltage, current and time were tabulated at each of the time increments. The data was then punched on IBM cards for computer analysis. The computer solution follows the procedure outlined by the flow diagram shown in Figure F.2.

Samples of the computer output are shown in Figures F.3 and F.4. The last column on the right of Figure F.3 is the list of the cumulative energy values for each time increment up to the total. The transition point between the E_H and E_L components of the spark was chosen at the knee of the curve shown in Figure F.4. The corresponding value of P_{LA}/P_{HA} is found in the second set of tabulated values in Figure F.3. The following symbols are used in the computer program and in the flow diagram.

A = voltage divider attenuation ratio

AVHP(J) = PHA

AVHP(J) = PLA

B = constant required in calculation in amperes from centimeters

BAR = barometer reading

CA(J) = amplitude of current trace in centimeters at DELTA(J)

CAP = capacitance setting in pulse circuit

CBAR = corrected barometer

C(J) = current in milliamperes

CS = oscilloscope setting for current

DELTA(J) = time increment in centimeters measured from point of breakdown

DELT(J) = time interval between each point in centimeters

E (J) = energy in millijoules for each time interval T (J)

GAP = electrode spacing

K = a constant used in calculation of corrected pressure

M = constant referring to total number of elements the voltage and current traces were broken up into

PC = primary current

P (J) = power in milliwatts

PRESS 1 = initial pressure in psig or inches of mercury absolute

PRESS 2 = initial pressure converted to inches of mercury absolute

R = resistance setting in pulse circuit

RATIO = P_{LA}/P_{HA}

RN = run number

SRT = oscilloscope setting for sweep rate, in μsec/cm

SUM(J) = cummulative energy for all T(J) before it

T 1 = barometer temperature

TA(J) = same as DELTA(J) in real time units of microseconds

TEMP 1 = initial temperature

T (J) = same as DELT(J) in real time units of microseconds

V (J) = actual voltage

VS = oscilloscope setting for voltage

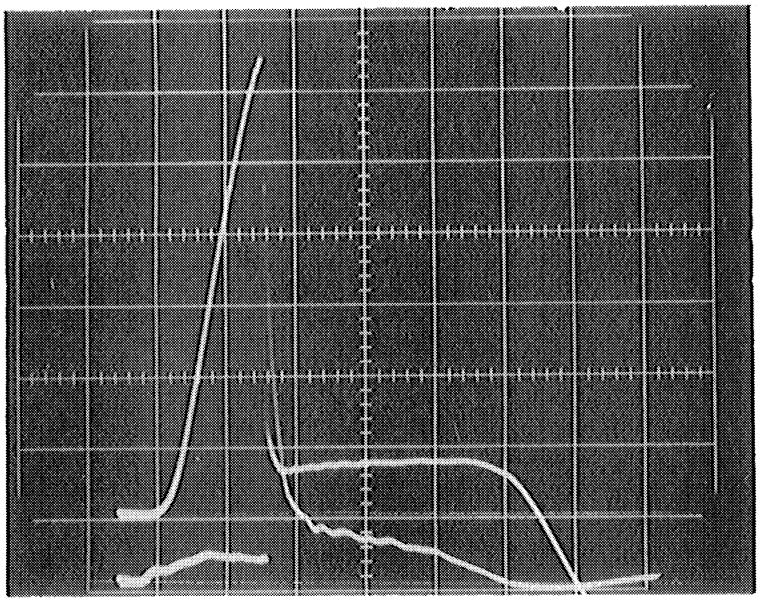

Figure F.1. Photographic Record of Spark Voltage and Current as a Function of Time.

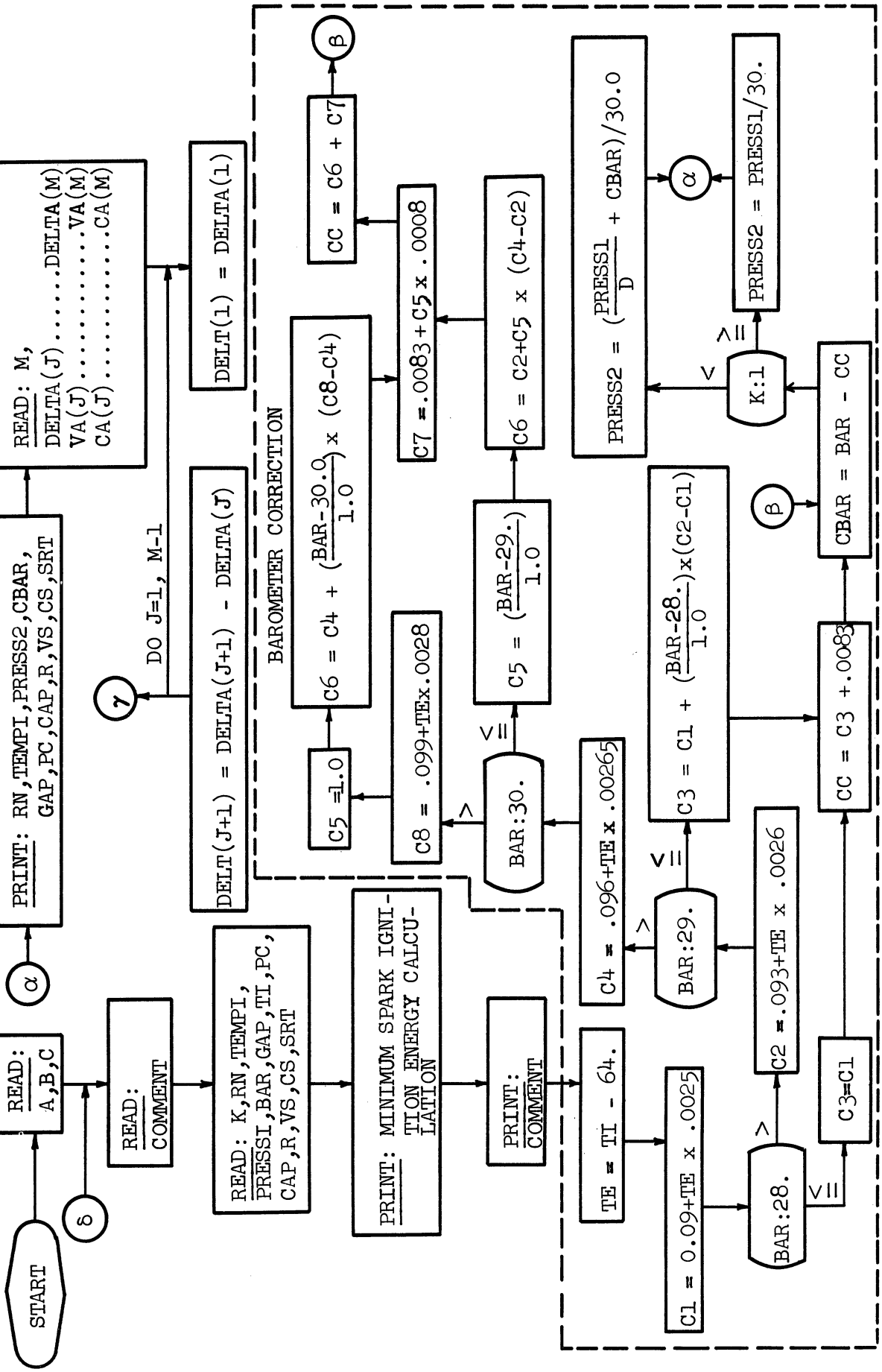

Figure F.2. Computer Flow Diagram.

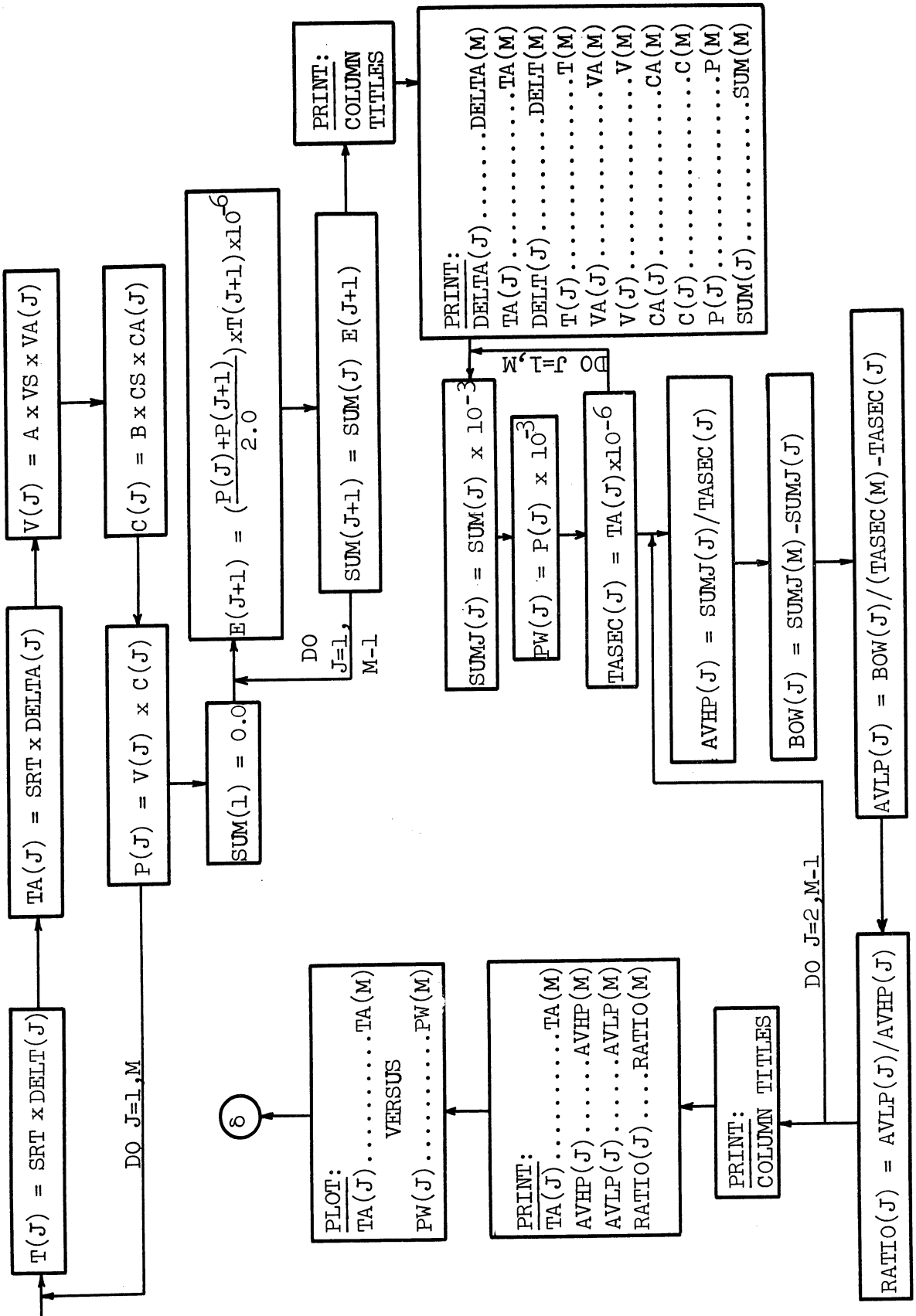

Figure F.2. (Continued).

MINIMUM SPARK IGNITION ENERGY CALCULATION

7/24/63,DELCO+249.5,25PF,149.5K,ER=.69,

RUN NO 56017

INITIAL TEMPERATURE= 79.0F INITIAL PRESSURE,ATM.= 1.0

CORRECTED BAROMETER=29.27IN.HG.

ELECTRODE GAP= .254IN. PRI. CURRENT=5.0AMPS. CAPACITY=1.0 R=1.40

OSC. SETTINGS VOLTAGE= 2 V/CM. CURRENT= 2 V/CM. SWEEP RATE,MICROSEC./CM.= 54

TIME INCREMENT IN,CM.	TIME INCREMENT IN,MICROSEC.	TIME INTERVAL IN,CM.	TIME INTERVAL IN,MICROSEC.	VOLTAGE INCREMENT IN,CM.	CURRENT INCREMENT IN,CM.	INSTANTANEOUS VALUES OF CURRENT IN,MILLIAMP	VOLTAGE IN,VOLT	POWER IN,MILLIWATT	NET ENERGY FOR TIME INCREMENT: IN,MILLIJOULES
.00	.00	.00	.00	6.40	.32	4.27	12800.0	54616.06	.000
.05	2.67	.05	2.67	1.10	5.55	74.00	2200.0	162808.13	.291
.11	5.88	.06	3.21	1.02	3.22	42.94	2040.0	87588.38	.693
.22	11.77	.11	5.88	.65	2.00	26.67	1300.0	34668.40	1.052
.36	19.26	.14	7.49	.60	1.22	16.27	1200.0	19520.98	1.255
.58	31.03	.22	11.77	.65	.95	12.67	1300.0	16467.49	1.467
.80	42.80	.22	11.77	.68	.78	10.40	1360.0	14144.71	1.647
2.52	134.82	1.72	92.02	.75	.43	5.73	1500.0	8600.43	2.694
3.50	187.25	.98	52.43	.60	.00	.00	1200.0	.00	2.919

TIME INCREMENT IN,MICROSEC.	AVERAGE HIGH RATE POWER IN WATTS	AVERAGE LOW RATE POWER IN WATTS	RATIO
2.67	108.71	14.24	.131
5.88	117.70	12.28	.104
11.77	89.42	10.64	.119
19.26	65.18	9.90	.152
31.03	47.28	9.30	.197
42.80	38.49	8.81	.229
134.82	19.98	4.30	.215

FIGURE F.3 SAMPLE COMPUTER OUTPUT

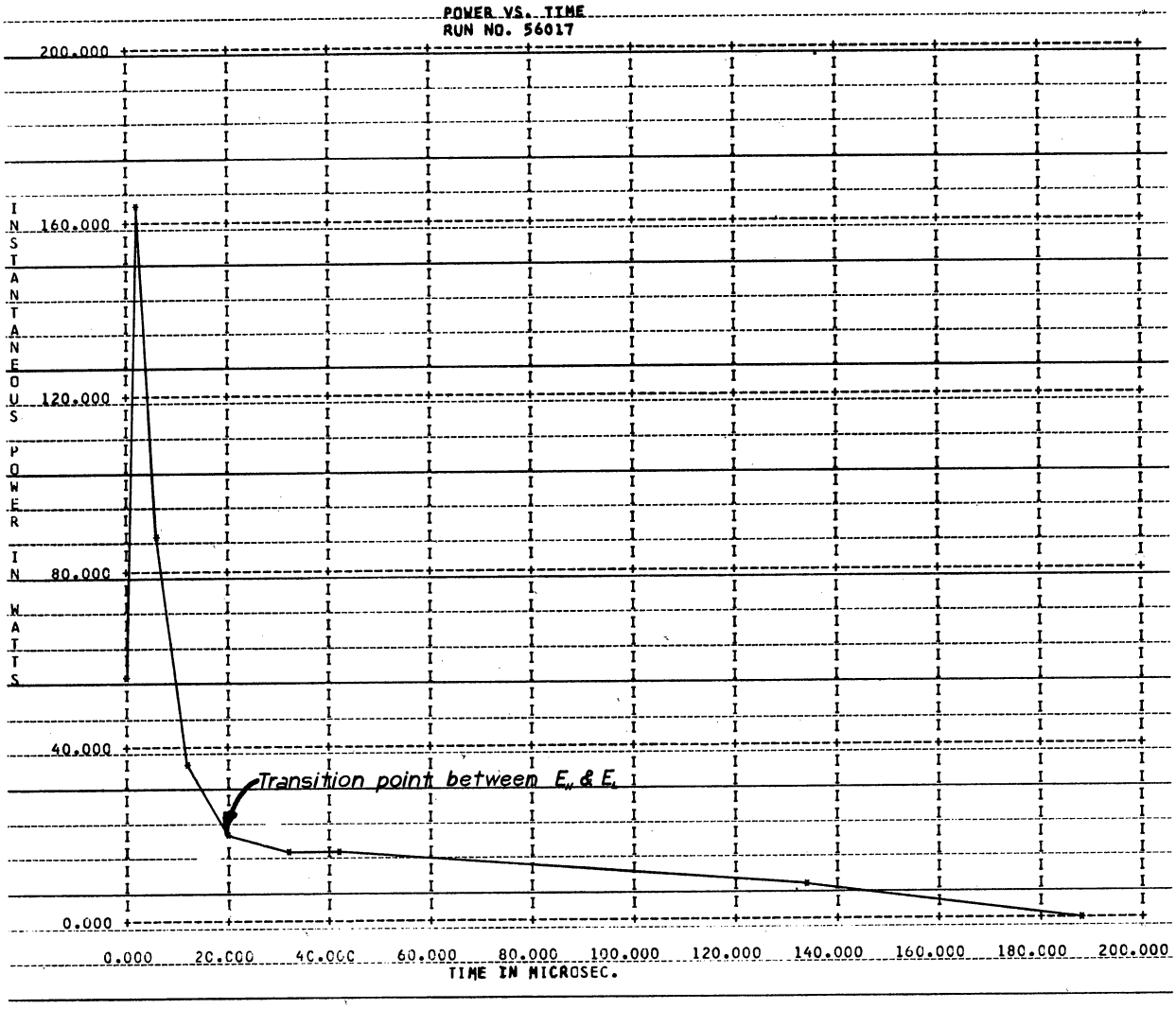

FIGURE F.4 SAMPLE POWER vs. TIME COMPUTER PLOT

BIBLIOGRAPHY

1. Silsbee, F. B., Loeb, L. B., and Fonseca, E. L., "Part I. Method of Measuring Heat Energy of Ignition Sparks," Fifth Annual Report of NACA, Report No. 56, (1919), 163.

2. Silsbee, F. B., and Fonseca, E. L., "Part II. Measurement of Heat Energy per Spark of Various Ignition Systems," Fifth Annual Report of NACA, Report No. 56, (1919), 169.

3. Wheeler, R. V., "The Ignition of Gases. Part I. Ignition by Impulsive Electrical Discharge. Mixtures of Methane and Air," J. Chem. Soc., 117, Part 2, (1920), 903.

4. Wheeler, R. V., "The Ignition of Gases. Part III. Ignition by Impulsive Electrical Discharge. Mixtures of Paraffins with Air," J. Chem. Soc., 125, Part 2, (1924), 1858.

5. Taylor-Jones, E., Morgan, J. D., Wheeler, R. V., "On the Form of the Temperature Wave Spreading by Conduction from Point and Spherical Sources; with a Suggested Application to the Problem of Spark Ignition," Lond. Phil. Mag., 43, (1922), 359.

6. Taylor-Jones, E., "Spark Ignition," Lond. Phil. Mag., Ser. 7, 6, N. 40, (Dec. 1928).

7. Coward, H. F., and Meiter, E. G., "Chemical Action in the Electric Spark Discharge," J. Am. Chem. Soc., 49, (1927), 396.

8. Finch, G. I., and Thompson, H. W., "The Effect of Frequency on the Condensed Discharge Ignition of Carbonic Oxide-Air Detonating Gas," Proc. Royal Soc., A, 134, (1931), 343.

9. Bradford, B. W., and Finch, G. I., "The Mechanism of Ignition by Electric Discharges," Chem. Rev., 21, No. 2, (Oct. 1937).

10. Thompson, H. W., "The Explosive Combination of Hydrogen and Oxygen - The Function of Walls in Gaseous Reactions," Faraday Soc. Trans., 28, (1932), 299.

11. Linnett, J. W., Raynor, E. J., and Frost, W. E., "The Mechanism of Spark Ignition," Faraday Soc. Trans., 41, (March, 1945), 487.

12. Lewis, B., and von Elbe, G., Combustion, Flames and Explosions of Gases, New York: Academic Press, Inc., 1951.

13. Linnett, J. W., and Nutbourne, D. M., "The Spark Ignition of Nitrous Oxide-Hydrogen Mixtures," Third Symposium on Combustion, Flame and Explosion Phenomena, Baltimore: Williams and Wilkins, (1949), 336.

14. Morgan, J. D., "The Ignition of Explosive Gases by Electric Sparks," J. Chem. Soc. Trans., 115, (1919), 94.

15. Morgan, J. D., Principles of Ignition, London: Sir Isaac Pitman and Sons, Ltd., 1942.

16. Bradford, B. W., Finch, G. I., and Prior, A. M., "The Coil Ignition of Some Explosive Gaseous Mixtures," J. Chem. Soc., Paper 63, (1933), 227.

17. Finch, G. I., and Sutton, R. W., "The Control of Ignition - Coil Discharge Characteristics," Proc. Royal Soc. Lond., 45, (1933), 288.

18. Jost, W., Explosion and Combustion Processes in Gases, New York: McGraw-Hill Book Co., Inc., 1946.

19. Finch, G. I., and Mole G., "The Mechanism of Electrical Ignition," Proc. Inst. Auto. Eng., 29, (1934), 71.

20. Blanc, M. V., Guest, P. G., von Elbe, G., and Lewis, B., "Ignition of Gas Mixtures by Electric Sparks. I. Minimum Ignition Energies and Quenching Distances of Mixtures of Methane, Oxygen, and Inert Gases," J. Chem. Phys., 15, No. 11, (Nov. 1947), 797.

21. Blanc, M. V., Guest, P. G., von Elbe, G., and Lewis, B., "Ignition of Explosive Gas Mixtures by Electric Sparks. III. Minimum Ignition Energies and Quenching Distances of Mixtures of Hydrocarbons and Ether with Oxygen and Inert Gases," Third Symposium on Combustion and Flame and Explosion Phenomena, Baltimore: The Williams and Wilkins Co., (1948), 363.

22. Guest, P. G., "Apparatus for Determining Minimum Energies for Electric-Spark Ignition of Flammable Gases and Vapors," U.S. Bur. Mines Rept. Invest., 3753, (1944).

23. Lewis, B., and von Elbe, G., "Ignition and Flame Stabilization in Gases," ASME Trans., 70, (1948), 307.

24. Morris, H., "Ignition of Gas Mixtures by Electric Sparks," Third Symposium on Combustion, Flame and Explosion Phenomena, Baltimore: Williams and Wilkins, (1949), 361.

25. Lewis, B., and von Elbe, G., "Ignition of Explosive Gas Mixtures by Electric Sparks. II. Theory of the Propagation of Flame from an Instantaneous Point Source of Ignition," J. Chem. Phys., 15, No. 11, (Nov. 1947), 803.

26. Belles, F. E., and Swett, C. C., "Ignition and Flammability of Hydrocarbon Fuels," Basic Considerations in the Combustion of Hydrocarbon Fuel with Air, NACA Report 1300, (1959), 83.

27. Friedman, R., and Johnston, W. C., "The Wall Quenching of Laminar Propane Flames as a Function of Pressure Temperature, and Air-Fuel," J. Appl. Phys., 21, No. 8, (Aug., 1950), 791.

28. Harris, M. E., Grumer, J., von Elbe, G., and Lewis, B., "Burning Velocities, Quenching, and Stability Data on Nonturbulent Flames of Methane and Propane with Oxygen and Nitrogen-Application of Theory of Ignition, Quenching, and Stabilization of Flames of Propane and Air," Third Symposium on Combustion, Flame and Explosion Phenomena, Baltimore: The Williams and Wilkins Co., (1948), 80.

29. Priede, T., and Rose, H. E., "An Investigation of the Characteristics of Spark Discharges as Employed in Ignition Experiments," Seventh Symposium (International) on Combustion, London: Butterworths Scientific Publications, (1959), 454.

30. Priede, T., and Rose, H. E., "Ignition Phenomena in Hydrogen-Air Mixtures," Seventh Symposium (International) on Combustion, London: Butterworths Scientific Publications, (1959), 436.

31. Swett, C. C., Spark Ignition of Flowing Gases, Part 1. Energies to Ignite Propane-Air Mixtures in Pressure Range of 2 to 4 Inches of Mercury Absolute, NACA RM-E9E17, (Aug., 1949).

32. Swett, C. C., Spark Ignition of Flowing Gases, Part 2, Effect of Electrode Parameters on Energy Required to Ignite a Propane-Air Mixture, NACA RM-E51J12, (Dec., 1951).

33. Swett, C. C., and Donlon, R. H., Spark Ignition of Flowing Gases, Part 3, Effect of Turbulence Promoter on Energy Required to Ignite a Propane-Air Mixture, NACA RM-E52J28, (Jan. 1953).

34. Swett, C. C., "Effect of Gas Stream Parameters on the Energy and Power Dissipated in a Spark and on Ignition," Third Symposium on Combustion and Flame and Explosion Phenomena, Baltimore: The Williams and Wilkins Co., (1949), 354.

35. Swett, C. C., "Spark Ignition of Flowing Gases Using Long Duration Discharges," Sixth Symposium (International) on Combustion, New York: Reinhold Publishing Corp., (1956), 523.

36. Guest, P. G., Lewis, B., Roth, W., and von Elbe, G., "Heat Generation by Electric Sparks and Rate of Heat Loss to the Spark Electrodes," J. Chem. Phys., 19, No. 12, (Dec. 1951), 1530.

37. Olsen, H. L., Gayhart, E. L., and Edmonsen, R. B., "Application of Ideal Gas Theory to the Gaseous Expansion from an Electric Spark," J. Appl. Phys., 25, No. 8, (Aug., 1954), 1008.

38. Olsen, H. L., Gayhart, E. L., and Edmonsen, R. B., "Microchronometric Schlieren Study of Gaseous Expansion from an Electric Spark," J. Appl. Phys., 23, No. 10, (Oct. 1952), 1157.

39. Olsen, H. L., Gayhart, E. L., and Edmonson, R. B., "Propagation of Incipient Spark-Ignited Flames in Hydrogen-Air Mixtures," Fourth Symposium on Combustion, Baltimore: Williams and Wilkins, (1953), 144.

40. Arnold, J. S., and Sherburne, R. K., "Obervations of the Ignition and Incipient Flame Growth in Hydrocarbon-Air Mixtures," Fourth Symposium on Combustion, Baltimore: Williams and Wilkins, (1953), 139.

41. Kumagai, Seuchiro, Tadami Sakai, and Itsuro Kimura,"Effect of Ultrasonic Waves on Flame Propagation and Spark Ignition," Fourth Symposium on Combustion, Baltimore: Williams and Wilkins, (1953), 148.

42. Calcote, H. F., Gregory, C. A., Barnett, C. M., and Gilmer, R. B., "Spark Ignition. Effect of Molecular Structure," Ind. Engr. Chem., 44, (1952), 2656.

43. Metzler, A. J., Minimum Spark-Ignition Energies of 12 Pure Fuels at Atmospheric and Reduced Pressure, NACA RM-E53H31, (Oct. 1953).

44. King. I. R., and Calcote, H. F., "Effect of Initial Temperature on Minimum Spark-Ignition Energy," J. Chem. Phys., (Letters to the Editor), 23, No. 12, (Dec. 1955), 2444.

45. Harnsberger, D. A. and Van Wylen, G. J., Effects of Radiation at Ignition Point of Constant-Volume Combustion, Ann Arbor: University of Michigan College of Engineering Industry Program, IP-171, 1956.

46. Souka, A. F., Influence of Alpha-Radiation on Some Aspects of Constant Volume Combustion, Ph.D. Dissertation, University of Michigan, 1957.

47. Clarke, J. S., "Initiation and Some Controlling Parameters of Combustion in the Automobile Engine," SAE Trans., (1962), 240.

48. Miller, W., "Fast Break Induction," SAE, Paper 652D, 1963.

49. Obert, E. F., Internal Combustion Engines Analysis and Practice, Scranton, Pa.: International Textbook Co., 1950.

50. Ethyl Corporation. Effect of Ignition Source on Spark Plug Electrode Erosion, Report No. A. R. 102, prepared by Ethyl Corporation, Detroit, Dec. 1943.

51. Ethyl Corporation. Effect of Internal Resistors on Spark Plug Electrode Erosion, Report No. A. R. 101, prepared by Ethyl Corporation, Detroit, Dec. 1943.

52. Ethyl Corporation. Effect of Low and High Values of Capacitance on Spark Plug Electrode Erosion, Report No. A. R. 100, prepared by Ethyl Corporation, Detroit, Dec., 1943.

53. Ethyl Corporation. The Effect of Different Center Electrode Materials on Sparking Voltage During Actual Engine Operation, Report No. A. R. 139, prepared by Ethyl Corporation, Detroit, Apr., 1945.

54. Allsop, G., and Guenault, E. M., "The Incendivity of Electric Sparks in Relation to the Characteristics of the Circuit," Third Symposium on Combustion, Flame and Explosion Phenomena, Baltimore, (1949), 341.

55. Cipriani, C., and Middleton, L. H., "Ignition Theory Uncovers Electrical Design Facts," SAE Journal, 56, No. 10, (Oct., 1948), 47.

56. Loeb, L. B., and Meek, J. M., The Mechanism of the Electric Spark, Stanford University, Calif.: Stanford University Press, 1941.

57. Loeb, L. B., Fundamentals of Electricity and Magnetism, New York: Dover Publication, Inc. (Unabridged and corrected republication of 3rd edition punlished by John Wiley and Sons, Inc., 1947), 1961.

58. Dow, W. G., Fundamentals of Engineering Electronics, New York: John Wiley and Sons, Inc., 1937.

59. Wheatcroft, E. L. E., Gaseous Electrical Conductors, England: Oxford at the Clarendon Press, 1938.

60. Devins, J. C., and Sharbaugh, A. H., "The Fundamental Nature of Electric Breakdown," Electro-Tech., (Feb., 1961), 103.

61. Meek, J. M., and Craggs, J. D., Electrical Breakdown of Gases, Great Britain: Oxford at the Clarendon Press, 1953.

62. Cobine, J. D., Gaseous Conductors, (Unabridged republication of the 1st edition with corrections by Author 1941), New York: Dover Publications, Inc., 1958.

63. Townsend, J. S., Electricity in Gases, London and New York: Oxford at the Clarendon Press, 1915.

64. Loeb, L. B., Fundamental Processes of Electrical Discharge in Gases, New York: John Wiley and Sons, Inc., 1939.

65. Loeb, L. B., Basic Processes of Gaseous Electronics, Los Angeles and Berkeley: University of California Press, 1960.

66. Meek, J. M., "A Theory of Spark Discharge," Phys. Rev., 57, (1940), 722, cited in Reference 61.

67. Raether, H., Arch. Electrotech., 34, (1940), 49, cited in Reference 61.

68. Eason, W. R., "Voltage Risetime - A New Ignition Criterion?", SAE, Paper 652C, Jan., 1963.

69. Semenov, N. N., Thermal Theory of Combustion and Explosion, NACA Tech. Memo No. 1024, (1942) from Progress of Physical Science (U.S.S.R.) Vol. 23, No. 3, (1940).

70. Vulis, L. A., Thermal Regimes of Combustion, New York: McGraw-Hill Book Co., Inc., (Translated by M. D. Friedman and G. C. Williams), 1961.

71. Frost, A. A., and Pearson, R. G., Kinetics and Mechanism, 2nd Ed., New York: John Wiley and Sons, Inc., 1961.

72. Benson, S. W., The Foundations of Chemical Kinetics, New York: McGraw-Hill Book Co., Inc., 1960.

73. Tenn, J. B., "Lean Flammability Limit and Minimum Spark Ignition Energy," Ind. and Engr. Chem., 43, (July-Dec., 1951), 2865.

74. Swett, C. C., Spark Ignition of Flowing Gases, Part IV. Theory of Ignition in Nonturbulent and Turbulent Flow Using Long-Duration Discharges, NACA RM-E-54F29a, Aug., 1954.

75. Swett, C. C., Spark Ignition of Flowing Gases, Part V. Application of Fuel-Air Ratio and Initial Temperature Data to Ignition Theory, NACA RM-E55I16, Nov. 1955.

76. Yang, C. H., "Theory of Ignition and Auto Ignition," Combustion and Flame, 6, (Dec., 1962), 215.

77. Mole, G., "The Ignition of Explosive Gases," Proc. Phys. Soc., 48, No. 61, (Oct., 1936), 857.

78. Landau, H. G., "The Ignition of Gases by Local Sources," Chem. Rev., 21, No. 2, (July, 1937), 245.

79. McAdams, W. H., Heat Transmission, New York: McGraw-Hill Book Co., Inc., 1954.

80. Radio Corporation of America, R.C.A. Transistor Manual, 1962.

81. Shea, R. F., (editor), Transistor Circuit Engineering, New York: John Wiley and Sons, Inc., 1957.

82. Strauss, L., Wave Generation and Shaping, New York: McGraw-Hill Book Co., Inc., 1960.

83. Basic Theory and Application of Transistors, New York: Dover Publication, 1963.

84. Larges, E. R., Frank, R. K., and Schneider, A., "Operating the Ignition Transistor within Safe Limits," SAE, Paper 652B, Jan., 1963.

85. Saad, M. A., Evaporation and Combustion of Single Fuel Droplets in a Hot Atmosphere, Ph.D. Dissertation, University of Michigan, IP-140, 1956.

86. Stout, M. B., Basic Electrical Measurements, Second Edition, New Jersey: Prentice-Hall, Inc., 1960.

87. Orr, L. W., Roberts, G. A., Schulte, H. T., Jr., Butler, T. W. Jr., and Otterman, J., Research and Development of Improved Ignition Systems, ERI Report 2370:2-P-3, University of Michigan, May 1956.